

2. REVERSED-FIELD PINCH AS A FUSION REACTOR

Robert A. Krakowski

Farrokh Najmabadi

Contents

2.1.	INTRODUCTION	2-1
2.2.	RFP THEORY	2-5
2.2.1.	RFP Confinement Concept	2-5
2.2.2.	Equilibrium	2-13
2.2.3.	Stability	2-16
2.2.4.	Relaxation and Sustainment	2-20
2.2.5.	Transport and Confinement	2-22
2.3.	RFP EXPERIMENTS	2-24
2.3.1.	Start-Up and Formation	2-28
2.3.2.	Typical Temperature and Density Responses	2-35
2.3.3.	Density Control	2-36
2.3.4.	Plasma Fluctuations	2-40
2.3.5.	Scaling	2-42
2.3.6.	Highly Radiating Plasma	2-57
2.3.7.	Current Termination	2-61
2.3.8.	Current Drive	2-61
2.3.9.	Operation with Resistive Shells	2-65
2.4.	SUMMARY	2-70
	REFERENCES	2-71

2. REVERSED-FIELD PINCH AS A FUSION REACTOR

2.1. INTRODUCTION

The TITAN research program is a multi-institutional [1] effort to determine the potential of the reversed-field-pinch (RFP) magnetic fusion concept as a compact, high-power-density, and “attractive” fusion energy system from economics (cost of electricity, COE), safety, environmental, and operational viewpoints.

In recent reactor studies, the compact reactor option [2 - 5] has been identified as one approach toward a more affordable and competitive fusion reactor. The main feature of a compact reactor is a fusion power core (FPC) with a mass power density in excess of 100 to 200 kWe/tonne. Mass power density (MPD) is defined [2] as the ratio of the net electric power to the mass of the FPC, which includes the plasma chamber, first wall, blanket, shield, magnets, and related structure. The increase in MPD is achieved by increasing the plasma power density and neutron wall loading, by reducing the size and mass of the FPC through decreasing the blanket and shield thicknesses and using resistive magnet coils, as well as by increasing the blanket energy multiplication. A compact reactor, therefore, strives toward a system with an FPC comparable in mass and volume to the heat sources of alternative fission power plants, with MPDs ranging from 500 to 1000 kWe/tonne and competitive cost of energy.

Other potential benefits for compact systems can be envisaged in addition to improved economics. The FPC cost in a compact reactor is a small portion of the plant cost and, therefore, the economics of the reactor will be less sensitive to changes in the unit cost of FPC components or the plasma performance. Moreover, since a high-MPD FPC is smaller and cheaper, a rapid development program at lower cost should be possible, changes in the FPC design will not introduce large cost penalties, and the economics of learning curves can be readily exploited throughout the plant life.

The RFP has inherent characteristics which allow it to operate at very high mass power densities. This potential is available because the main confining field in an RFP is the poloidal field, which is generated by the large toroidal current flowing in the plasma. This feature results in a low field at the external magnet coils, a high plasma beta, and a very high engineering beta (defined as the ratio of the plasma pressure to the square

of the magnetic field strength at the coils) as compared to other confinement schemes. Furthermore, sufficiently low magnetic fields at the external coils permit the use of normal coils while joule losses remain a small fraction of the plant output. This option allows a thinner blanket and shield. In addition, the high current density in the plasma allows ohmic heating to ignition, eliminating the need for auxiliary heating equipment. Also, the RFP concept promises the possibility of efficient current-drive systems based on low-frequency oscillations of poloidal and toroidal fluxes and the theory of RFP relaxed states. The RFP confinement concept allows arbitrary aspect ratios, and the circular cross section of plasma eliminates the need for plasma shaping coils. Lastly, the higher plasma densities particularly at the edge, together with operation with a highly radiative RFP plasma, significantly reduce the divertor heat flux and erosion problems.

These inherent characteristics of the RFP [6] allow it to meet, and actually far exceed, the economic threshold MPD value of 100 kWe/tonne. As a result, the TITAN study also seeks to find potentially significant benefits and to illuminate main drawbacks of operating well above the MPD threshold of 100 kWe/tonne. The program, therefore, has chosen a minimum cost, high-neutron wall loading of 18 MW/m^2 as the reference case in order to quantify the issue of engineering practicality of operating at high MPDs. The TITAN study has also put strong emphasis on safety and environmental features in order to determine if high-power-density reactors can be designed with a high level of safety assurance and with low-activation material to qualify for Class-C waste disposal.

Two different detailed designs, TITAN-I and TITAN-II, have been produced to demonstrate the possibility of multiple engineering design approaches to high-MPD reactors. TITAN-I is a self-cooled lithium design with a vanadium-alloy structure. TITAN-II is a self-cooled aqueous “loop-in-pool” design with ferritic-steel alloy, 9C, as the structural material. Both designs use RFP plasmas operating with essentially the same parameters.

The operating space of a compact RFP reactor has been examined using a comprehensive parametric systems model which includes the evolving state of knowledge of the physics of RFP confinement and embodies the TITAN-I and TITAN-II engineering approaches (Section 3). Two key figures of merit, the cost of electricity (COE) and mass power density (MPD), are monitored by the parametric systems model and are displayed in Figure 2.1-1 as functions of the neutron wall loading. Figure 2.1-1 shows that the COE is relatively insensitive to wall loadings in the range of 10 to 20 MW/m^2 , with a shallow minimum at about 19 MW/m^2 . The MPD is found to increase monotonically with the wall load. For designs with a neutron wall load larger than about 10 MW/m^2 , the FPC is physically small enough such that single-piece FPC maintenance is feasible. These considerations point to a design window for compact RFP reactors with neutron wall

loading in the range of 10 to 20 MW/m². The TITAN-class RFP reactors in this design window have an MPD in excess of 500 kWt/tonne, and an FPC engineering power density in the range of 5 to 15 MWt/m³; these values represent improvements by factors of 10 to 30 compared with earlier fusion reactor designs. The FPC cost is a smaller portion of the total plant cost (typically about 12%) compared with 25% to 30% for earlier RFP designs [4,5]. Therefore, the unit direct cost (UDC) is less sensitive to related physics and technology uncertainties.

Near-minimum-COE TITAN-I and TITAN-II design points, incorporating distinct blanket thermal-hydraulic options, materials choices, and neutronics performances have been identified in Figure 2.1-1. The major parameters of the TITAN reactors are summarized in Table 2.1-I. In order to permit a comparison, the TITAN reference design points have similar plasma parameters and wall loadings allowing for certain plasma engineering analyses to be common between the two designs.

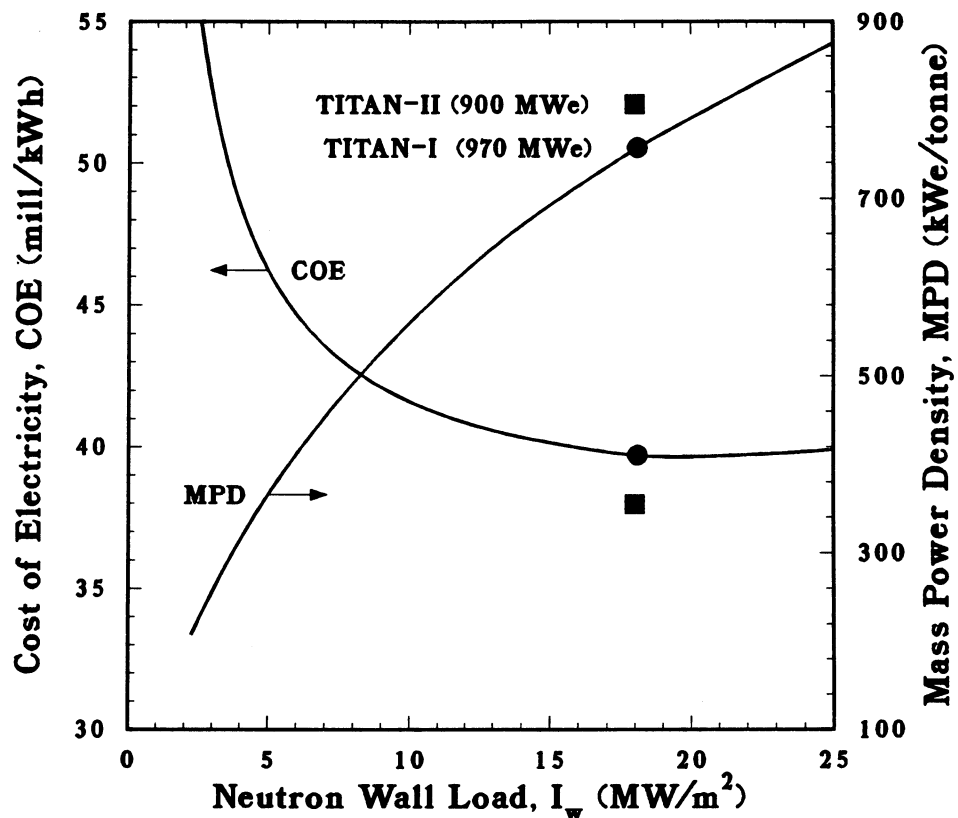


Figure 2.1-1. The COE (in 1986\$) and MPD as functions of neutron wall loading for the TITAN-class RFP reactors. TITAN-I (filled circle) and TITAN-II (filled squares) reference design points are also shown.

Table 2.1-I.
OPERATING PARAMETERS OF TITAN FUSION POWER CORES

	TITAN-I	TITAN-II
Major radius (m)	3.9	3.9
Minor plasma radius (m)	0.60	0.60
First wall radius (m)	0.66	0.66
Plasma current (MA)	17.8	17.8
Toroidal field on plasma surface (T)	0.36	0.36
Poloidal beta	0.23	0.23
Neutron wall load (MW/m ²)	18	18
Radiation heat flux on first wall (MW/m ²)	4.6	4.6
Primary coolant	Liquid lithium	Aqueous solution
Structural material	V-3Ti-1Si	Ferritic steel 9-C
Breeder material	Liquid lithium	LiNO ₃
Neutron multiplier	none	Be
Coolant inlet temperature (°C)	320	298
First-wall-coolant exit temperature (°C)	440	330
Blanket-coolant exit temperature (°C)	700	330
Coolant pumping power (MW)	48	49
Fusion power (MW)	2301	2290
Total thermal power (MW)	2935	3027
Net electric power (MW)	970	900
Gross efficiency	44%	35%
Net efficiency	33%	30%
Mass power density, MPD (kWe/tonne)	757	806
Cost of electricity, COE (mill/kWh)	39.7	38.0

In this section, the theoretical principles and understanding of the RFP confinement scheme are described, emphasizing those features that are relevant to a fusion reactor. The experimental data base is summarized in Section 2.3. More detailed descriptions of the theoretical and experimental aspects of RFP confinement concept are given in References [6,9,10] and the references contained therein. A detailed description of the plasma engineering for TITAN reactors is given in Sections 4 through 7. Section 8 summarizes the major physics issues for realizing TITAN-class RFP reactors.

2.2. RFP THEORY

2.2.1. RFP Confinement Concept

The RFP, like the tokamak, belongs to a class of axisymmetric, toroidal confinement systems that uses both toroidal, B_ϕ , and poloidal, B_θ , magnetic fields to confine the plasma. Stability in the tokamak is provided by a strong toroidal field ($B_\phi \gg B_\theta$ everywhere) such that the safety factor, $q = r_p B_\phi / (R_T B_\theta)$, exceeds unity, where R_T and r_p are, respectively, the major and minor radii of the plasma. In the RFP, on the other hand, strong magnetic shear produced by the radially varying (and decreasing) toroidal field stabilizes the plasma with $q < 1$ at relatively modest levels of B_ϕ . Theoretically, an electrically conducting shell surrounding the plasma is required to stabilize the long-wavelength MHD modes. In both the RFP and the tokamak, equilibrium may be provided by either an externally produced vertical field, a conducting toroidal shell, or a combination of both. Figure 2.2-1 compares the radial variation of the poloidal and toroidal fields and the safety factors for the tokamak and RFP.

The RFP magnetic topology is dominated by the poloidal field generated by the current flowing in the plasma. This feature has several reactor-relevant advantages. The poloidal field decreases inversely with the plasma radius outside the plasma. The toroidal field is also weak outside the plasma relative to the tokamak. The magnetic field strength at the external conductors, therefore, is small, and a high engineering beta (defined as the ratio of the plasma pressure to the magnetic field pressure at the magnets) results; less-massive resistive coils with a low current density are possible. The RFP experiments operate at reactor-relevant values of total beta (5% to 10%). Furthermore, by relying on the magnetic shear to stabilize the plasma, the RFP can support a large ratio of plasma current to toroidal field, and stability constraints on the aspect ratio, R_T/r_p , are removed; the choice of the aspect ratio, therefore, can be made solely on the basis of engineering constraints. High-current-density operation and strong ohmic heating to ignition are

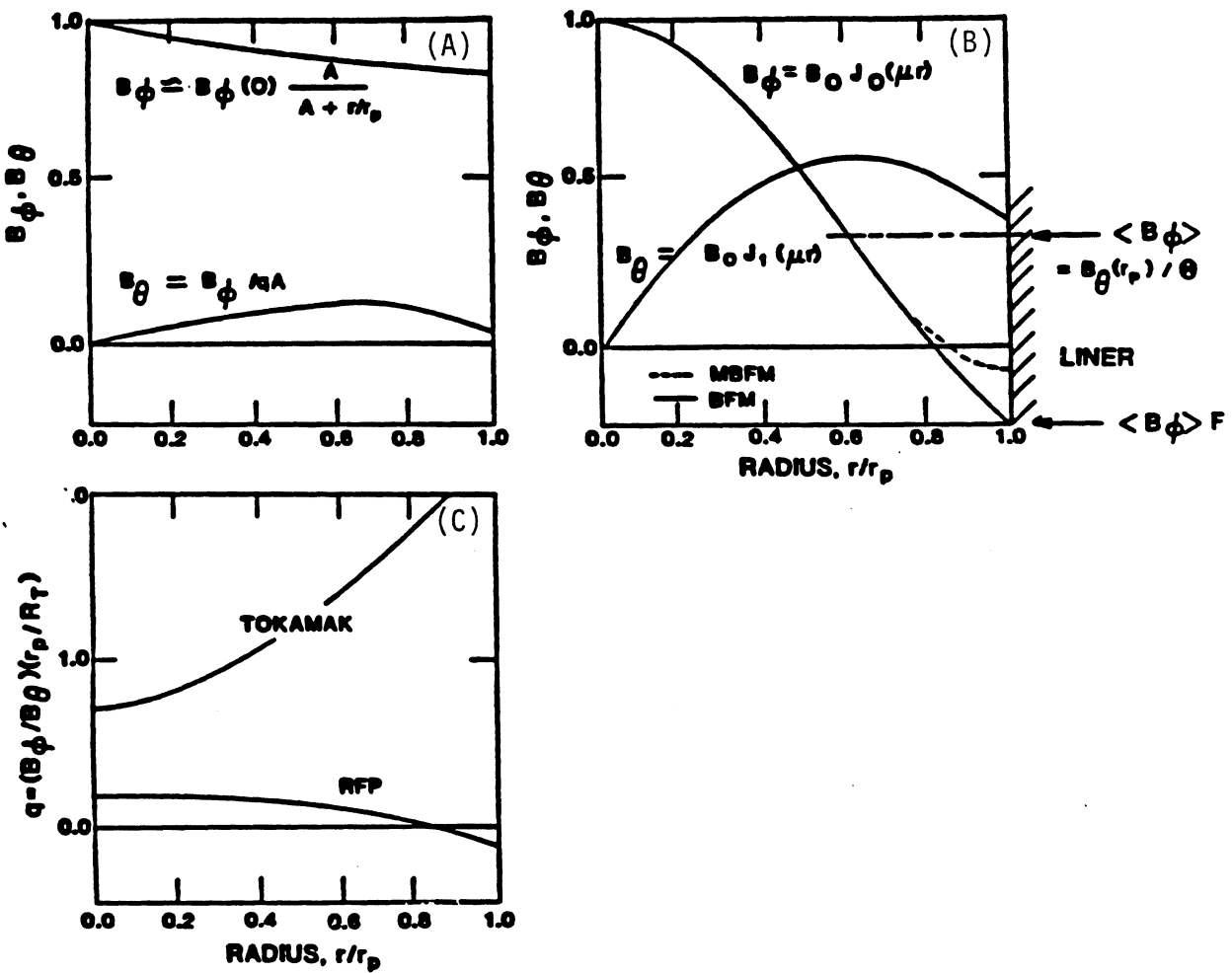


Figure 2.2-1. Magnetic-field distribution for tokamak (A) and RFP (B) and the q profiles for tokamak and RFP (C).

also positive consequences of the shear-stabilized RFP. Lastly, the close coupling of the current and magnetic-field components within the RFP plasma also promises a unique and highly efficient current-drive technique.

The field configuration and toroidal-field reversal in the RFP are the result of the relaxation of the plasma to a near-minimum-energy state. A theory of relaxed states developed by Taylor [11] postulates that a pinch should relax to a magnetic-field configuration determined by minimizing the magnetic energy subject to constraints imposed on allowed motion or magnetic-field variation. Taylor then considered the relaxation of a plasma with small but finite resistivity in a flux-conserving cylinder, subject to the invariance of the magnetic helicity $K \equiv \int \mathbf{A} \cdot \mathbf{B} dV_p$, where $\mathbf{B} \equiv \nabla \times \mathbf{A}$ and the integration is over the plasma volume. The helicity is a measure of the linkage between the poloidal and toroidal magnetic flux. The relaxed, minimum-energy state was found to be force-free and described by $\nabla \times \mathbf{B} = \mu \mathbf{B}$, where $\mu = \mu_0 \mathbf{j} \cdot \mathbf{B} / B^2$ is the ratio of local parallel current and field. For the minimum-energy Taylor state, the μ profile is uniform across the plasma. The solution to the equilibrium equation in cylindrical geometry for a spatially constant μ gives the Bessel-function model (BFM), with $B_\phi \propto J_1(\mu r)$ and $B_\theta \propto J_0(\mu r)$, where J_1 and J_0 are Bessel functions of the first kind. These relaxed states can be described solely in terms of two dimensionless quantities: the reversal parameter, F , and the pinch parameter, Θ , where

$$F \equiv \frac{B_\phi(r_p)}{\langle B_\phi \rangle}, \quad (2.2-1)$$

$$\Theta \equiv \frac{B_\theta(r_p)}{\langle B_\phi \rangle}. \quad (2.2-2)$$

The average toroidal field within the conducting shell, $\langle B_\phi \rangle$, is defined as

$$\langle B_\phi \rangle = \frac{2}{r_p^2} \int_0^{r_p} B_\phi(r) r dr. \quad (2.2-3)$$

The locus of relaxed states then form a curve in $F-\theta$ space, as is shown in Figure 2.2-2 (labeled as BFM). The same figure also shows the experimental data which lie to the right of the curve predicted by the BFM model. The experimental equilibria represented in Figure 2.2-2 differ from the Taylor model because plasma has finite pressure, μ is not uniform across the plasma, and a perfectly conducting wall is not used. These data represent “near-minimum-energy” states. The concept of a preferred locus of relaxed states in $F-\theta$ space, as originally postulated by Taylor, remains applicable, however.

Near the cool edge of practical RFPs, the μ profile deviates away from $\mu(r) \simeq \text{constant}$ condition of the minimum-energy assumption. At the highly resistive plasma edge, μ is

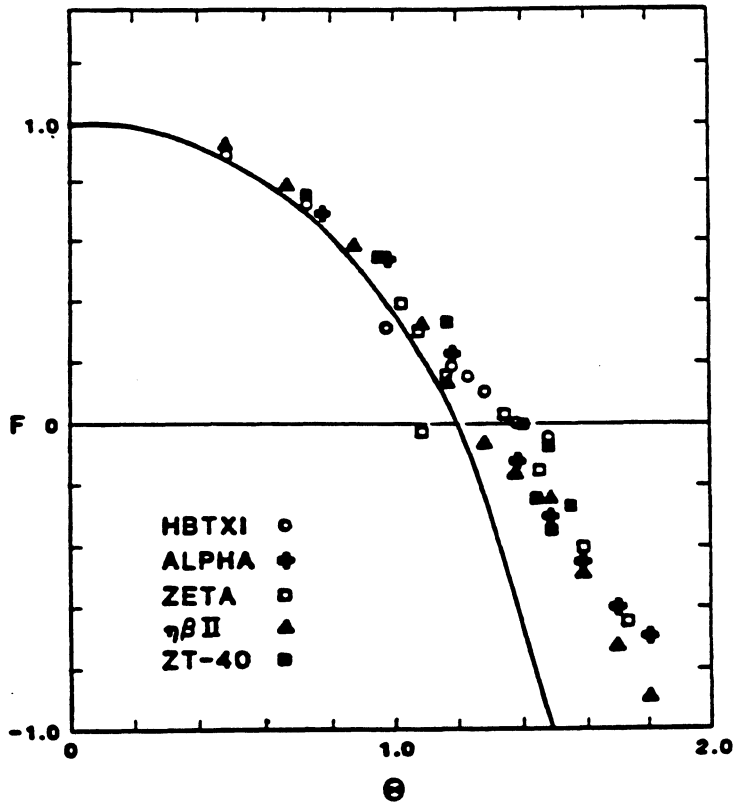


Figure 2.2-2. Locus of operating points on the F - Θ diagram. The solid line (BFM) is the curve predicted by Taylor's theory [11] and the data points are from several RFP experiments.

assumed to decrease to zero in order to model the decreasing current expected in the edge region. These differences can be seen in Figure 2.2-3 [12] which compares the magnetic field profiles from experiments to the BFM model. The smaller magnitude of the toroidal fields observed in experiment reflects the falloff of μ and j_θ in the cold plasma edge. Typically, the following expressions for $\mu(r)$ describes experimental results [13].

$$\frac{\mu(r)}{\mu(0)} = 1 - \left(\frac{r}{r_p}\right)^\alpha, \quad (2.2-4)$$

where $\alpha \simeq 6$ to 8 and $\mu(0) \equiv 2\Theta_0/r_p = 2q(0)A/r_p$ are fitting parameters used to model the experimental profiles with finite plasma beta. The impact of the cold plasma edge (smaller value of α) on the F - Θ diagram is shown in Figure 2.2-4 along with experimental results form the ETA-BETA-II RFP experiment [12].

The theory of relaxed states as applied to the RFP concept has several important consequences. Firstly, the theory predicts that the relaxed states depend only on the

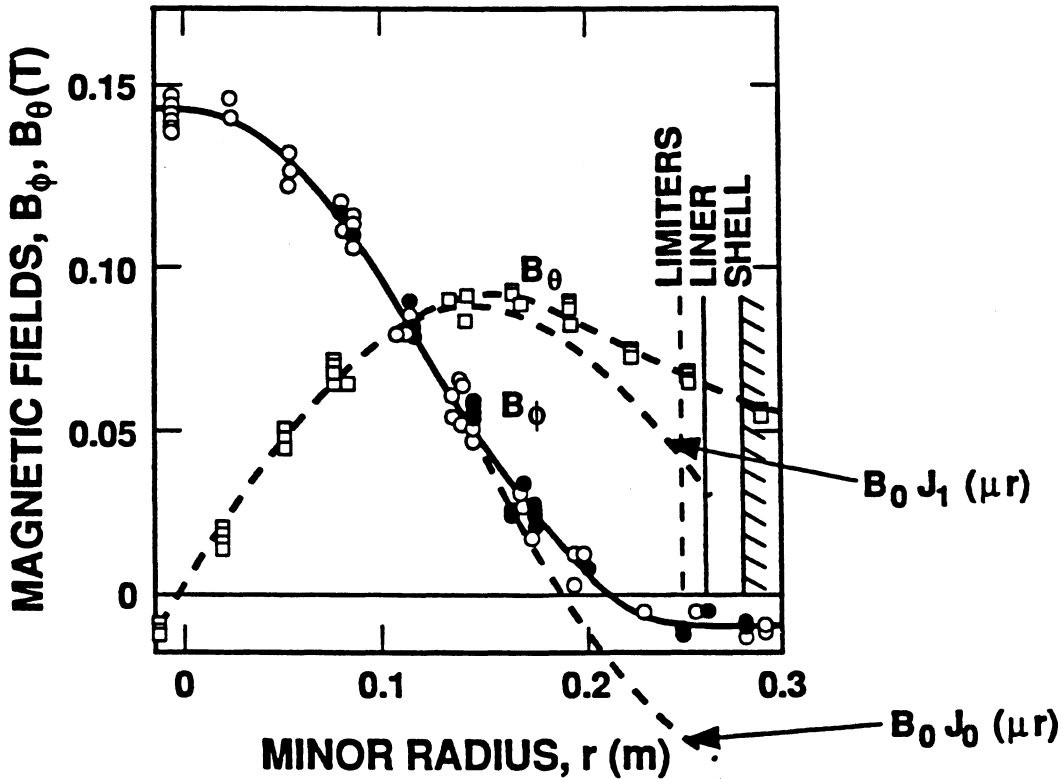


Figure 2.2-3. Magnetic-field profiles from the HBTX experiments [12] showing the derivation from the BFM for $\mu(r)$ profiles that are not constant across the plasma radius.

pinch parameter, Θ , and these states are independent of initial conditions provided that the time scale is sufficiently long for the relaxation process to occur. Secondly, if the plasma current and toroidal flux are maintained constant in time (*i.e.*, constant Θ), then the relaxed-state equilibrium will be sustained. Experimentally, the RFP configuration shown in Figure 2.2-3 exists for times much larger than the resistive decay time of the field profiles. This sustainment process involves continuous generation of the toroidal field within the plasma to compensate for the resistive decay of the toroidal field and to maintain the field profile; this process is often called the RFP “dynamo.” The RFP dynamo converts poloidal flux or toroidal currents to poloidal currents or toroidal flux and is driven by localized plasma fluctuations of fluid velocity, δu , and magnetic field, δB , to give a non-zero time-averaged electric field, $\langle \delta u \times \delta B \rangle$.

The F - Θ relationship (Figure 2.2-2) reflects a strong coupling between the toroidal and poloidal fields within the plasma: the toroidal field is continuously regenerated by

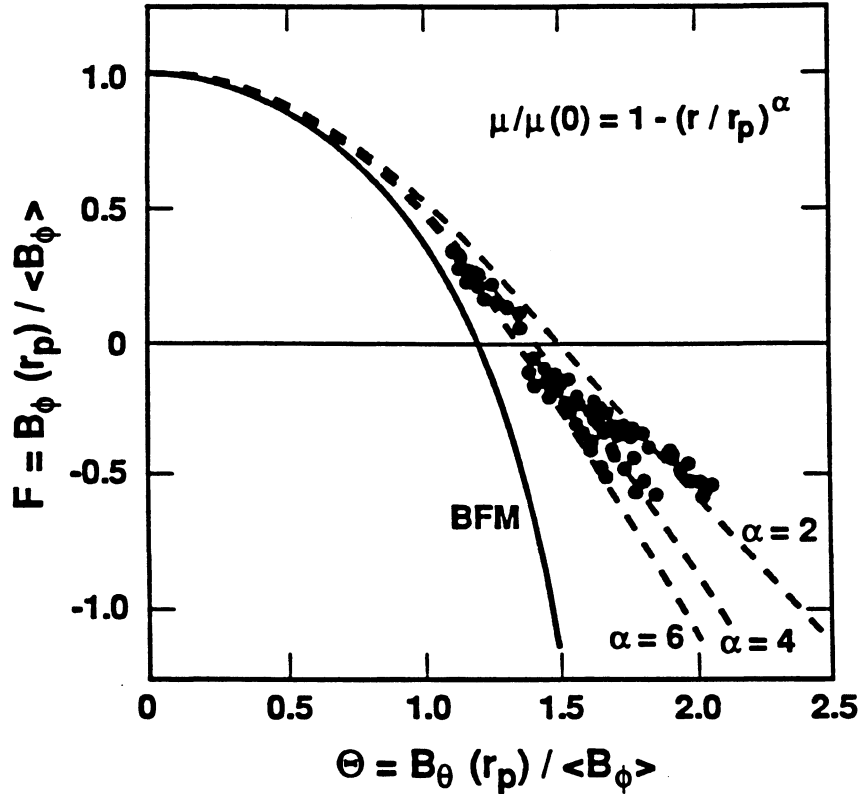


Figure 2.2-4. F - Θ diagram for Taylor's relaxed state and an equilibrium model with different values of the experiment, α , describing the flatness of the μ profile (Equation 2.2-4). Circles indicate experimental configuration for the ETA-BETA-II experiment [12].

driving toroidal current with an external poloidal-field circuit. Indeed, such a relaxation-assisted plasma current ramp has been demonstrated in RFP experiments and is envisioned for RFP reactors. Figure 2.2-5 illustrates a typical “matched-mode” RFP start-up [14]. After the vacuum toroidal field, B_ϕ , reaches a maximum value, the plasma breakdown occurs, and current, I_ϕ , is initiated, with B_ϕ at and beyond the plasma surface, $B_\phi(r \geq r_p)$, actually reversing direction while the average toroidal field, $\langle B_\phi \rangle$, and toroidal flux, Φ , within the conducting shell remain positive. Upon reversal of the toroidal field and establishment of the quiescent near-minimum-energy RFP state, Figure 2.2-5 shows a dramatic decrease in the plasma resistive, R_p , which nevertheless remains large in comparison with the tokamak. Figure 2.2-6 [15,16] illustrates explicitly the generation of toroidal flux within the plasma by the RFP dynamo, which assists and maintains the toroidal field during a slow current ramp-up on a time scale that is an order of magnitude greater than the resistive decay time for the toroidal field.

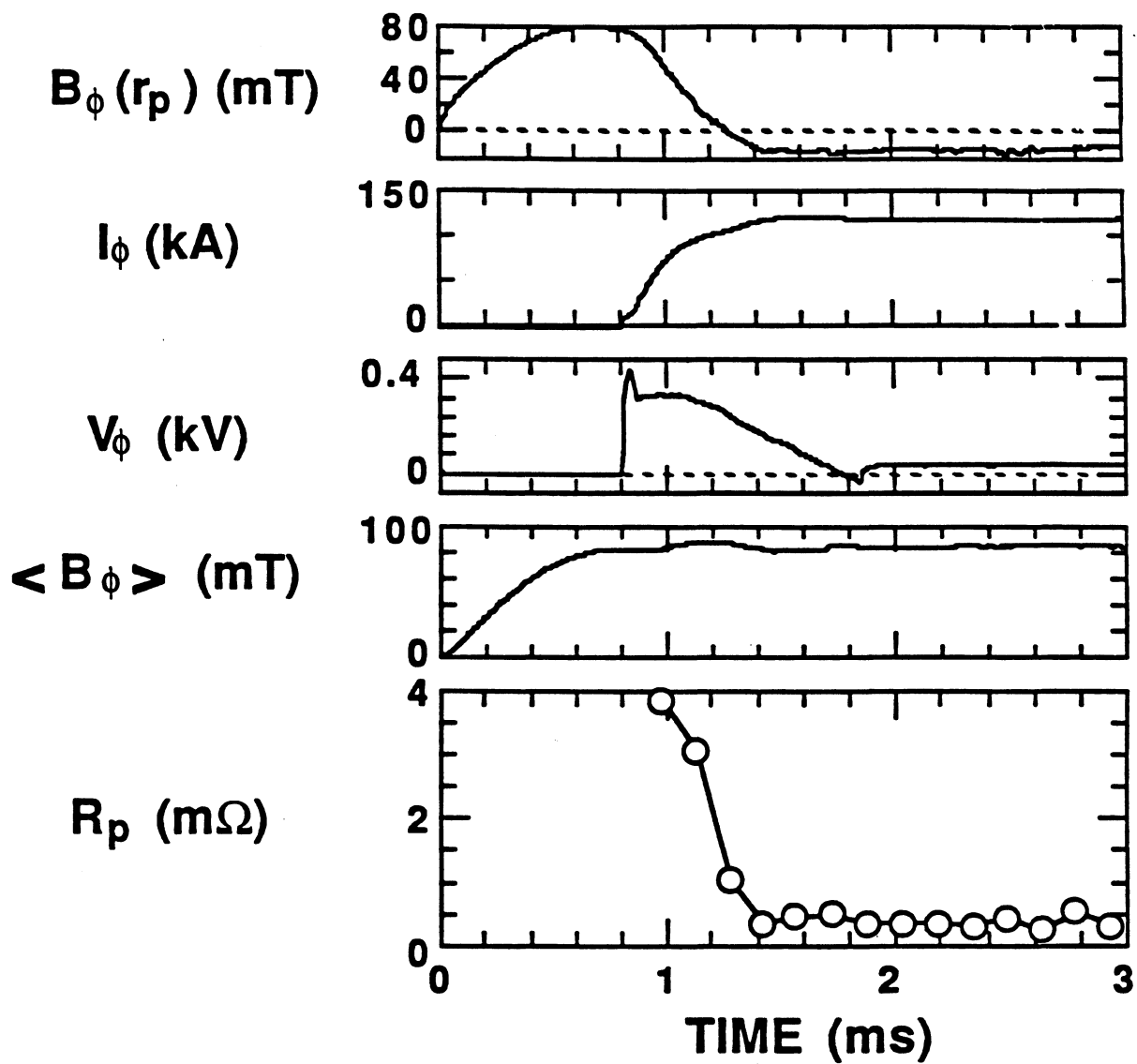


Figure 2.2-5. Typical “matched-mode” formation and start-up of an RFP wherein the net transfer of toroidal flux across the conducting shell is zero.

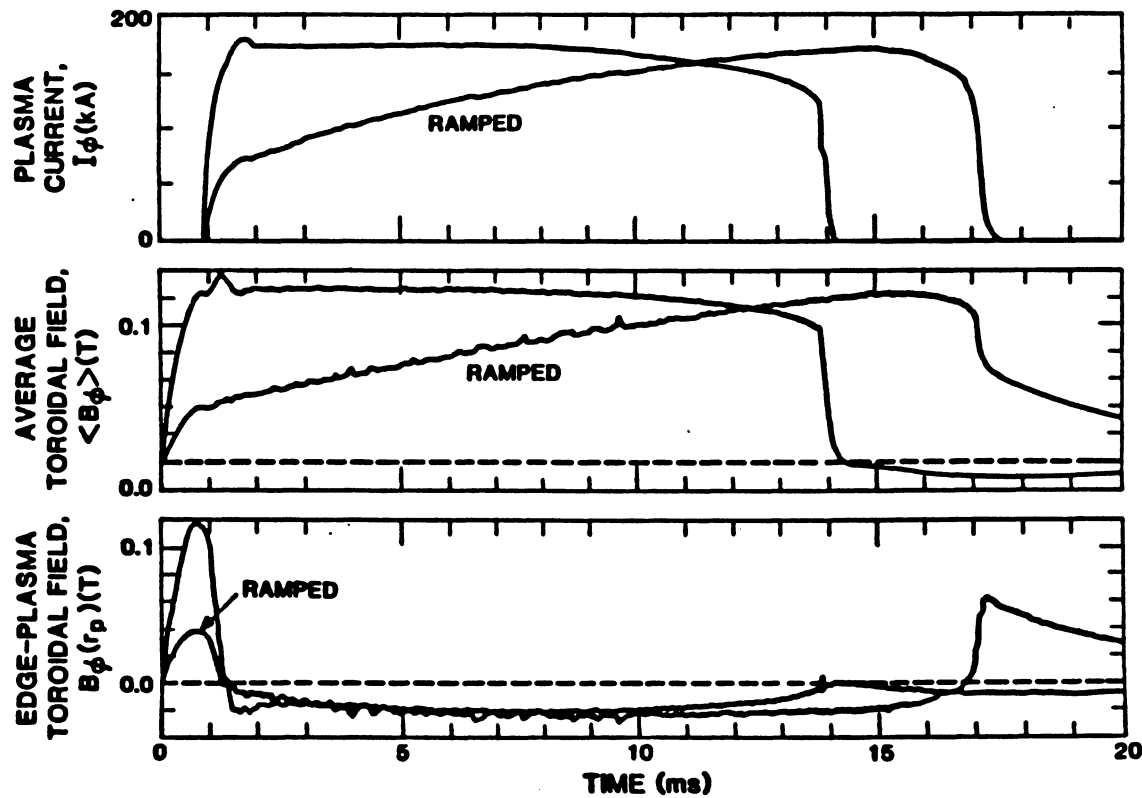


Figure 2.2-6. Dynamo-assisted current ramp-up wherein a majority of the toroidal flux, $\Phi = \pi r_p^2 \langle B_\phi \rangle$, within the plasma is generated by fluid motion within the plasma, since $B_\phi(r_p)$ is fixed by the external circuit [15,16].

The strong coupling of the poloidal and toroidal fields in RFPs also offers the possibility of a steady-state current-drive mechanism based on “magnetic helicity injection” [17] because the resistive decay of plasma currents can be viewed as a dissipation of magnetic helicity. Current drive through “electrostatic helicity injection” has been experimentally demonstrated in spheromaks [18], which are also relaxed-state systems like RFPs. Another helicity injection technique is the oscillating-field current drive (OFCD) [17,19]. In this scheme, oscillating voltages are applied to the toroidal and poloidal circuits in the appropriate phase to drive a DC toroidal current in the plasma with the plasma, in effect, behaving as a nonlinear rectifier. The experiments on OFCD are not yet conclusive but are encouraging [16, 19 - 21]. Helicity injection as applied to TITAN is discussed in more detailed in Section 7, with Section 2.3.8 summarizing experimental results.

The general characteristics of a dynamo-sustained RFP, therefore, describe a system where $B_\phi \simeq B_\theta$ within the plasma, and fluctuation and transport are enhanced because

of the dynamic sustainment of field and current profiles. Also, loop voltages and plasma resistance should be higher than in a comparable tokamak, and significant ohmic heating by the larger current densities in the low- q , shear-stabilized plasma is expected.

2.2.2. Equilibrium

As for any toroidal plasma, equilibrium in the RFP is described by the static ideal-MHD equations,

$$\nabla p = \mathbf{j} \times \mathbf{B}, \quad (2.2-5)$$

$$\nabla \times \mathbf{B} = \mu_0 \mathbf{j}, \quad (2.2-6)$$

where $p = 2k_B(T_e + T_i)$ is the plasma pressure, $k_B = 1.602 \times 10^{-16}$ J/keV is the Boltzmann constant, and $\mu_0 = 4\pi \times 10^{-7}$ H/m is the permeability of free space. The analysis of equilibrium and stability in RFPs usually invokes the high-aspect-ratio (straight cylinder) approximation. Such a model encompasses z-pinches ($q = 0$), θ -pinches ($q \rightarrow \infty$), large-aspect-ratio tokamaks ($q > 1$), and RFPs ($q < 1$). The radial pressure balance in these systems is described by

$$\frac{d}{dr} \left(p + \frac{B_\theta^2 + B_\phi^2}{2\mu_0} \right) + \frac{B_\theta^2}{\mu_0 r} = 0. \quad (2.2-7)$$

Information on the current and pressure profiles is required in order to find the equilibrium magnetic-field profiles. Because of the strong tendency for RFPs to relax towards a near-minimum-energy state, the field distributions obtained in modern experiments (Figure 2.2-3) are close to those given in Figure 2.2-1. The theory of relaxed states [11] predicts that $\mathbf{j} = \mu \mathbf{B}$, with $\mu \equiv \mu_0 j_{||}/B$ assumed to be spatially uniform across the plasma and leading to BFM field profiles (Figure 2.2-3). As noted previously, a constant μ profile implies a large parallel-current density in the outer region of cold, resistive plasma. A μ profile that is nearly constant over the bulk of the plasma and decreases in the outer region to match the practical condition that \mathbf{j} and $\mu(r_p) \approx 0$ eliminates an unphysical feature of the BFM. Sample profiles used are as given by Equation 2.2-4 with $\alpha \approx 6$ to 8 or a μ profile that is constant for $r < r_r$ (the radius of reversal surface) and decreases linearly to zero at r_p .

For any toroidal plasma system, including the RFP, equilibrium requires the compensation of the outward force from the plasma pressure and the plasma current (*i.e.*, poloidal-field pressure). A perfectly conducting wall, a vertical field produced by the

external circuits, or a combination of both is necessary to provide toroidal equilibrium. The required value of this vertical field is given by [22,23]

$$B_V = \frac{\mu_0 I_\phi}{4\pi R_T} \left[\ln \left(\frac{8R_T}{r_p} \right) + \beta_\theta + \frac{\ell_i}{2} - 1.5 \right], \quad (2.2-8)$$

where

$$\ell_i = \frac{1}{\pi r_p^2 B_\theta^2(r_p)} \int_0^\pi \int_0^{r_p} B_\theta^2 r dr d\theta \quad (2.2-9)$$

is the normalized plasma internal inductance and β_θ is the poloidal beta $\beta_\theta = 2\mu_0 p / B_\theta^2$. Typically, the vertical field required for equilibrium is small, and the ratio $B_V/B_\theta(r_p)$ is of the order of the inverse aspect ratio, $\epsilon = 1/A = r_p/R_T$.

A toroidal shift, δ , develops between the center of a conducting shell of radius r_w and the center of a circular plasma of radius r_p in the process of compensating for the force acting on the plasma and achieving an equilibrium. A detailed analysis [22,23] gives the following expression for the equilibrium shift:

$$\frac{\delta}{r_p} = \frac{\epsilon}{2x^2} \left[-\ln(x) + (1-x^2) \left(\beta_\theta - \frac{\ell_i - 1}{2} \right) \right], \quad (2.2-10)$$

where $x \equiv r_p/r_w$. Present-day RFP experiments use a conducting shell to provide equilibrium (and stability), with vertical fields being applied, largely at insulating gaps provided in the shell, prior to or during the discharge. On longer time scales, these equilibrium-producing magnetic fields will diffuse into the shell, and externally produced vertical fields will be required to maintain a force equilibrium. Externally produced vertical fields will in fact be required for the next generation of RFP experiments [24], as are presently used on most modern tokamaks.

It follows from the ideal-MHD theory (Equation 2.2-5) that the current and the magnetic-field lines lie on constant-pressure surfaces. For axisymmetric, toroidal, current-carrying plasma, the equilibrium, therefore, consists of toroidal flux surfaces that are nested about a magnetic axis. Each surface is generated by a large number of toroidal traverses of the helical magnetic-field lines. If the toroidal symmetry is violated (e.g., because of errors in the alignment of magnet coils), the nested toroidal surfaces break up, resulting in a more complicated structure which includes helical magnetic islands [25]. The existence and interaction of these islands in the regions near the plasma edge impact plasma transport. Although both tokamaks and RFPs are susceptible to magnetic-island formation, the number and location of the resonant flux surfaces, as indicated in

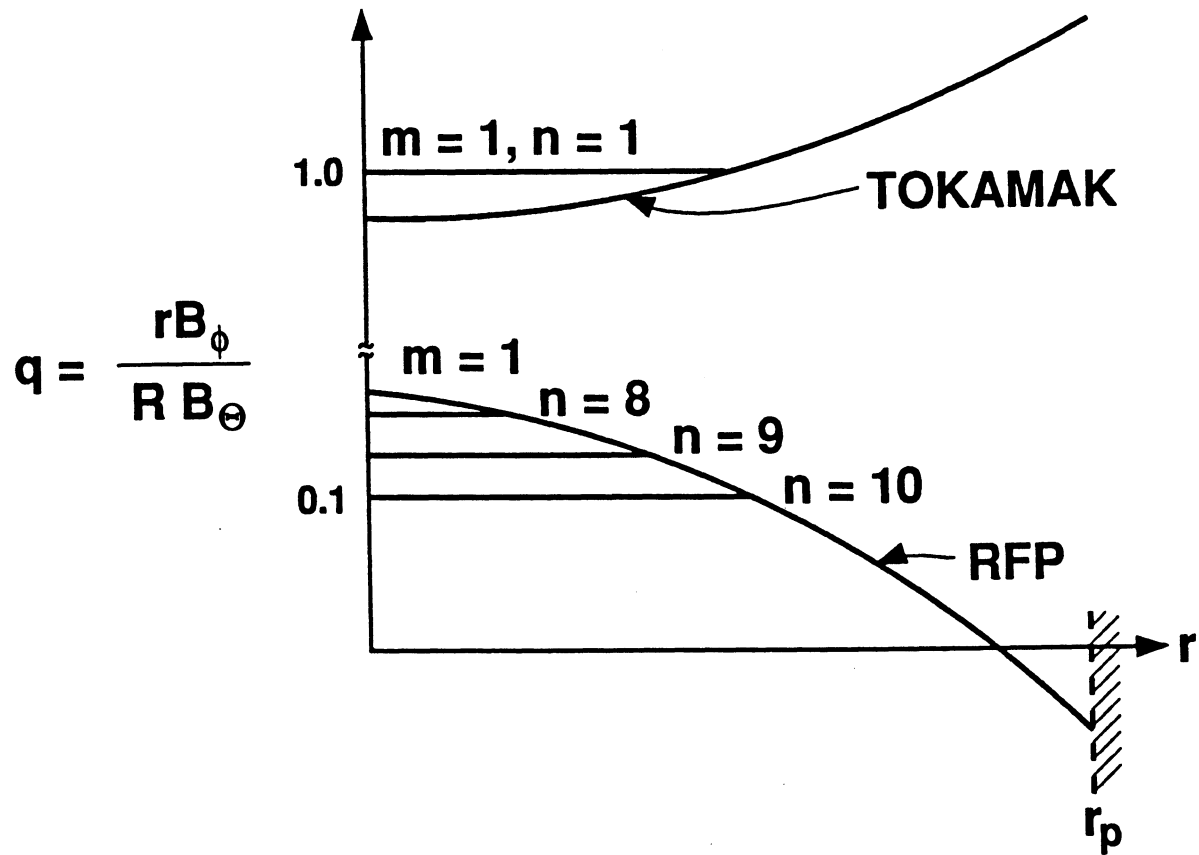


Figure 2.2-7. Comparison of magnetic-plasma configurations between RFPs and tokamaks, indicating the large number of toroidally resonant flux surfaces in the RFP compared with the tokamak.

Figure 2.2-7, are significantly different in the two concepts. Whereas the admission of a rational surface into the tokamak plasma nonlinearly leads to instability (disruptions), the inclusion of a large number of helically interacting, rational surfaces in the RFP give rise to a large number of degrees of freedom for field-line reconnection and a mechanism (e.g., dynamo) for moving towards the Taylor minimum-energy state [11]. The large number of rational surfaces, however, makes field errors a greater concern in RFPs [24].

Since the plasma edge in RFPs plays an important role in plasma confinement and helicity dissipation [26 - 29], changes in this region through the equilibrium shift and/or field errors can be important in determining plasma performance. Figures 2.2-8 and 2.2-9 illustrate, respectively, the reduction in loop voltage and the increase in energy confinement time as a result of better control of field errors and the equilibrium shift.

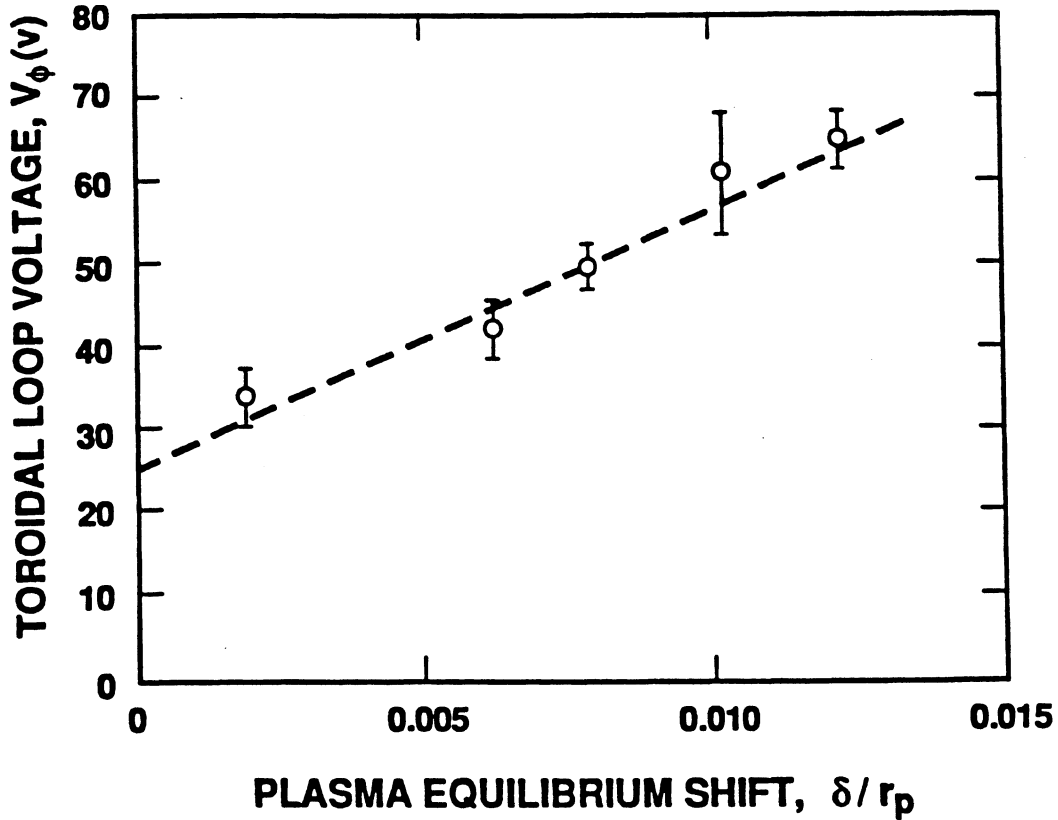


Figure 2.2-8. Impact of plasma equilibrium shift and wall contact on the toroidal loop voltage in the HBTX experiment [27].

2.2.3. Stability

The equilibrium-pressure profile described by Equation 2.2-7 must be subjected to stability analysis using the energy principle [30] or normal-mode analysis. The Suydam criterion [31] gives the following necessary condition for stability against ideal-MHD pressure-driven modes for a straight cylinder:

$$\frac{r}{4} \left(\frac{1}{q} \frac{dq}{dr} \right)^2 + \frac{2\mu_o}{B_\phi^2} \frac{dp}{dr} > 0, \quad (2.2-11)$$

where $q(r) = (r/R)(B_\phi/B_\theta)$ is a relative measure of field-line pitch at minor-radial position r . This criterion simply states that the negative pressure gradient associated with the confinement of a hot plasma has a destabilizing effect and can be compensated for only by a sufficiently large radial variation in the field-line pitch $P(r) = (B_\phi/B_\theta)r = qR$ (*i.e.*, large magnetic shears).

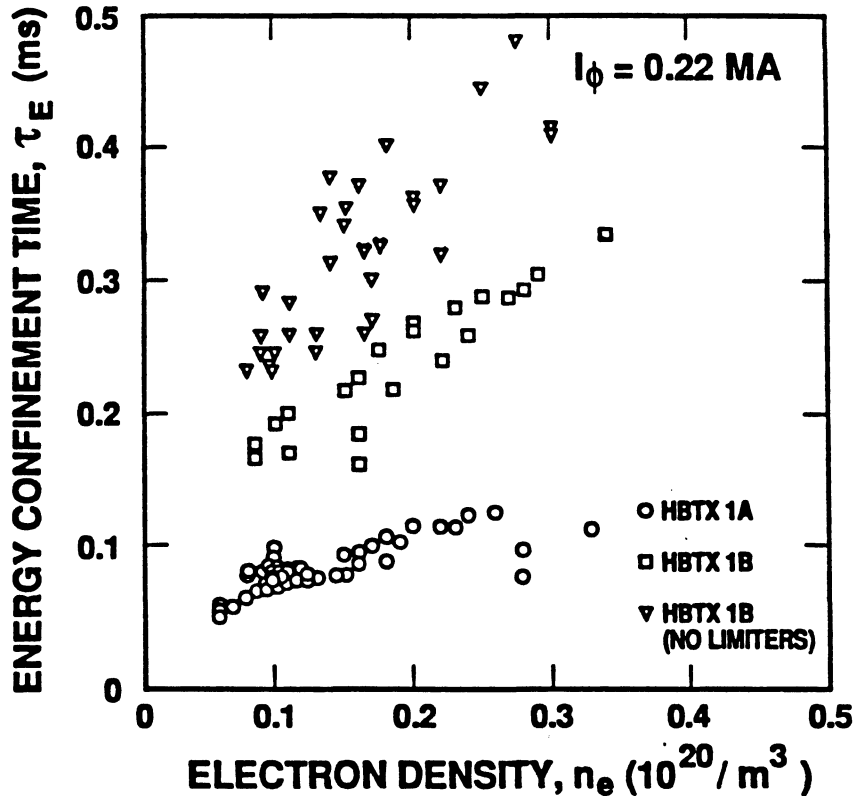


Figure 2.2-9. Impact of field errors and DC vertical field on the energy confinement in the HBTX experiments [12]. Compared to HBTX1A, the field errors in HBTX1B have been reduced by a factor of 15 [0.3% to 0.02%, expressed as a percentage of error flux intersecting the wall relative to $B_\theta(r_p)$].

Inclusion of first-order toroidal effects into the stability analysis leads to the Mercier criterion [32]

$$\frac{r}{4} \left(\frac{1}{q} \frac{dq}{dr} \right)^2 + \frac{2\mu_o}{B_\phi^2} \frac{dp}{dr} (1 - q^2) > 0. \quad (2.2-12)$$

The Mercier criterion indicates that if $q(r) > 1$ everywhere, the system is ideally stable, even without the magnetic shear. This condition is the primary approach to stability used in the tokamak. Physically, the $q > 1$ condition forces the wave length of the potentially unstable $m = 1$ kink mode to exceed the major circumference of the torus, $2\pi R_T$. Since $q < 1$ in RFPs, sufficient shear must be present in order to satisfy the Mercier criterion. Moreover, a pitch minimum (*i.e.*, $dq/dr = 0$) within the plasma must be avoided.

Necessary conditions for stability against ideal-MHD current-driven modes have been derived by Robinson [33] on the basis of the energy principle [30]. The necessary condition

can be expressed as $|P(r_w)| < 3P(0)$, where r_w is the location of the conducting wall. This condition can be approximately expressed as follows:

$$\left(\frac{r_w}{r_p}\right)^2 < 3 \left| \frac{B_\phi(0)}{B_\phi(r_w)} \right|, \quad (2.2-13)$$

$$\Phi > 0, \quad (2.2-14)$$

where Φ is the total toroidal flux inside the conducting wall. These conditions do not include a vacuum boundary and require that both the amplitude and the region of the field reversal not be large.

In summary, the conducting wall should be close to the plasma to stabilize current-driven modes. Furthermore, stability against current-driven modes also excludes a pitch minimum in the plasma. These conditions are usually well satisfied for experimental profiles and are also monitored and satisfied for the profiles calculated for the TITAN designs. The necessary conditions given by Equations 2.2-13 and 2.2-14 are in practice close to being sufficient. Based on ideal-MHD theory, RFP profiles are possible with plasma beta values as high as 0.3. The Taylor theory predicts that all states described by the F - Θ diagram (Figure 2.2-2), including those with $F > 0$, are near-minimum-energy states and, therefore, are stable. Profiles without toroidal-field reversal, however, exhibit pressure-driven and current-driven modes. This conclusion is confirmed experimentally and an example is given in Figure 2.2-10 showing the plasma resistance in the HBTX1A experiment [34] as a function of the pinch parameter; as Θ increases, the resistance falls dramatically, particularly as Θ exceeds the value where the field reversal occurs. For larger values of Θ and $|F|$, the plasma resistance increases again because of enhanced dynamo activity and the appearance of sawtooth-like oscillations in the plasma [35].

The ideal-MHD theory assumes a zero plasma resistivity. This assumption constrains magnetic-field lines to be “frozen” in the plasma, thereby limiting the class of potentially unstable modes. Resistive-MHD stability analysis has to be performed to provide a more realistic picture of the plasma behavior [33]. In general, the criteria for resistive stability are more stringent, and a closer fitting conducting wall and a lower value of β generally result. A detailed analysis of current-driven resistive tearing modes has been made [36] and stable RFP configurations have been found with $\beta \simeq 0.2$. These configurations, however, have been found to be unstable to the so-called resistive g-modes (the “g” is used to emphasize the “gravity” analogy). Moreover, analyses show that resistive g-modes can become unstable for pressure gradients substantially smaller than those needed to drive ideal-MHD instabilities. These resistive g-modes are localized and may ultimately affect the confinement time. In fact, certain theoretical estimates of the confinement time

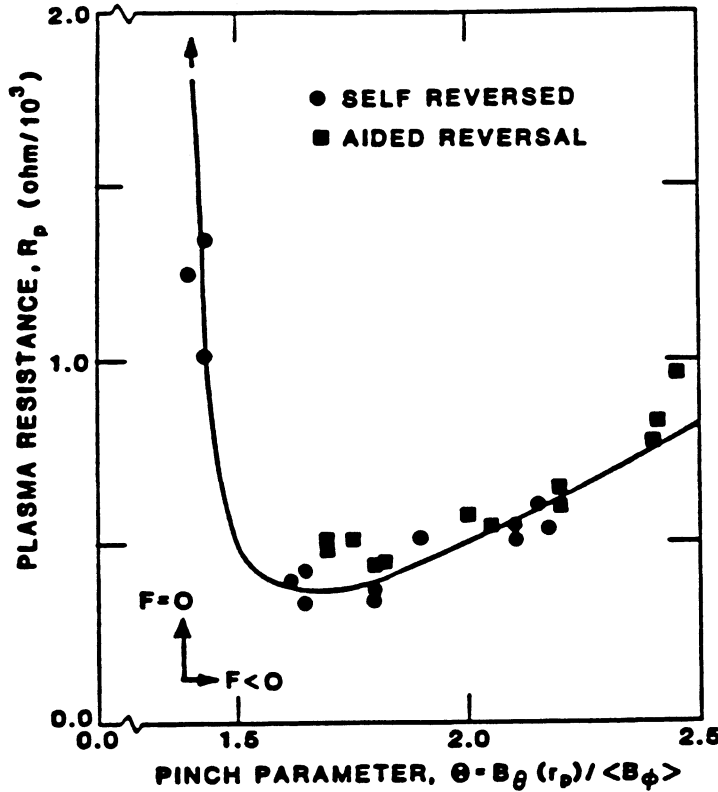


Figure 2.2-10. Plasma resistance in the HBTX1A experiment as a function of the pinch parameter, Θ [34].

have been proposed that are based on transport along stochastic field lines created by resistive g-mode turbulence [37] and are discussed in Section 2.2.5.

The current-driven MHD instabilities have more recently been analyzed for an RFP in contact with a perfectly conducting wall [13], and even more recently for conditions where a vacuum annulus exists between the RFP and the conducting wall [38]. Figure 2.2-11 gives an example of a stability diagram [13,38] for the fastest growing $m = 1$ mode as a function of the μ -profile shape factors, $\mu(0)$ and α , as given in Equation 2.2-4. These analytic results show that a completely stable region exists for ideal and resistive current-driven modes in an RFP over a range of $\Theta \simeq \Theta_o$ and degrees of current-density peaking, and for a range of free-boundary conditions, $\delta_v \simeq (r_w - r_p)/r_p$. Generally, the external $m = 1$ modes do not appear to be significant. These external modes occur for deep-reversal conditions that rarely arise for most experiments and are not of interest for reactors because of cost and technology demands (Section 8). A lower limit on $q(0) A = \Theta_o \geq 2/3$ is identified which weakly depends on the profile exponent α . This

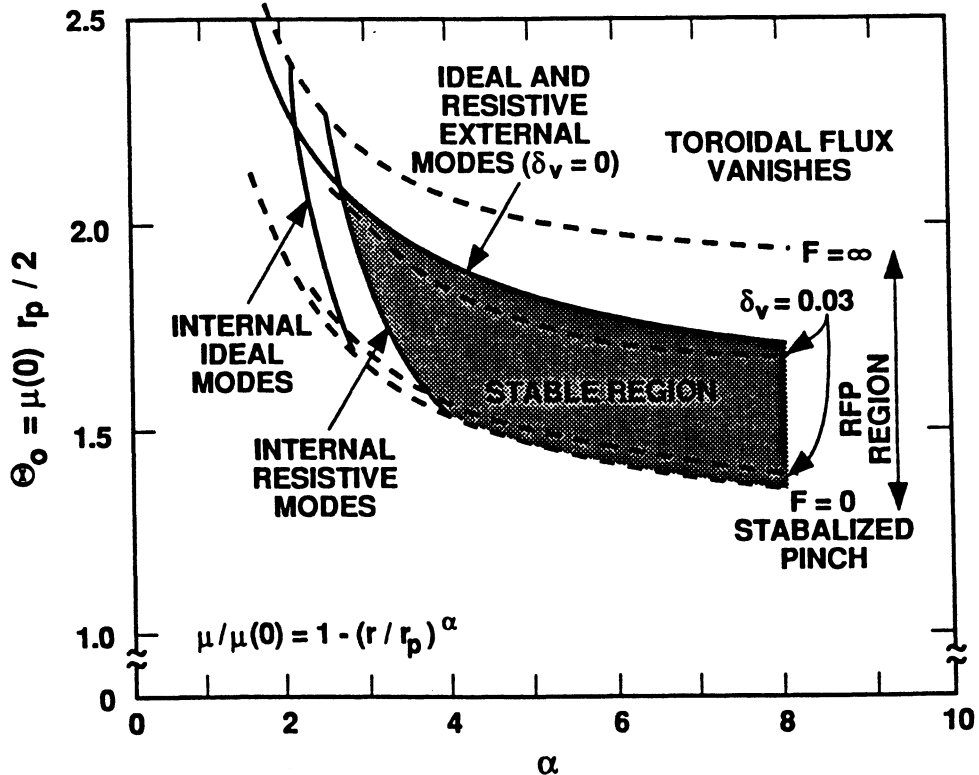


Figure 2.2-11. Stability diagram for $m = 1$ internal (inside reversal layer) and external resistive current-driven modes for an RFP with a vacuum annulus equal to $\delta_v = 0.0$ and 0.3 of the plasma radius [13,38].

lower limit is associated with the internal $m = 1$ resistive mode, and imposes an upper limit on the on-axis current density [13,38] of $j_\phi(0) \leq 3B_\phi(0)/(\mu_0 r_p)$. As noted in Reference [13], resistive diffusion tends to peak the on-axis current, lowering $q(0)$ to below this critical limit and exciting internal current-driven instabilities, redistributing (*i.e.*, flattening) the current-density profile, and recovering the initial configuration that is stable to tearing modes. Hence, the field profiles in RFPs are a result of periodic relaxations that oppose processes related to resistive diffusion; such oscillations around near fields have been observed in a number of large- Θ RFP discharges [39,40].

2.2.4. Relaxation and Sustainment

The RFP magnetic topology is maintained against diffusion by instability-driven fluctuations and described by an evolving series of plasma-configurational relaxations. The theory of relaxed states has successfully predicted the behavior of RFPs in terms of the

characteristics of the F - Θ diagram (Figure 2.2-2). The details of the process of relaxation to near-minimum-energy states are neither invoked nor required in this theory. These details are understood only in the broadest terms, but a complete description is ultimately required to explain and understand the sustainment, stability, and transport in RFPs.

Of particular interest is a more detailed account of RFP profile sustainment. Consider a cylindrically symmetric, resistive plasma with reversed-field profiles, and possibly with anisotropic resistivity. According to Ohm's law, a poloidal electric field, E_θ , corresponding to the poloidal current at the reversal point should exist. To sustain this resistive electric field, Faraday's law requires a resistive decay of the toroidal flux inside the reversal radius. Reversed-field-pinch discharges, however, are maintained for times far longer than the resistive diffusion time with $E_\theta = 0$. A mechanism is necessary to drive the poloidal current at the plasma surface and cancel the resistive electric field at that point. This dynamo mechanism generates a magnetic field that opposes the resistive field diffusion.

Several mechanisms for toroidal-flux regeneration have been proposed, each offering a different explanation for the origin of the poloidal current at the toroidal-field reversal surface. For example, second-order effects of low-level MHD fluctuations resulting from nonlinear evolution of resistive-MHD modes can drive a poloidal current at the reversal surface that is sufficient to sustain the field reversal [41]. Alternatively, a plasma model with stochastic field lines has been proposed, wherein a global rather than a local Ohm's law applies. In this mode, the poloidal current at the reversal surface is driven by electromagnetic fields originating elsewhere in the plasma [26,42 - 44].

In summary, quasi-stationary RFP equilibria are sustained through continuous relaxation and field generation. These time-averaged equilibria are stable to ideal and resistive-tearing modes because the relaxation process acts to maintain the stability. Relaxation and field-generation processes are driven continuously by a complex spectrum of resistive MHD modes and related nonlinear interactions [44]. These processes also involve field-line reconnection and profile modification that can impact the cross-field transport. The plasma confinement and beta, therefore, are intimately related to and affected by the relaxation process [37]. A detailed explanation of the mechanisms that drive the relaxation and dynamo activities in RFPs, however, has yet to be devised. Lastly, resistive g-modes or pressure-driven interchange modes are always unstable for RFP field profiles. These modes, however, are highly localized, should contribute to transport, and in principle should become less a factor in hotter, reactor-grade plasmas with high magnetic Reynolds numbers ($S \equiv \tau_\Omega/\tau_A$, where τ_Ω is the ohmic time and τ_A is the Alfvén time).

2.2.5. Transport and Confinement

Theoretical models for the transport in RFPs based on micro-turbulence have been proposed [45]. A detailed transport model is not yet available for RFPs, however, and the precise scaling of the energy confinement is unknown. Empirical approaches can be used to evaluate present experimental results from ohmically heated RFPs and used to form a basis for the extrapolation of these results to reactor regimes. The details of the transport physics, therefore, are not considered here but instead, experimental observations are used to guide the formulation of a scaling theory. Pressure balance in the RFP (*i.e.*, $p \propto \beta_\theta I_\phi^2/r_p^2$) can be expressed as follows:

$$T = \frac{\mu_o}{16\pi k_B} \left(\frac{I_\phi}{N} \right) \beta_\theta I_\phi, \quad (2.2-15)$$

where $N = n\pi r_p^2$ is the plasma line density and T is the density-weighted plasma temperature. Firstly, Equation 2.2-15 predicts that $T/I_\phi \propto I_\phi/N \simeq \text{constant}$; this behavior is observed experimentally. Secondly, the plasma pressure under certain conditions is found to scale approximately as $I_\phi^{1.7} \rightarrow I_\phi^2$ over a wide range of conditions, indicating an approximately constant β_θ . In fact, experimental evidence exists that RFPs operate near a beta limit; plasma energy transport and loss mechanisms in RFPs appear to self-adjust to lose energy at a rate that is sufficient to maintain β_θ nominally constant (Sections 2.3.5 and 2.3.6). Equation 2.2-15 then suggests that the temperature varies linearly with the current for a fixed value of I_ϕ/N , as has been reported for a number of experiments.

The constant-beta assumption, however, remains an open question, since a strict linear relation between T and I_ϕ is not observed under all RFP experimental conditions. Specifically, evidence is emerging from a number of RFP devices that the average plasma pressure may be scaling with current raised to a power less than two, indicating that under certain conditions β_θ may be decreasing somewhat with plasma current. Interpretation of scaling results from present devices is difficult because of less-than-ideal density control, impurity effects, Z_{eff} , and operation close to or within the electron runaway condition, $\xi = v_D/v_{THE} \propto (I_\phi/N) T_e^{-1/2} \geq 0.1$.

Using the definition of energy confinement derived from the energy balance for a steady-state, ohmically heated discharge, and substituting from Equation 2.2-15 for T , the following expression for τ_B results:

$$\tau_B \equiv \frac{3n k_B T}{\eta j_\phi^2} = \frac{3\mu_o}{16} \frac{\beta_\theta r_p^2}{\eta}, \quad (2.2-16)$$

where $j_\phi \equiv I_\phi / (\pi r_p^2)$ is the plasma current density and η is the plasma electrical resistivity evaluated at the density-weighted average plasma temperature. The plasma resistance measured on a number of RFP experiments over a wide range of parameters is observed to have classical temperature dependence, $\eta \propto T_e^{-3/2}$. Using the assumptions of constant β_θ and linear dependence of T on I_ϕ , the energy confinement time is found to scale with the plasma current according to $\tau_E \propto I_\phi^{3/2} r_p^2$.

Geometrical effects (*i.e.*, spatial dependence of field-line pitch), impurities, and the anomalous resistance associated with the electric fields needed to drive the RFP dynamo must be considered in calculating the plasma resistance. The dynamo represents an added dissipation of the currents and, therefore, appears as a resistivity anomaly. The resistivity in RFP experiments over a wide range of conditions is close to the classical values, taking into account the geometrical and impurity effects. The dissipation associated with the dynamo effect, therefore, is generally small, and the ohmic power delivered to the plasma under optimal conditions is not expected to exceed the classical prediction by a significant amount. At low plasma densities (or high values of I_ϕ/N or streaming parameter, ξ) the resistance-anomaly factor is too high to be explained solely by geometrical or impurity effects.

Theories have been proposed to estimate the energy confinement time associated with the electron parallel-field transport along stochastic magnetic-field lines caused by resistive-fluid turbulence. Turbulence caused by pressure-driven resistive-interchange modes has been considered [37] and gives a diffusion coefficient that scales as follows:

$$D \propto \eta \left(\frac{M}{m} \right)^{1/2} \beta_\theta^2, \quad (2.2-17)$$

where M and m are ion and electron masses, respectively. Using this diffusion coefficient for ohmically heated discharges, the value of beta is found to be $\beta_\theta \equiv (m/M)^{1/6}$ and is independent of machine parameters: the exponent of $1/6$ is a result of assuming a radial temperature profile that scales as $T \propto J_o(\mu r)$. This prediction combined with the pressure balance gives a linear temperature-current scaling, as reported in a number of experiments (Section 2.3.5).

Turbulence associated with resistive-tearing modes has been considered [44] and gives the following scaling:

$$\frac{1}{\beta_\theta} \propto \left(\frac{I_\phi}{N} \right)^{1/3} I_\phi^{1/3} r_p^{1/6}, \quad (2.2-18)$$

$$T \propto I_\phi^{2/3} r_p^{-1/6}. \quad (2.2-19)$$

Another theory based on current-driven drift-wave turbulence [46] gives the following scaling relationships:

$$\frac{1}{\beta_\theta} \propto \left(\frac{I_\phi}{N}\right) I_\phi^{1/7} r_p^{-2/7}, \quad (2.2-20)$$

$$T \propto I_\phi^{6/7} r_p^{-2/7}, \quad (2.2-21)$$

$$\tau_B \propto \left(\frac{I_\phi}{N}\right)^{-1} I_\phi^{8/7} r_p^{9/7}. \quad (2.2-22)$$

This theory predicts a weak dependence of plasma beta on machine parameters and a nearly linear temperature-current dependence. A clear resolution of these various theoretical predictions must await experiments with a broader range of plasma and machine parameters (*e.g.*, plasma current, current density, dimensions) and diagnostics (profiles, Z_{eff}) under a level of density control that is sufficient to eliminate considerations and possible secondary effects of runaway electrons.

2.3. RFP EXPERIMENTS

An important achievement for the RFPs was the discovery in 1965 of a period of improved stability and reduced turbulence on the ZETA device [47]. The quiescent period observed in ZETA was preceded by a turbulent phase with large energy losses and strong plasma-wall interactions. Furthermore, self-reversal of the external toroidal field relative to the on-axis field was observed, but the importance of these observations was not fully appreciated at the time. To reduce energy losses and plasma-wall interactions, experimental RFPs during the 1970s used fast magnetic-field programming with typical rise-times of a few microseconds to force the reversal externally. These experiments required electrically insulated discharge tubes to accommodate the high voltages needed to generate fast-rising magnetic fields. Many important advances in RFP physics were made in these machines, although the reactor relevance of these high-voltage, pulsed devices was minimal.

With experience from fast-programming machines and a general theory of relaxed states [11], modern RFP experiments in the late 1970s and 1980s have returned to slow-rising plasma current (0.1 to 1.0 ms) and the facility for slow B_ϕ control to assist and optimize the self-reversal process and to minimize RFP formation losses. These machines use a metallic liner around the plasma, are equipped with improved vacuum systems, and operate with improved magnetic-field geometry. The first of these modern machines

was ETA-BETA-II at Padova [48-50], which began operation in 1979. Today, high-temperature plasmas are routinely produced in many intermediate-size machines, such as TPE-1R(M) at ETL, Sakura-Mura [51,52], ZT-40M at Los Alamos National Laboratory [15,53,54], HBTX1A at Culham [55,56], and OHTE/RFP at General Atomics [57,58]. General parameters of these more recent RFP experiments are listed in Table 2.3-I. The design parameters of the TITAN reactor are also listed for comparison and Figure 2.3-1 gives a size comparison between existing, planned [24], and conceptual [59] RFP designs.

The plasma parameters obtained in these experiments have been improving steadily. Reactor-relevant values of β_θ in the range 0.1 to 0.2 are routinely achieved (total beta in RFPs is typically 50% of β_θ). Electron temperatures in the range 0.4 to 0.6 keV, densities exceeding 10^{20} m^{-3} , and energy confinement times approaching 1 ms are typical of these intermediate-size experiments. In addition, ion temperatures approaching 1 keV have been achieved under conditions where anomalous ion heating is observed (*i.e.*, high values of I_ϕ/N). Data from a number of machines indicate a nearly linear temperature-current scaling under some conditions, which suggests $\tau_e \propto T_e^{3/2}$. Furthermore, both experimental and theoretical evidence suggest a strong scaling of $n\tau_e$ with the plasma current ($n\tau_e \propto I_\phi^{5/2}$). The scaling of plasma pressure with current suggests $p \propto I_\phi^\nu$, where $\nu \leq 2.0$; the equality indicates a constant- β_θ scaling, although evidence exists for a slow decrease in β_θ with plasma current.

This section presents the experimental data from the key RFP experiments listed in Table 2.3-I with special emphasis on extrapolating the present data base to a reactor-relevant regime. The main scaling parameter is plasma current, I_ϕ , with the larger RFPs ranging almost a factor of 10 in this variable, while the smaller devices vary I_ϕ by only a factor of 2 to 3. As concluded at a recent RFP workshop [60], the overall picture on RFP scaling remains somewhat uncertain, and prediction of performance "...is subject to large errors." Specifically, on the basis of more than 4,000 ZT-40M discharges it was concluded [60] that the available information is "insufficient ... to formulate statistically defensible scaling laws, and that it may be more sensible to compare the data to predictions" at this point in the development of the RFP data base.

Reference [60] summarizes concisely the difficulties at this time in deriving statistically meaningful scaling laws for the present RFP data base; these difficulties are multifold and interconnected, and it is appropriate to list them here as follows:

- Each RFP device is improving performance with time (*e.g.*, reduced field errors, better B_V control, etc.) and, therefore, remains in an optimization process; parameters, consequently, are changing and evolving.

Table 2.3-I.
PARAMETERS OF MAJOR RFP DEVICES

Device	Major Radius	Minor Radius	Plasma Current	Current Density	Electron Temperature	Average Density	Poloidal Beta
	(m)	(m)	(MA)	(MA/m ²)	(keV)	(10 ²⁰ m ⁻³)	
TPE-1RM ^(a)	0.50	0.09	0.13	5.1	0.60	0.3	0.1
ETA-BETA-II ^(b)	0.65	0.125	0.15	3.0	0.08	1.0	0.1
HBTX1A ^(c)	0.80	0.26	0.32	1.5	0.10	0.2	0.05
OHTE/RFP ^(d)	1.24	0.20	0.50	4.5	0.4 - 0.6	0.5 - 3.0	0.1 - 0.2
ZT-40M ^(e)	1.14	0.20	0.44	3.5	0.3 - 0.5	0.4 - 0.9	0.1 - 0.2
RFX ^(f)	2.00	0.48	2.0	2.8	0.5 - 2.0	0.3 - 2.0	0.10
CPRF/ZTH ^(g)	2.40	0.40	4.0	8.0	0.5 - 5.0	0.3 - 5.0	0.10
FTF/RFP ^(h)	1.80	0.30	10.4	37.	10. - 20.	6.0 - 9.0	0.1 - 0.2
TITAN ⁽ⁱ⁾	3.80	0.60	18.2	16.	10. - 20.	9.0	0.2

(a) Existing experiment at ETL, Japan [51,52].

(b) Existing experiment at Padova, Italy [48 - 50].

(c) Existing experiment at Culham, U. K. [55,56].

(d) Existing experiment at General Atomics, U. S. A. [57,58].

(e) Existing experiment at Los Alamos National Laboratory, U. S. A. [53,54].

(f) Planned experiment at Padova, Italy [24].

(g) Planned experiment at Los Alamos National Laboratory, U. S. A. [24].

(h) Conceptual neutron source, a Los Alamos National Laboratory study, U. S. A. [59].

(i) Conceptual reactor design, a UCLA-led multi-institutional study, U. S. A.

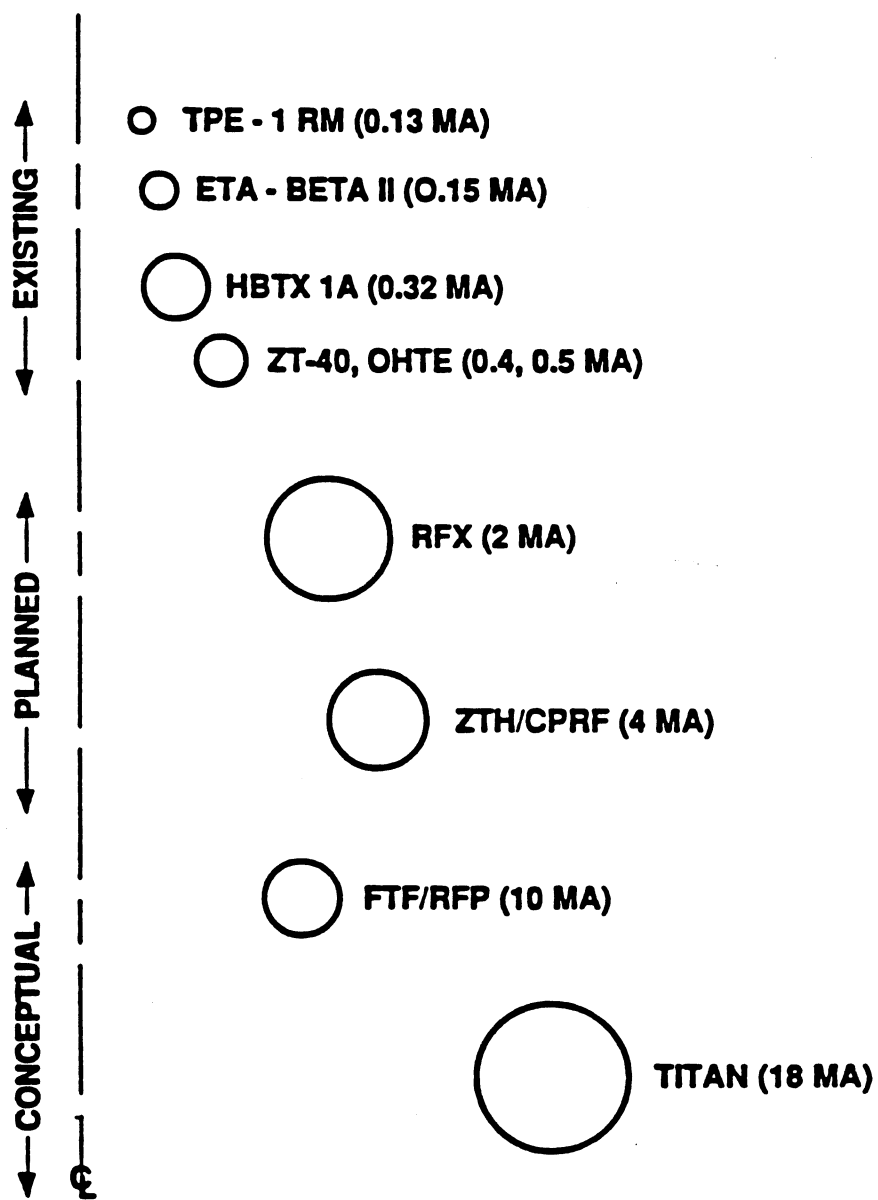


Figure 2.3-1. Comparison of plasma cross sections for present, planned, and conceptual RFP devices of Table 2.3-I.

- Diagnostics generally could be improved in all RFPs (*e.g.*, Z_{eff} , profiles, edge-plasma parameters, ion temperatures).
- Under some conditions, certain parameters presumed to be “independent” can be strongly correlated (*e.g.*, I_ϕ/N or β_θ dependence on I_ϕ).
- Most data bases are not sufficient in size or extent to permit statistically meaningful correlations to be made at this time.
- In addition to a constant improvement in machine parameters with time, sometimes within a given period machine performance is not reproducible, indicating unknown and/or uncontrollable parameter variations.
- Size scaling is highly limited for the existing RFPs with strong difference in field errors, diagnostics, construction, and other factors. It is, therefore, difficult to predict whether key confinement parameters are scaling with I_ϕ , I_ϕ^2/N , j_ϕ , or combinations thereof.

Many of these uncertainties will dissolve with the advent of the next generation of higher-current RFP experiments. The scaling of machine performance with I_ϕ and/or I_ϕ/N given in the following subsections, therefore, should be viewed as a comparison of sample data with the predictions of simplified theory, rather than the presentation of a fully corroborated RFP data base.

This section summarizes the experimental data base as applied to the physics assumed or extrapolated to describe the TITAN reactor. Emphasis is placed on the areas of start-up and formation, confinement, and transport. The status and experience in the areas of density control, highly radiating RFPs, current terminations, and RFP operation with resistive shells are also reviewed.

2.3.1. Start-Up and Formation

The time history of a typical RFP experimental discharge can be divided into three phases: (1) formation phase, (2) sustainment phase, and (3) termination phase. A representative time history of a RFP discharge is shown in Figures 2.2-5 and 2.2-6. The formation phase denotes the time from the start to the peak of the toroidal plasma current. The sequence of events during the formation phase begins by establishing a toroidal magnetic field inside the discharge chamber in the absence of the plasma. At the time of peak toroidal magnetic field, poloidal-field windings are activated to produce a flux

change through the center of the torus and, consequently, a toroidal voltage around the discharge chamber. This voltage typically ionizes the gas in a few microseconds and the toroidal current is initiated in the resulting plasma. The toroidal plasma current and the toroidal magnetic field within the plasma increase while the toroidal magnetic field at the wall decreases, keeping the average toroidal field (and the toroidal flux) in the chamber almost constant. Eventually the toroidal magnetic field at the wall changes sign and is crowbared in the reversed direction relative to the back-biased condition of the formation phase.

The duration of the RFP discharge is extended by using either a passive crowbar applied to the poloidal circuits, to give a decaying waveform, or an active (power) crowbar to produce a flat-top current waveform, as is illustrated in Figure 2.3-2 (upper trace). Figure 2.3-2 also gives the time dependence of plasma density and a soft-X-ray signal, which is measure of plasma temperature. It should be noted that the un-fueled RFP shows a density decrease or "pump-out," as does the tokamak. This pump-out can and must be controlled by wall conditioning in the short term and by gas-puffing, pellet injection, or both in the longer term.

Reversed-field-pinch discharges normally end abruptly and the plasma current decreases rapidly to zero. Accompanying this fast current "termination" is a positive pulse in the toroidal voltage at the liner, as is also shown on Figure 2.3-2. This current termination is in contrast to the negative spike in toroidal voltage that accompanies the current disruption in a tokamak, indicating a difference in the flow of magnetic energy to or from the plasma during the respective events. Furthermore, the RFP current termination can be influenced through the control of the density or toroidal magnetic (reversed) field [61], and in this sense also differs from a tokamak disruption; generally, the RFP terminates only when toroidal-field reversal is lost.

Three modes of operation are generally used for the RFP formation phase: self-reversal, matched, and aided-reversal. In the self-reversal mode, a conducting shell maintains and conserves the toroidal flux inside the chamber. The self-reversal mode of RFP formation is used on OHTE/RFP and often on HBTX1A. In the matched mode, the external circuits are programmed to conserve the toroidal flux inside the chamber by maintaining the poloidal electric field, E_θ , near zero at the liner, thereby, simulating the action of a conducting shell. This mode is usually used on ZT-40M. In the aided-reversal mode, the external circuits supplement the plasma self-reversal effect, as typically used on ETA-BETA-II. Field control during the formation phase provides flexibility in varying the pinch parameter, Θ , on which the configuration depends. The choice of the formation mode also affects the consumption of the poloidal flux during this phase of the RFP

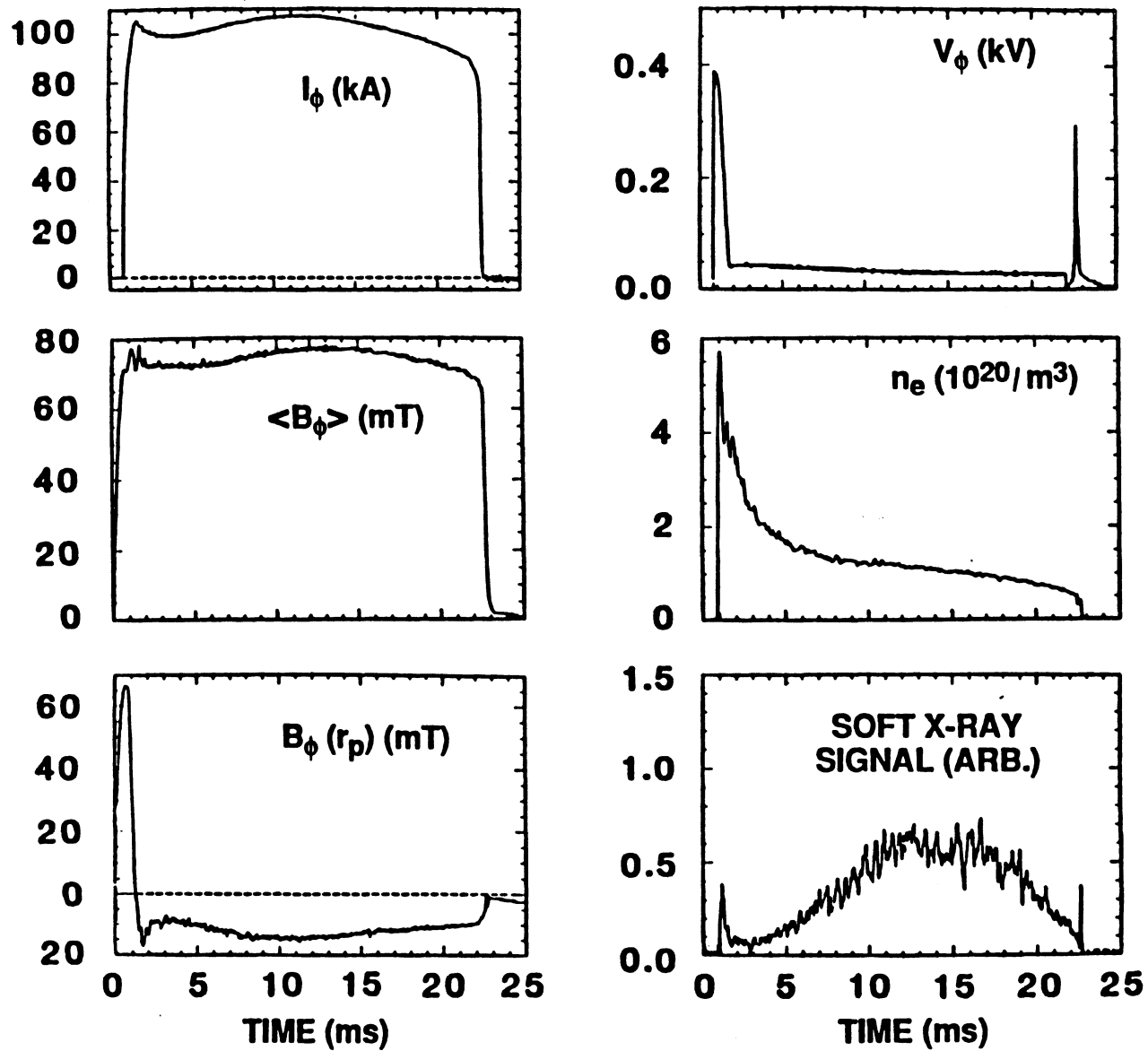


Figure 2.3-2. Typical waveforms for the toroidal current, I_ϕ , average toroidal field, $\langle B_\phi \rangle$, toroidal field at the plasma edge, $B_\phi(r_p)$, loop voltage, V_ϕ , plasma density, n_e , and soft-X-ray signals (measure of plasma temperature).

discharge (Figure 2.3-3). The final plasma parameters, however, are not particularly sensitive to the mode used for RFP formation.

The decrease in plasma resistance (Figure 2.2-10) or loop voltage (Figure 2.3-3) is typical of the attainment of the near-minimum-energy, reduced-turbulence RFP state. For larger values of Θ and deeper reversal, V_ϕ increases (Figure 2.3-3) because of the increased RFP-dynamo activity needed to maintain the larger toroidal fields within the plasma and the associated increase in the fluctuations and sawtooth-like oscillations. Start-up and formation modes, wherein the RFP is programmed to remain at the value of Θ where V_ϕ is minimum (minimum flux consumption), are desirable. This start-up mode has recently been achieved [62]. The ramp-scaling results shown in Figure 2.3-3, however, give a constant voltage, $V_\phi \simeq 32.5$ V, indicating that the plasma resistance, R_p , is decreasing only linearly with current, rather than as $R_p \propto T_e^{-3/2} \propto I_\phi^{-3/2}$.

Similar work on optimizing RFP formation and ramp-up has also been reported for HBTX1B [63], which now uses a matched-mode operation and is attempting to achieve constant- Θ operation. Figure 2.3-4 shows the value of plasma resistance as a function of the current for different start-up methods. The plasma resistance values are inferred from $R_p I_\phi = V_\phi^* + \delta V_\phi$, wherein V_ϕ^* is associated with collisional conductivity and δV_ϕ describes an anomaly, possibly caused by field lines intersecting walls [26,64]. In HBTX1B, $\delta V_\phi \sim 45$ to 55 V, this voltage can be reduced by reducing field errors [63].

Another mode of RFP start-up has been demonstrated on the ZT-40M experiment. This mode is called ramped start-up because the plasma current is slowly ramped to a final value after an initial low-current RFP is formed. Figure 2.2-6(C) shows such a ramped start-up. In a conventional start-up sequence, the peak current is nearly reached at the time the toroidal field at the wall reverses. This start-up mode is undesirable in a large experiment or a reactor because: (1) the RFP formation phase is power intensive until reversal is reached, and (2) large voltages are required. In a ramped start-up, however, the RFP configuration is set up in a relatively short time at a low current and low stored energy; the current is then slowly increased to the desired value while maintaining the RFP profiles. Ramped start-up operation has also recently been reported for the HBTX1B experiment [63].

The ramped start-up scenario relies on the plasma relaxation process. During the current ramp, the toroidal flux must be increased proportionally to the current to maintain the RFP profiles while holding F and Θ constant. This process requires the generation of toroidal flux by the RFP dynamo, since the toroidal field at the wall is negative while the average toroidal flux within the conducting shell is positive. The plasma must generate an equal and opposite amount of negative and positive flux to satisfy Faraday's

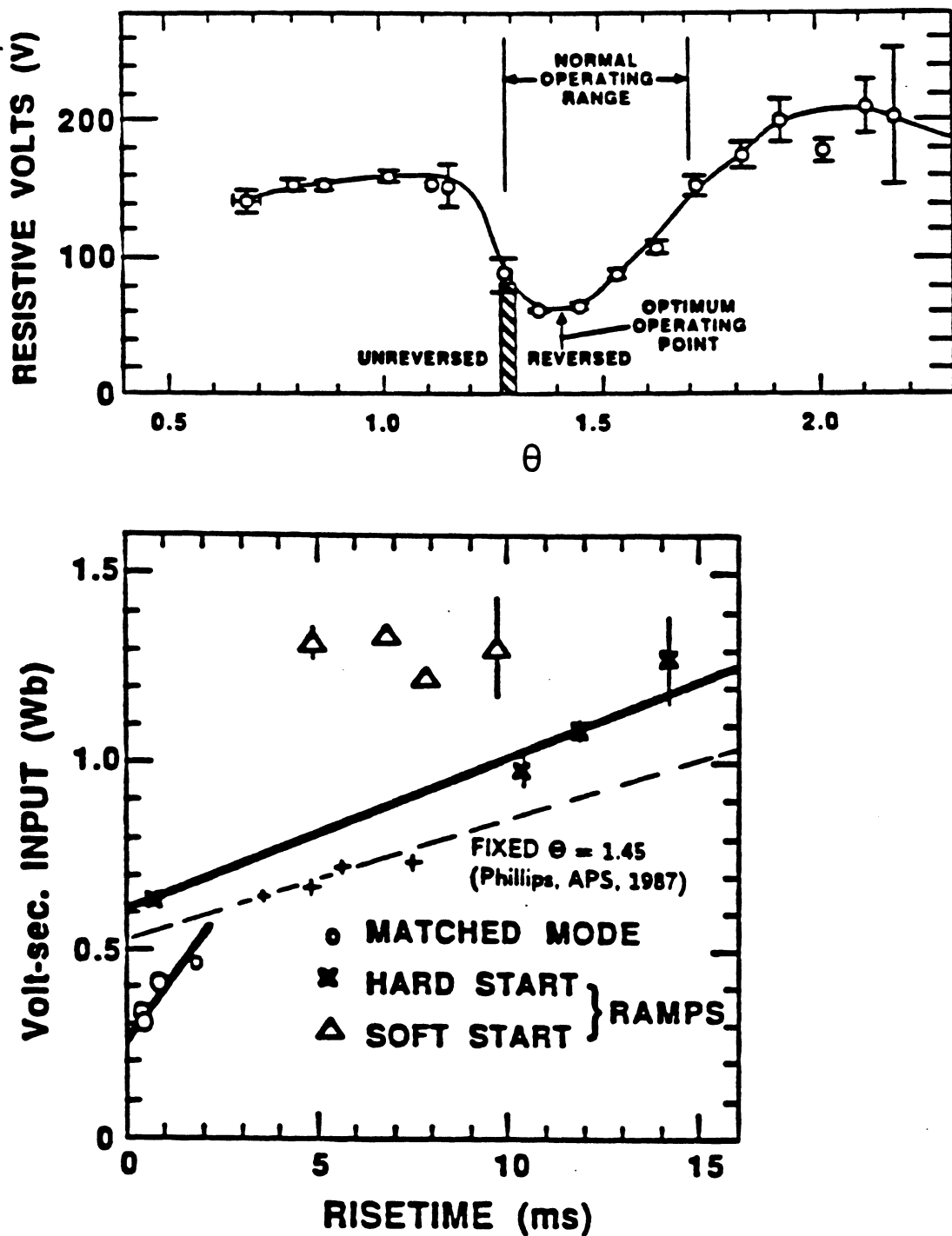


Figure 2.3-3. Dependence of loop voltage on pinch parameter, Θ , and flux consumption on current rise-time for ZT-40 [14,62].

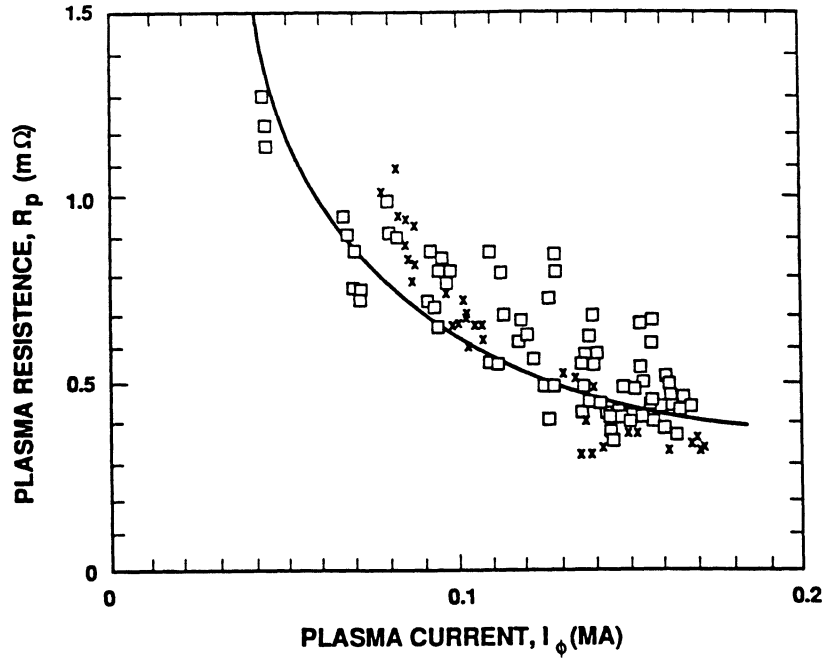


Figure 2.3-4. Plasma resistance as a function of the current in HBTX1B [63] for ramped (squares) and flat-top (x) discharges.

law and then expel the negative flux from the plasma to generate a net positive flux increase. Indeed, the ramped discharges show that toroidal flux (Figure 2.2-6) continues to be generated, and negative flux is expelled from the plasma; this process occurs on a multi-millisecond time scale.

The TITAN reactor design relies on a rapid formation of a “seed” RFP followed by a slow plasma current ramp to the final value (Section 6). Special attention is given to the RFP formation phase. Experimental results point to an RFP formation “window” in the parameter space constrained by the volt-second requirement (i.e., poloidal-flux consumption), equilibrium and field-error constraints, plasma density, current-density, etc. For example [65], the dependence of RFP formation on density and initial bias field is shown in Figure 2.3-5 for ZT-40M and is extrapolated to define a formation window for the reactor. Other constraints imposed on the RFP formation include the relationship between the initial bias toroidal field ($B_{\phi 0}$) and the average toroidal field ($\langle B_\phi \rangle$) and the value of I_ϕ/N upon formation. Figure 2.3-6 gives the relationship between $B_{\phi 0}$ and $\langle B_\phi \rangle$ derived from ZT-40M [65]. The dependence of the radiation burn-through and reduced loop voltage on I_ϕ/N for the ETA-BETA-II experiment is shown in Figure 2.3-7.

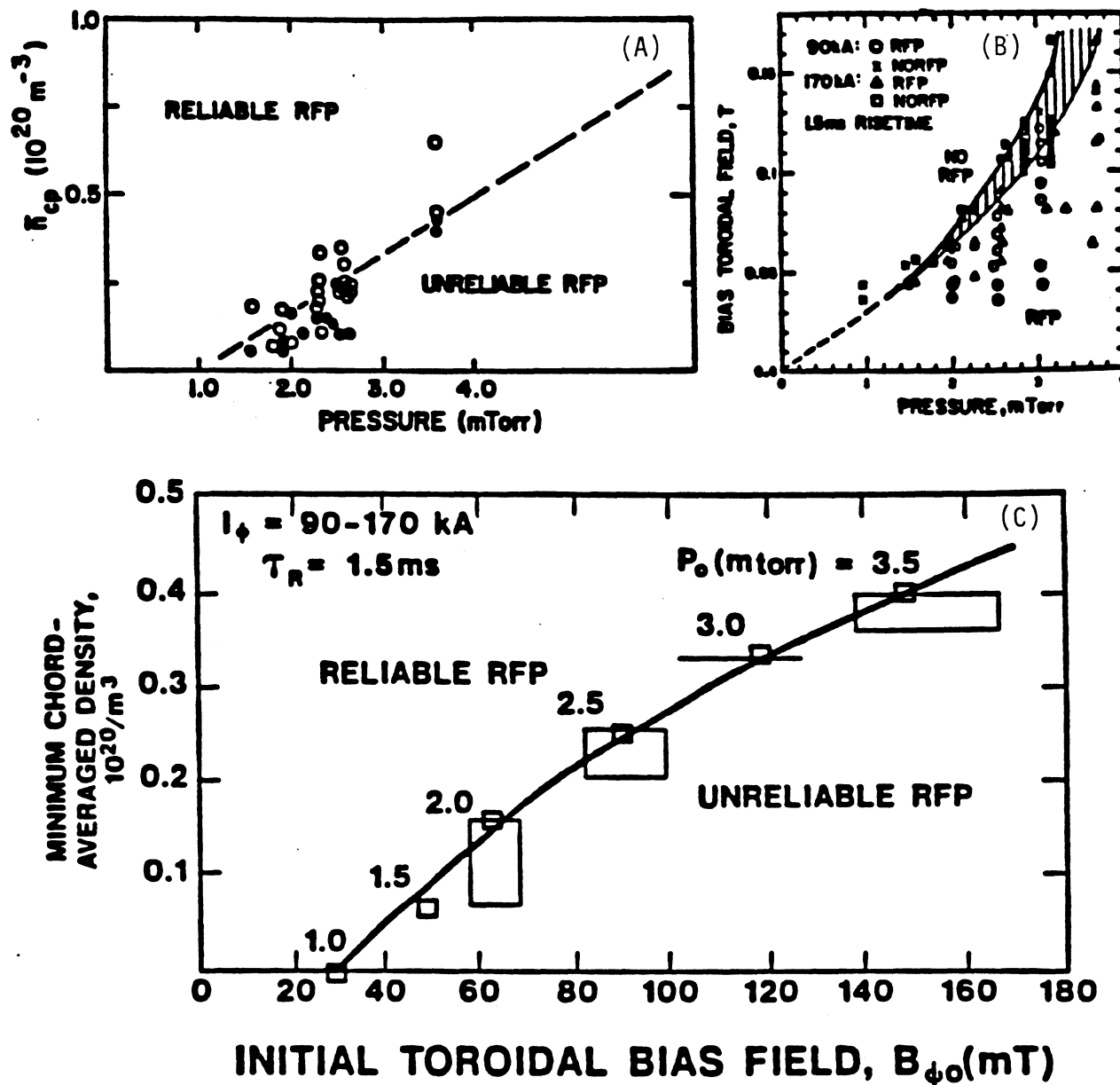


Figure 2.3-5. Typical RFP formation windows showing: (A) dependence on a critical plasma density, (B) magnitude of the original toroidal bias field, and (C) a combination of the two constraints.

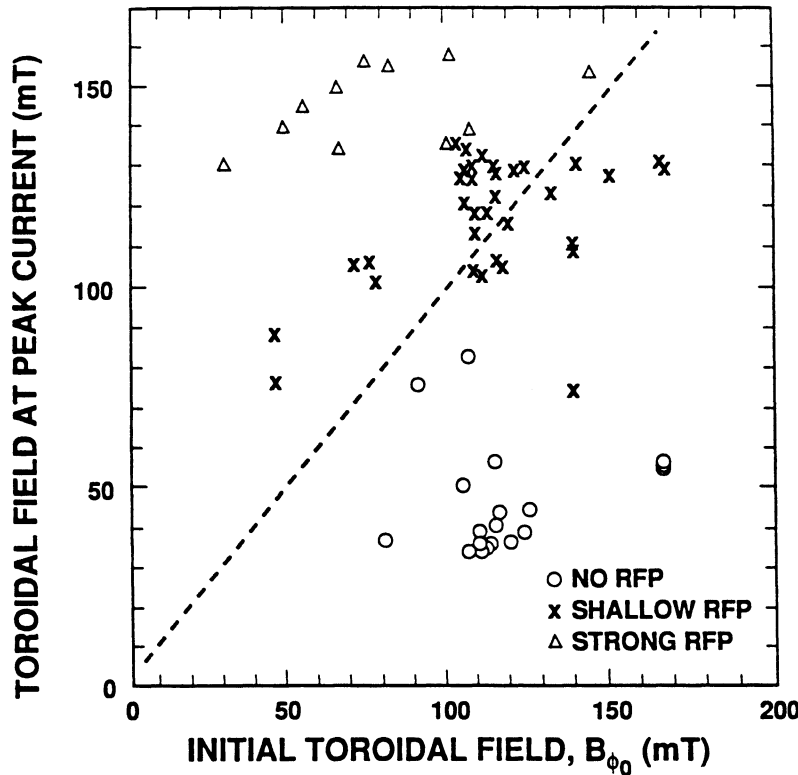


Figure 2.3-6. Relationship between B_{ϕ_0} and $\langle B_{\phi} \rangle$ for a range of ZT-40M discharges [65] where robust RFP formation occurred, as well as no RFP formation as very shallow, spheromak-like RFP were formed.

2.3.2. Typical Temperature and Density Responses

The time variation of the temperature from several machines is shown in Figure 2.3-8. For discharges with a flat-top current waveform (Figure 2.3-8) the electron temperature, T_e , rises rapidly, reaching approximately 100 to 200 eV near the time of peak current. Then T_e increases more slowly as the density drops, ultimately reaching values in the range of 300 to 500 eV. At later times during the discharge, the temperature remains approximately constant or decreases slightly. This latter behavior is attributed to wall effects, possibly caused by field errors or inadequate equilibrium control. Similar behavior of the electron temperature is seen on smaller devices, as is illustrated in Figure 2.3-8 for ETA-BETA-II, where the time scale is much shorter and T_e rises continuously during the pulse. The data from ZT-40M in Figure 2.3-8 shows that the temperature increases with increasing plasma current. Similar behavior is generally observed in all RFP experiments.

The ion temperature, T_i , is usually comparable to the electron temperature, but in certain cases $T_i > T_e$. Figure 2.3-8 also shows the time variation of the ion temperature

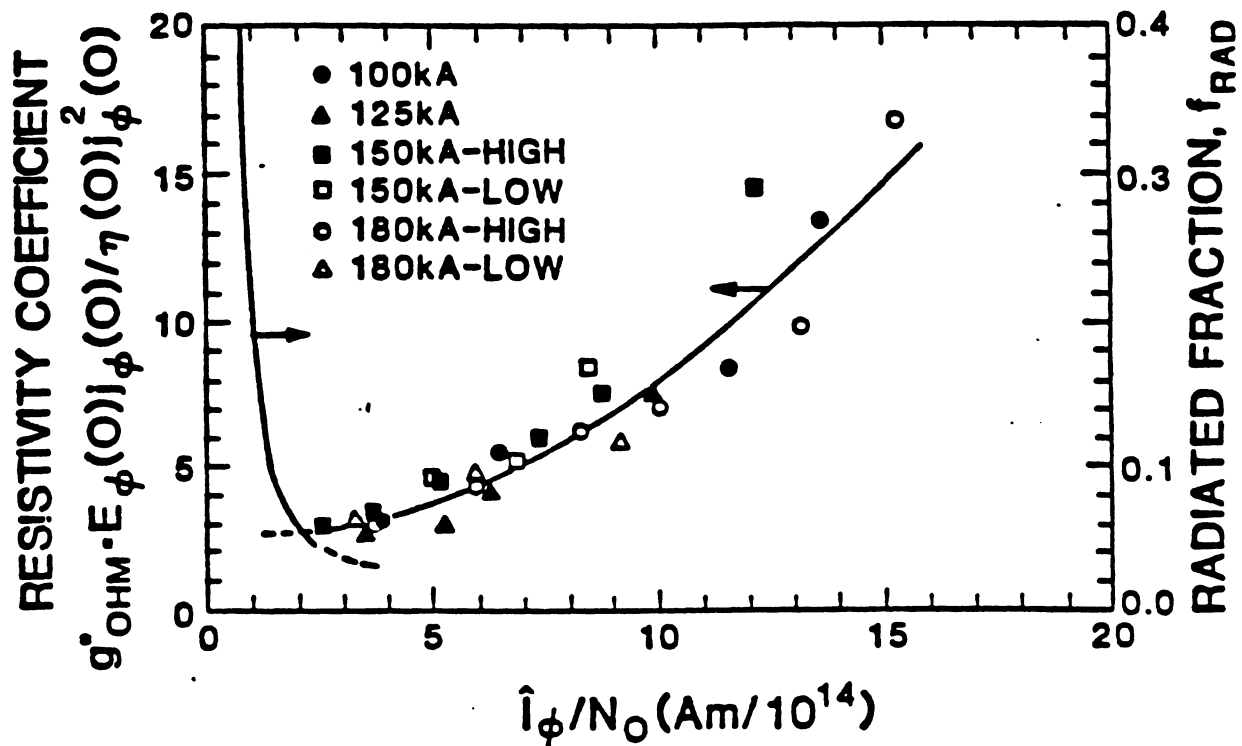


Figure 2.3-7. Dependence of burn-through and reduced-resistance constraints on \hat{I}_ϕ / N_o for the ETA-BETA-II RFP, where \hat{I}_ϕ is the peak current and $N_o = n_o \pi r_p^2$ is the initial filling pressure.

in TPE-1R(M). The electron-ion equilibration time is sufficiently long that the ions cannot be heated by collisions with electrons during the discharge, and some anomalous ion heating mechanism is apparent.

2.3.3. Density Control

Generally, RFP experiments operate without active refueling. The chamber is filled with gas prior to the discharge, and density is maintained by recycling with the chamber walls. Modern RFP discharges are of sufficient duration where active refueling by pellet injection has been used [16,66 - 68] (0.5- to 2.0-mm radius pellets injected at speeds of 1 to 1.5 km/s). Figure 2.3-9 shows the temporal variation of plasma density without pellet fueling. Typically, the electron density rises initially to a value corresponding to the filling density and then falls rapidly to 10% to 20% of the filling value during the formation phase. After this initial pump-out phase, the density decays more slowly. In

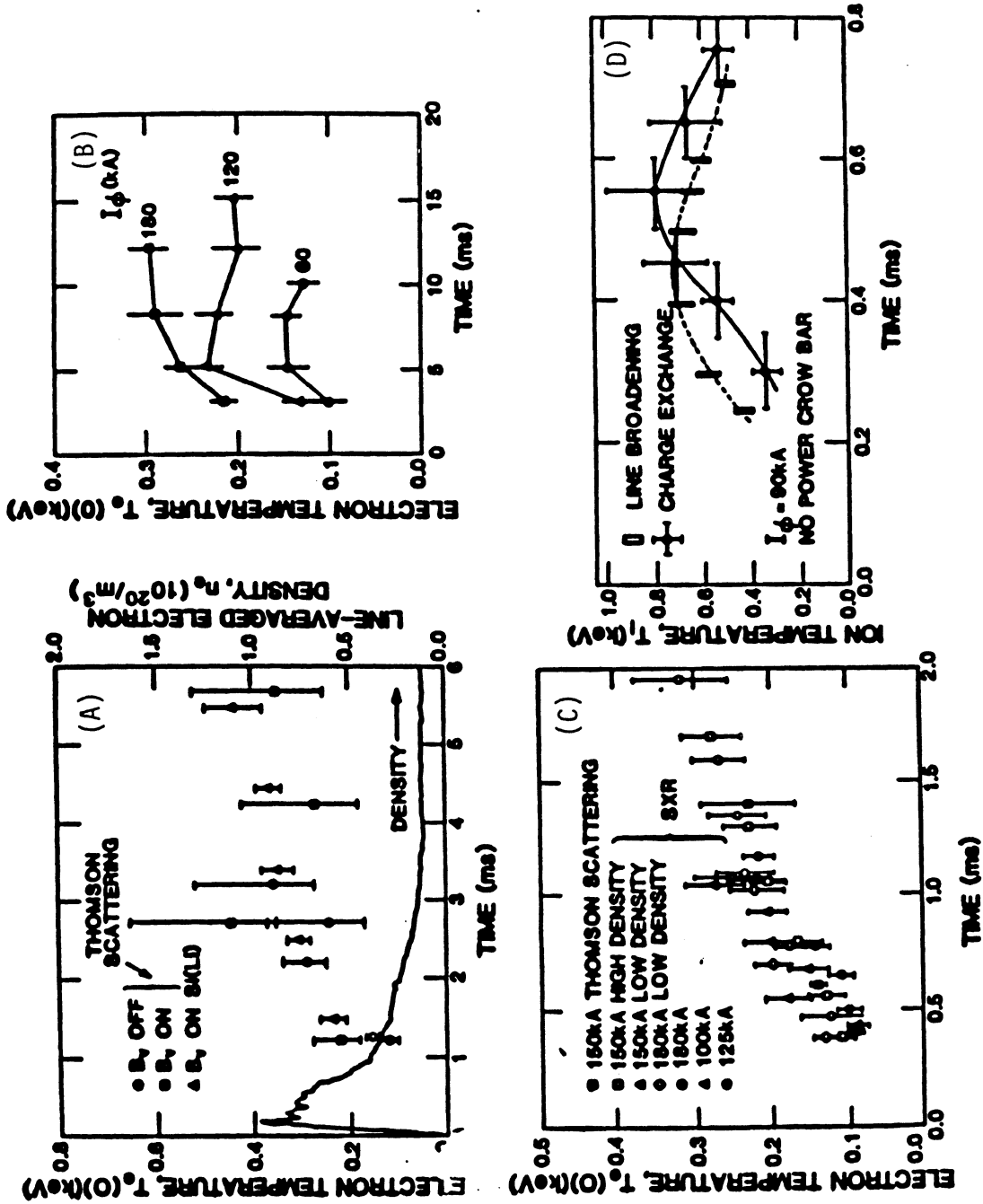


Figure 2.3-8. Time dependence of electron temperature for HBTX1A (A), ZT-40M (B), and ETA-BETA-II (C), and ion temperature for TPE-1R(M) (D).

long-pulsed devices, the density tends to reach a steady-state value that shows little dependence on the initial filling density, but some dependence on the plasma current and on the wall conditioning is observed.

The rate of intial pump-out depends strongly on the wall condition and is attributed to particles that leave the discharge and are not replaced sufficiently fast by wall recycling. This process can be affected by preconditioning the wall through pulsed discharge cleaning (PDC). In fact, by operating the PDC cycle at varying filling pressures a varying amount of hydrogen is “preloaded” into the vacuum-vessel wall and subsequently changes the plasma density as this gas is “unloaded” by subsequent plasma-wall interactions. In the HBTX1B and ZT-40M experiments shown on Figure 2.3-9, the walls were loaded with hydrogen or deuterium prior to the discharge initiation. The results show that the density decay can be reduced considerably, and the density is sustained approximately constant for up to 5 ms or longer without active refueling.

Gas-puffing through external fast-acting valves has been performed on both HBTX1A and ZT-40M. The gas valves inject a steady stream of gas for a preprogrammed portion of discharge. In these experiments, gas-puffing raised the density by at least a factor of two and also increased the duration of the current pulse. The electron temperature, however, decreased when the density was increased. Because gas-puffing often changes the equilibrium at a faster rate than can be controloed by the feedback systems presently used on these experiments, additional gas-puffing experiments await better equilibrium control.

Figure 2.3-10 gives the density response to the injection of four hydrogen pellets in ZT-40M discharges with $I_\phi = 120$ and 180 kA [66]. A single deuterium pellet has also been injected into the ETA-BETA-II experiment [68]. The strong poloidal currents flowing in the outer regions of the RFP cause substantial deflection of the pellet in the poloidal and toroidal directions because of the asymmetry of ablation driven by electrons streaming along field lines. On-axis density peaking was achieved, however, by off-axis injection to compensate for this ablation-driven deflection [67].

Pellet injection increases the density, but the temperature of both electrons and ions decrease in a way that holds β_θ approximately constant. Typically, ion temperature is 200 to 250 eV prior to the injection, decreases to 90 to 100 eV after the injection, and then recovers to ~ 200 eV on a 1 to 2 ms time scale. For the $I_\phi = 120$ -kA discharge on ZT-40M, the edge-chordal density rises higher and more rapidly than the central-chordal density. The pellet deposition appears to be more central for the $I_\phi = 180$ -kA discharges. Because of the large size of the pellet and the shortness of the discharge in the single-pellet injection experiments on ETA-BETA-II [68], the pellet is not fully consumed and

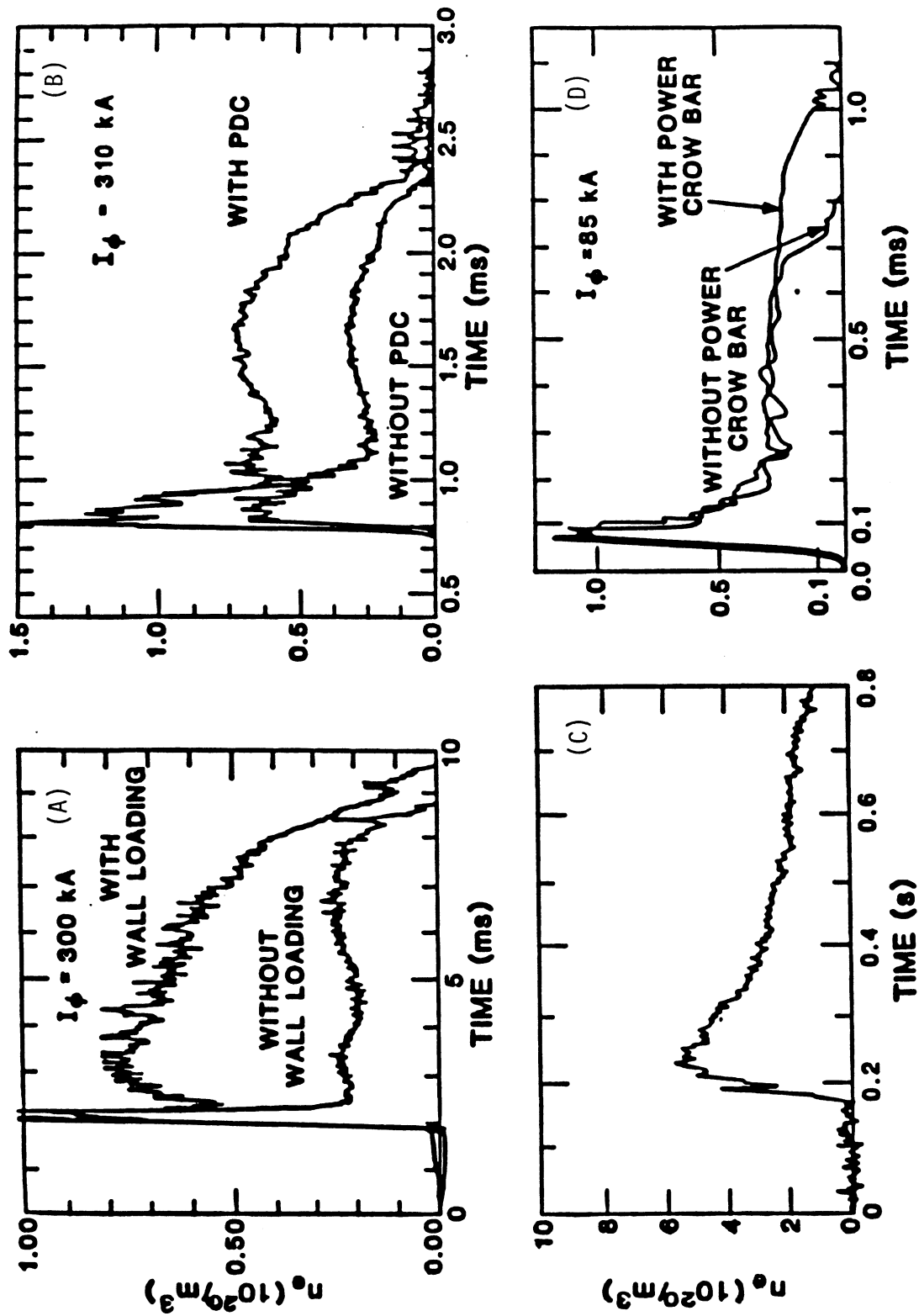


Figure 2.3-9. Time dependence of plasma density for HBTX1B (A), ZT-40M (B), ETA-BETA-II (C), and TPE-1R(M) (D).

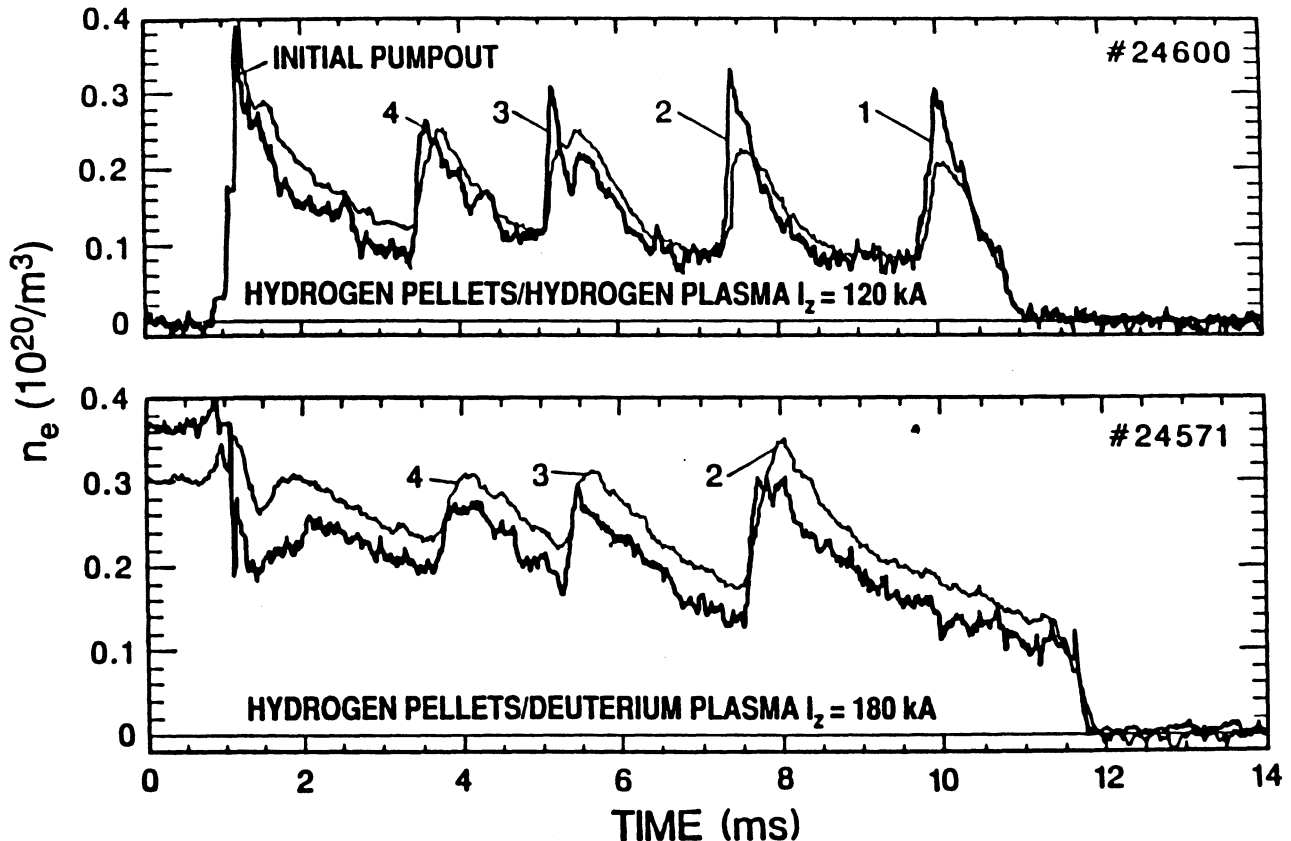


Figure 2.3-10. Density response in ZT-40M along a central chord (dark line) and an edge-plasma chord to the injection of four hydrogen pellets into $I_\phi = 120$ and 180-kA discharges.

the significant increase in density accompanying pellet injection is maintained throughout the discharge. In experiments on ETA-BETA-II, pellet injection is accompanied by a decrease in $T_e(0)$, similar to the ZT-40M experiments, but instead of constant beta, the ETA-BETA-II experiment indicates a slight increase in β_θ .

2.3.4. Plasma Fluctuations

The RFP is intrinsically turbulent since, according to Figure 2.2-7, many unstable, helically coupled MHD modes simultaneously reside in the plasma. Fluctuations of MHD origin are thought to be important for toroidal-field generation and sustainment. Fluctuations can also enhance cross-field transport because of the breakup of the magnetic surfaces and the resulting ergodic field-line behavior. Field and density fluctuations have been studied primarily on the HBTX and ETA-BETA-II experiments [69 - 73]. Measurements of magnetic-field fluctuations in HBTX1A, for example, indicate dominant global

modes with $m = 1$ and a broad spectrum in toroidal mode number centered around $n = -8$, corresponding to the aspect ratio of the device. The minus sign in the toroidal mode number indicates that these modes are resonant inside the reversal surface. Fine-scale activity with a short transverse correlation length, containing comparable power to the global modes, was also found in the core of the discharge. Modes with $m = 0$ and small toroidal mode numbers were also observed. These dominant modes were observed throughout the discharge, including the formation phase where the amplitude was a factor 5 to 10 times higher. These oscillations, therefore, appear to play a fundamental role in maintaining the RFP configuration.

More recent studies of magnetic fluctuations in HBTX1B [73] normal discharges ($\Theta = 1.4$, $F = -0.1$) indicate modes with $m < 2$ and $|n| < 6, 10, 13$, and 16 that are resonant inside the reversal surface. Magnitude of the magnetic-field fluctuations at edge-plasma is $\tilde{B}/B \simeq 0.01$ to 0.02, with toroidal fluctuations dominating the poloidal component by a factor of 3 to 5 and the power being concentrated at frequencies below 150 kHz. Deep reversal discharges on HBTX1B give field-fluctuation amplitudes of 5% to 10%, with the toroidal component being larger than the poloidal fluctuations by only a factor of 2 to 3.

In contrast to HBTX1A, coherent quasi-continuous $m = 1$ activity in the center of the plasma was observed to dominate in low- Θ discharges in ZT-40M [75]. The $m = 1$ modes were consistent with the predictions of the resistive instability theory. Estimates of the width and separation of magnetic islands resulting from the $m = 1$ modes indicate that the field lines are stochastic inside the reversal surface, and probably throughout the plasma when the $m = 0$ modes are taken into account. Qualitative estimates of the energy confinement time based on stochastic field-line diffusion from the $m = 1$ modes are similar in magnitude to those observed on HBTX1A.

Density fluctuations driven by pellet injection on ETA-BETA-II [68] were reported [74] to be $\tilde{B}/B = 0.01$ to 0.02. These density fluctuations are poorly correlated with fluctuations of other quantities such as fields, D_α signals, etc.

The level of magnetic-field fluctuations in RFPs is about $\tilde{B}/B \simeq 0.01$, which is approximately 10 or more times greater than the fluctuations typically observed in tokamaks. The magnetic-field fluctuation levels are observed to decrease with increasing plasma current or magnetic Reynolds number, $S \equiv \tau_\Omega/\tau_A$, where τ_Ω and τ_A are, respectively, the plasma resistive and Alfvén times. This behavior is shown in Figure 2.3-11 for OHTE/RFP, where fluctuation levels appear to decrease as $S^{-1/2}$. Similar behavior is also reported for ETA-BETA-II [76].

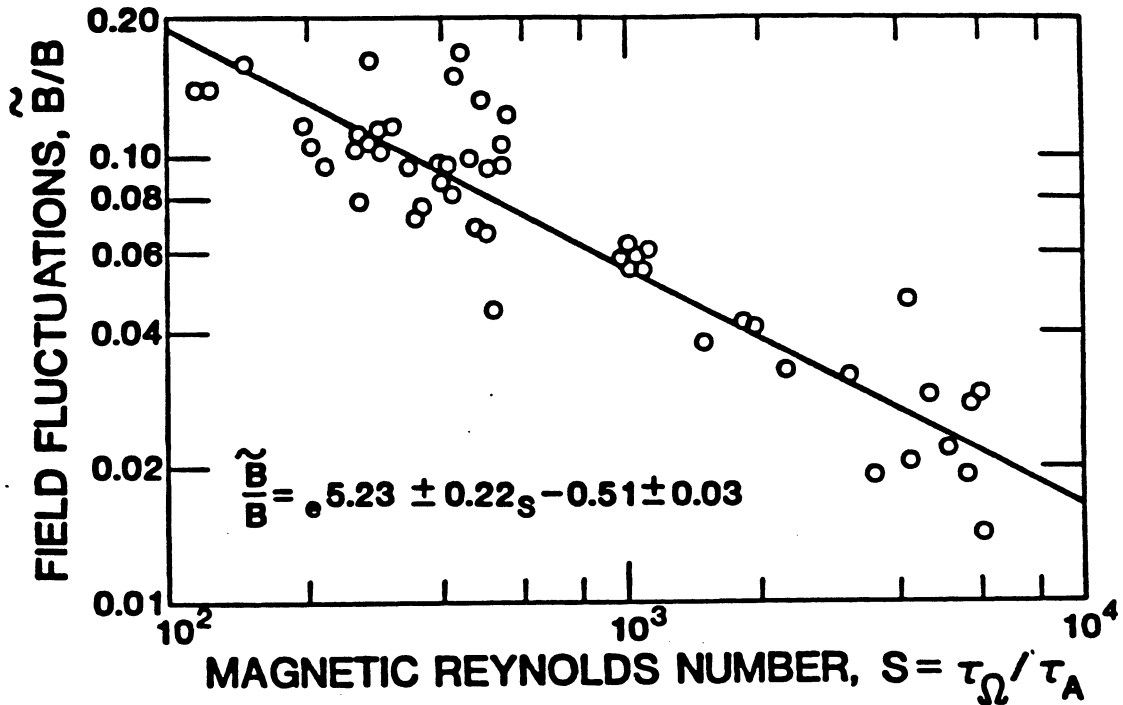


Figure 2.3-11. Magnetic-fluctuation amplitude as a function of magnetic Reynolds number for the OHTE/RFP device, where the plasma resistive and Alfvén times are τ_Ω and τ_A , respectively.

The cross-field transport caused by stochastic field-line diffusion corresponds to the correlation of fluctuations with S , given in Figure 2.3-11. This correlation gives a favorable temperature-current scaling that is consistent with the observed linear dependence of electron temperature on plasma current. Since the RFP dynamo is thought to be closely associated with MHD-driven fluctuations related to the simultaneous admission of many instabilities into the plasma, some concern arises as to the ability of the dynamo to maintain the minimum-energy state if the RFP becomes too quiescent in the high- S reactor regime.

2.3.5. Scaling

The experimental determination of the dependence of plasma resistance, density and temperature (pressure and beta), and confinement time as size and current is the main means by which present-day RFPs provide “scaling” to the next experiment [24], ignition devices [59], and the reactor. Since stability, transport, confinement, and heating are closely related in RFPs (or any ohmically heated device for that matter), the scaling

of each of these phenomena is closely coupled and interdependent. Recognizing this interdependence, the experimental status of RFP scaling is summarized here in a format that divides according to (1) plasma resistance, (2) density and temperature (pressure and beta), and (3) confinement time. In summarizing these results it should be emphasized that experimentally reported densities and temperatures generally refer to line-averaged and centerline values, respectively, with n referring to the volume-averaged density and $T_{e,i}$ being the density-weighted volume average for the TITAN study.

It is recalled (Equation 2.2-15) that expressing the pressure balance in terms of a poloidal beta and setting $T_e = T_i \equiv T$ leads to

$$T = \frac{\mu_0}{16\pi k_B} \beta_\theta I_\phi \left(\frac{I_\phi}{N} \right), \quad (2.3-1)$$

where $N \equiv n\pi r_p^2$ is the line density and the ratio $I_\phi/N = j_\phi/n$ is related to the electron streaming parameter, ξ :

$$\xi = \frac{v_D}{v_{THE}} = \left(\frac{10^6 m_e}{k_B^3} \right)^{1/2} \left(\frac{j_\phi}{n_e} \right) T_e^{-1/2}, \quad (2.3-2)$$

where $\xi \geq 0.1$ for the present experiment and $\xi \leq 0.004$ for the TITAN reactor designs.

Using the definition of energy confinement time in an ohmically heated plasma given by Equation 2.2-16 and defining the thermal diffusivity as $\chi_B \equiv (3/16) r_p^2 / \tau_B$ lead to

$$\chi_B = g_{OHM} \frac{\eta}{\mu_0 \beta_\theta}, \quad (2.3-3)$$

where $\eta \simeq 1.65 \times 10^{-9} Z_{eff} T_e^{-3/2} \ln \Lambda$ is the Spitzer resistivity. The composite profile factor, g_{OHM} , includes both density and temperature profiles as well as the average effects of the magnet-field “screw-up” factor which is larger for RFPs.

Equation 2.3-1 suggests that if β_θ , I_ϕ/N , and $T(0)/T$ are constants, then $T(0) \propto I_\phi$. Furthermore, if η scales classically with temperature and g_{OHM} and Z_{eff} are constant, then $\eta \propto I_\phi^{-3/2}$. Unfortunately, the scaling data base described below contains some uncertainty and diffusiveness because of the variability of profiles (*i.e.*, either g_{OHM} or $T(0)/T$), Z_{eff} , the contribution from locally nonclassical resistivities, and the relatively high value of ξ and the potential for significant runaway electron populations, at least through the latter stages of a given discharge (*i.e.*, n decreasing because of pump-out). The general trends suggested by the purely classical scaling described in Equations 2.3-1 and 2.3-3, however, are generally substantiated by experiment and serve as the primary basis from which the TITAN physics performance is extrapolated. It should be noted that profiles and Z_{eff} can vary with current, and this variation can significantly impact the measured dependence of T or τ_B on I_ϕ .

2.3.5.1. Resistance scaling

The decrease in plasma resistance, R_p , with current for HBTX1B was shown in Figure 2.3-4. Figure 2.3-12 illustrates a similar behavior for OHTE/RFP indicating $R_p \propto I_\phi^{-\nu}$, where $\nu \simeq 1$ to 1.5. Figure 2.3-13 gives the dependence of R_p on $T_e(0)$ for ZT-40M, with $R_p \propto T_e^{-\nu}$ and $\nu \simeq 1$ to 1.5 being indicated. Noting the validity of the above-mentioned assumptions leading to the $T_e \propto I_\phi$ prediction, these data indicated a Spitzer-like temperature dependence of R_p . The $R_p \propto T_e^{-3/2}$ curve in Figure 2.3-13 correlates with a value of $[T(0)/T]^{3/2} Z_{eff} g_{OHM} = 23.3$ which for $T(0)/T \simeq 2$ results in $Z_{eff} g_{OHM} = 8.2$. The profile factor g_{OHM} is expected to range from 2.9 to 5.1, respectively, for the profile used for TITAN (Equation 2.2-4 with $\alpha = 8$) and BFM. Hence, the data in Figure 2.3-13 match the Spitzer resistivity for Z_{eff} values in the range of 1.6 to 2.8.

Although this scaling of resistance with temperature, and indirectly with current, is favorable, the ZT-40M results for ramped discharge given in Figure 2.3-3 are less optimistic (*i.e.*, $R_p I_\phi \simeq 32.5$) and need further resolution. The sensitivity of R_p to field errors (Figure 2.2-9) and equilibrium shifts (Figure 2.2-8), and general edge-plasma conditions are also noted. Generally, the scaling of plasma resistance and/or loop voltage represents the most near-term, premier issue for RFPs, closely followed by and related to confinement of hot plasma (β_θ) and transport (χ_s).

2.3.5.2. Density and temperature (β_θ) scaling

All major RFP experiments show an increase in confinement plasma pressure with increased current and a general tendency for β_θ (Equation 2.3-1) to be constant or possibly to decrease slightly with current. It should be noted that the experimental values of β_θ generally refer to the average density, but the on-axis electron temperature, $T_e(0)$, is used. Hence, decreases in this experimental β_θ with current can also reflect changes in $T(0)/T$, as well as T_e/T_i which is assumed generally to be unity.

Figure 2.3-14 gives the results of a two-point electron-temperature measurement on ZT-40M, where I_ϕ was held fixed at 0.3 MA and the filling pressure, P_o , was varied to give the desired variation in n and I_ϕ/N . These data illustrate the general trade-off of density with temperature at the most basic experimental level. Figure 2.3-15 gives the variation of central electron temperature, $T_e(0)$, and density, $n_e(0)$, with plasma current for the OHTE/RFP device. A similar data correlation from the TPE-1R(M) experiment is given in Figure 2.3-16. Figure 2.3-17 gives the variation of the on-axis temperature

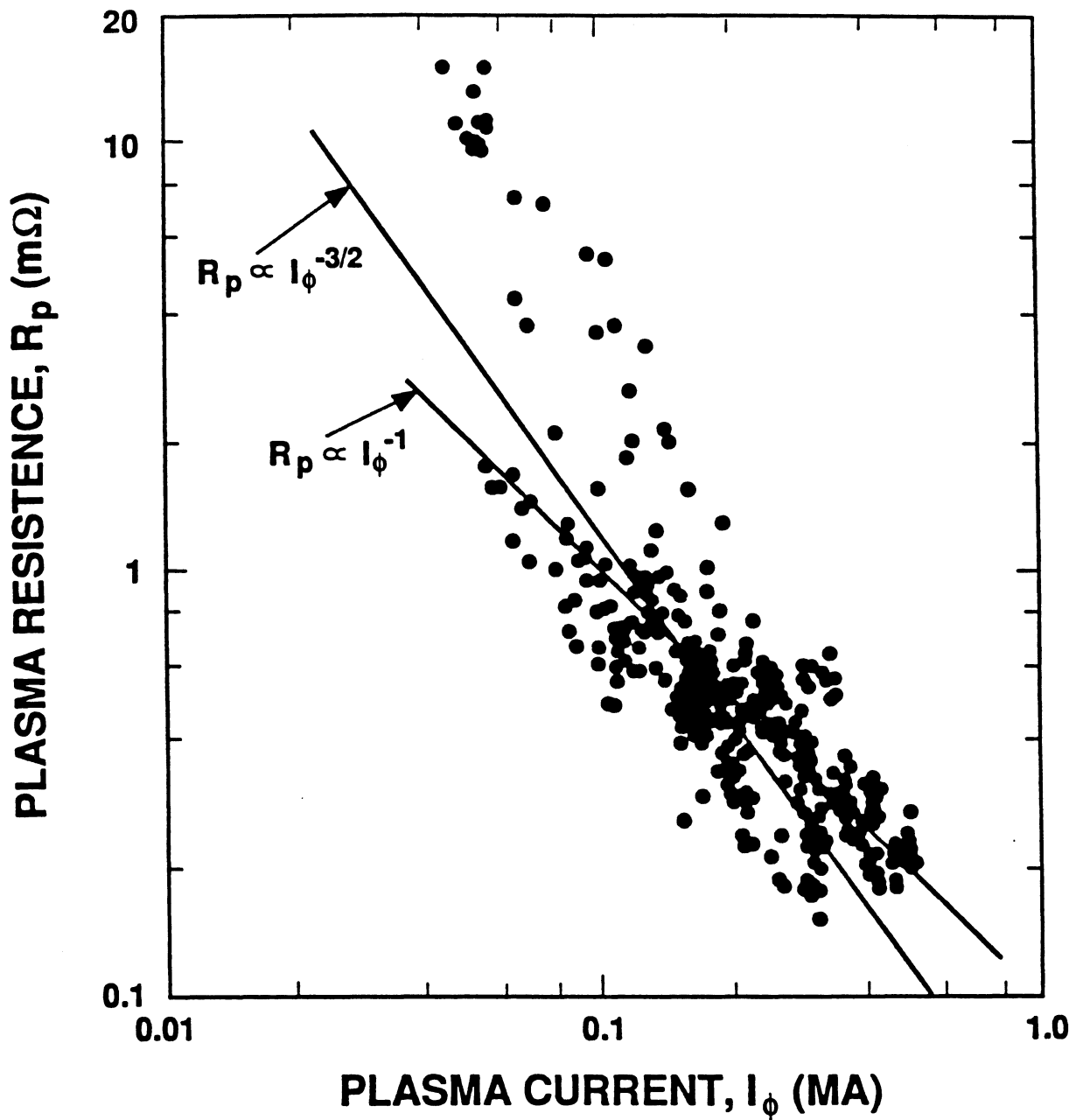


Figure 2.3-12. Dependence of plasma resistance on current for the OHTE/RFP experiment.

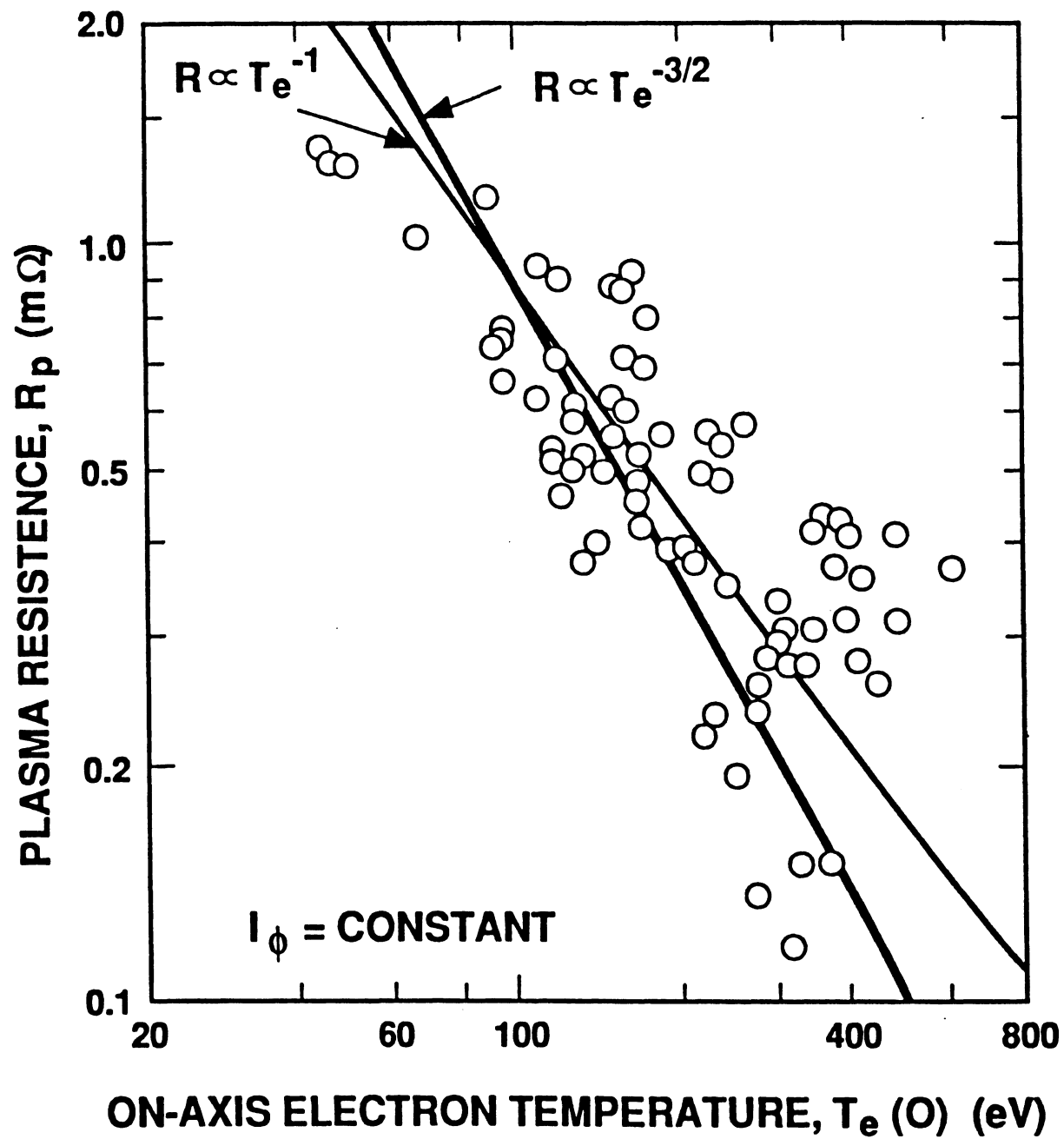


Figure 2.3-13. Dependence of plasma resistance on central electron temperature for ZT-40M experiment.

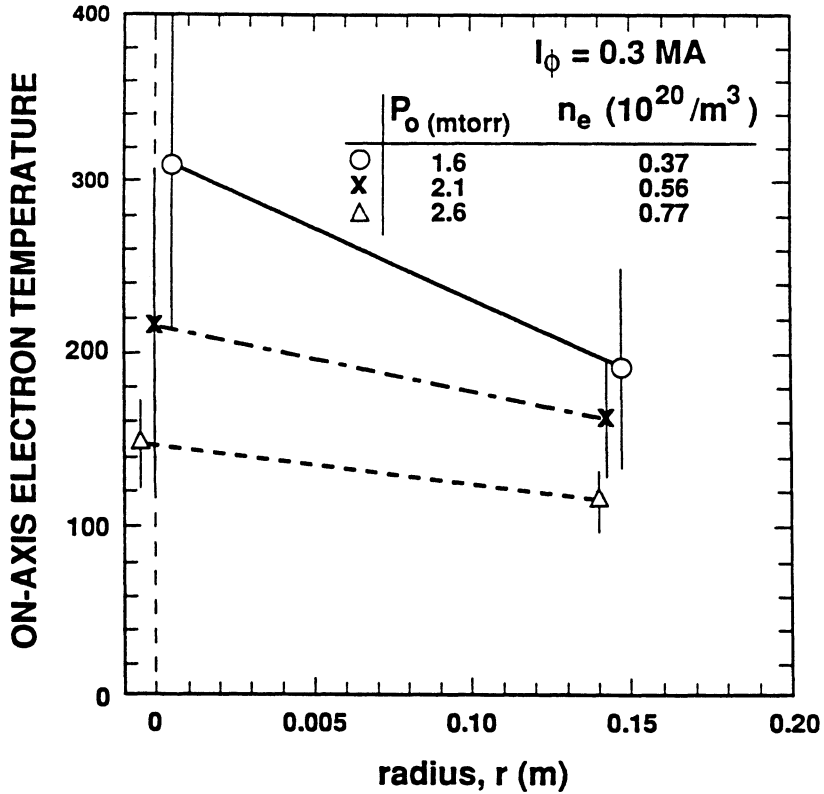


Figure 2.3-14. Two-point electron-temperature profiles for $I_\phi = 0.3$ MA and three values of I_ϕ/N for the ZT-40M experiment.

and the product $nT_e(0)$ with plasma current for ZT-40M. The latter set of data gives a linear increase of $T_e(0)$ with I_ϕ and $nT_e(0) \propto I_\phi^2$, with the slope indicating a nominally constant value of poloidal beta of $\beta_\theta \simeq 0.05$.

The ZT-40M and OHTE/RFP pressure-scaling data are given in Figure 2.3-18. Correlation of this data with Equation 2.3-1 shows that poloidal beta values in the range of 0.05 to 0.30 are possible. A correlation of selected data from a number of RFP experiments are shown on Figure 2.3-19, again substantiating the nominal constancy of β_θ in the range of 0.05 to 0.30. The best-fit curve gives an “international” β_θ of 0.064, nevertheless, a wide range of beta values are possible for a given machine, with the OHTE/RFP and TPE-1R(M) devices consistently reporting somewhat higher β_θ values.

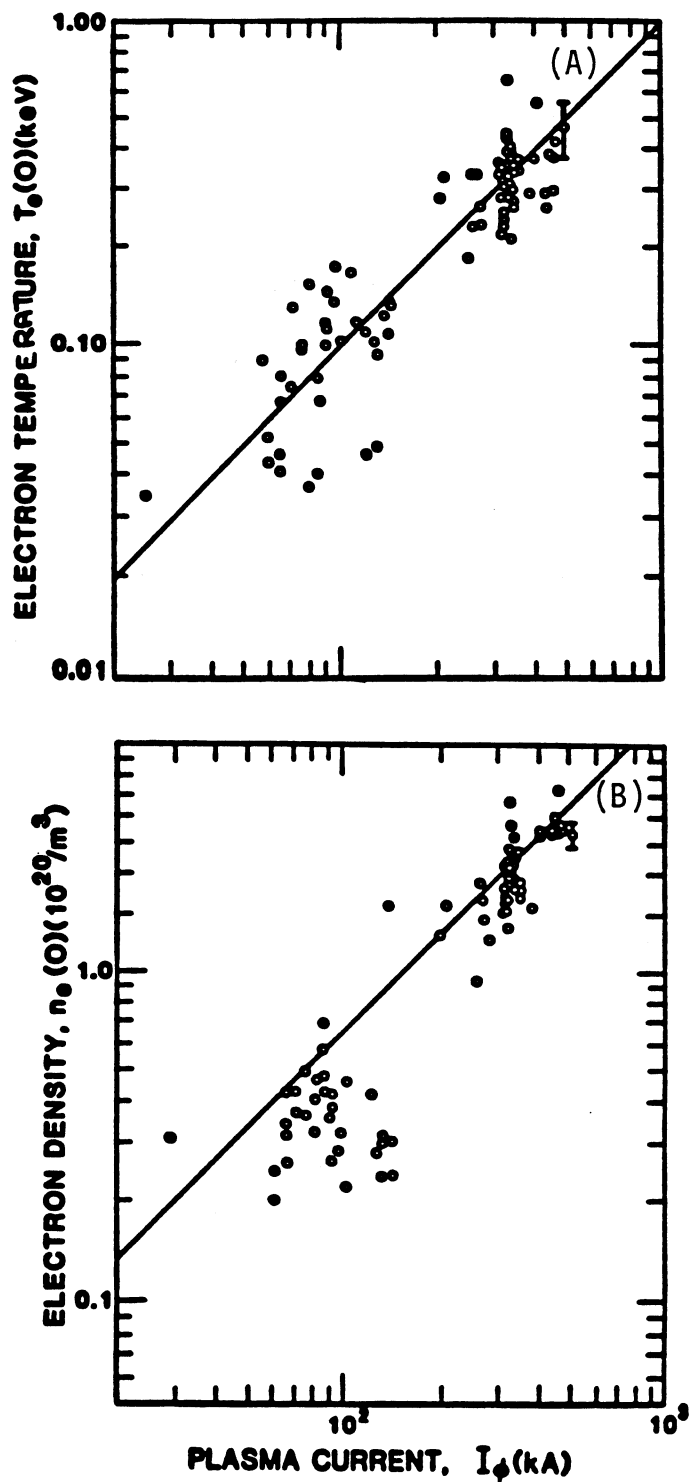


Figure 2.3-15. Variation of central electron temperature (A) and central electron density (B) with the plasma current for the OHTF/RFP experiment.

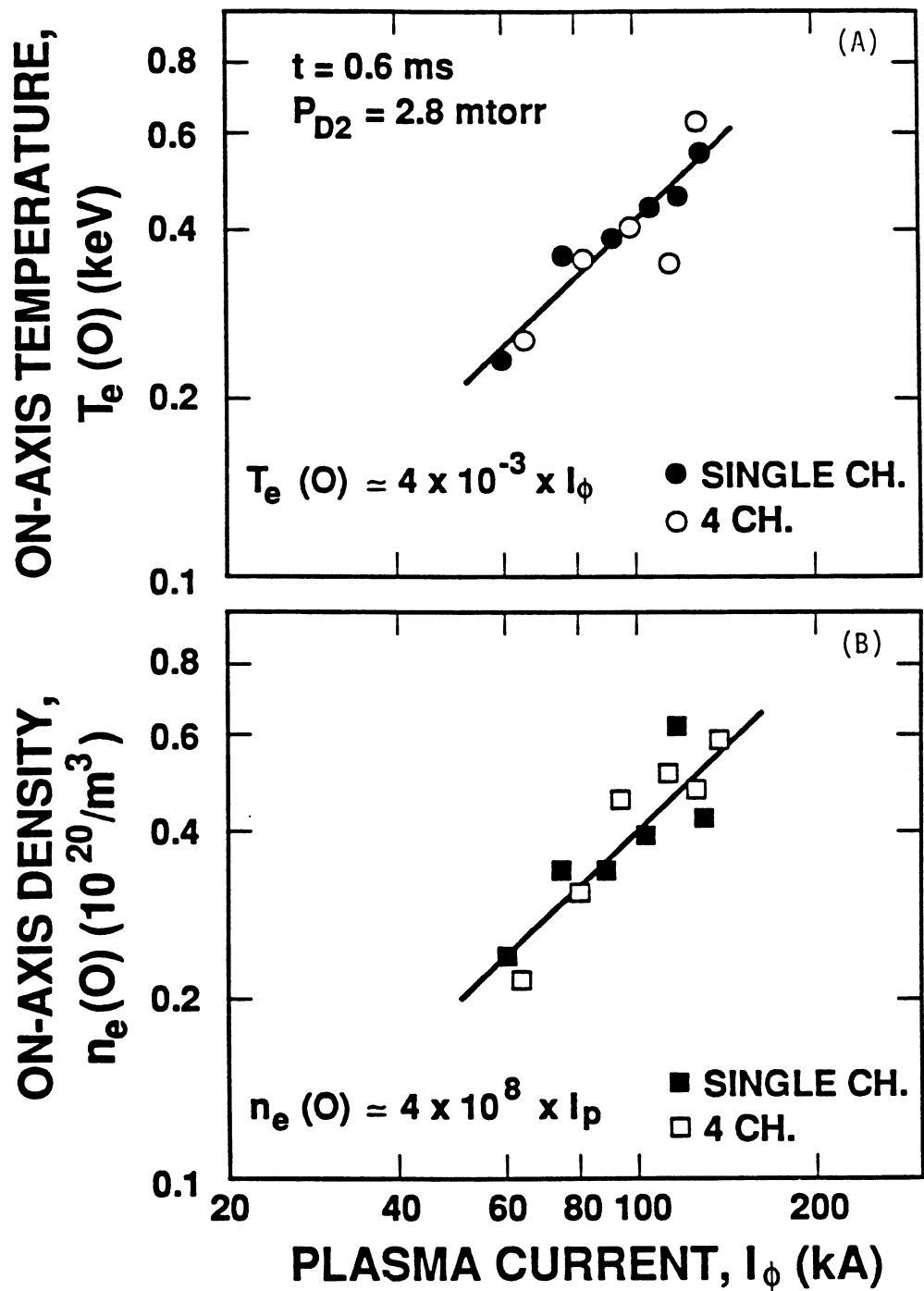


Figure 2.3-16. Variation of central electron temperature (A) and central electron density (B) with the plasma current for the TPE-1R(M) experiment.

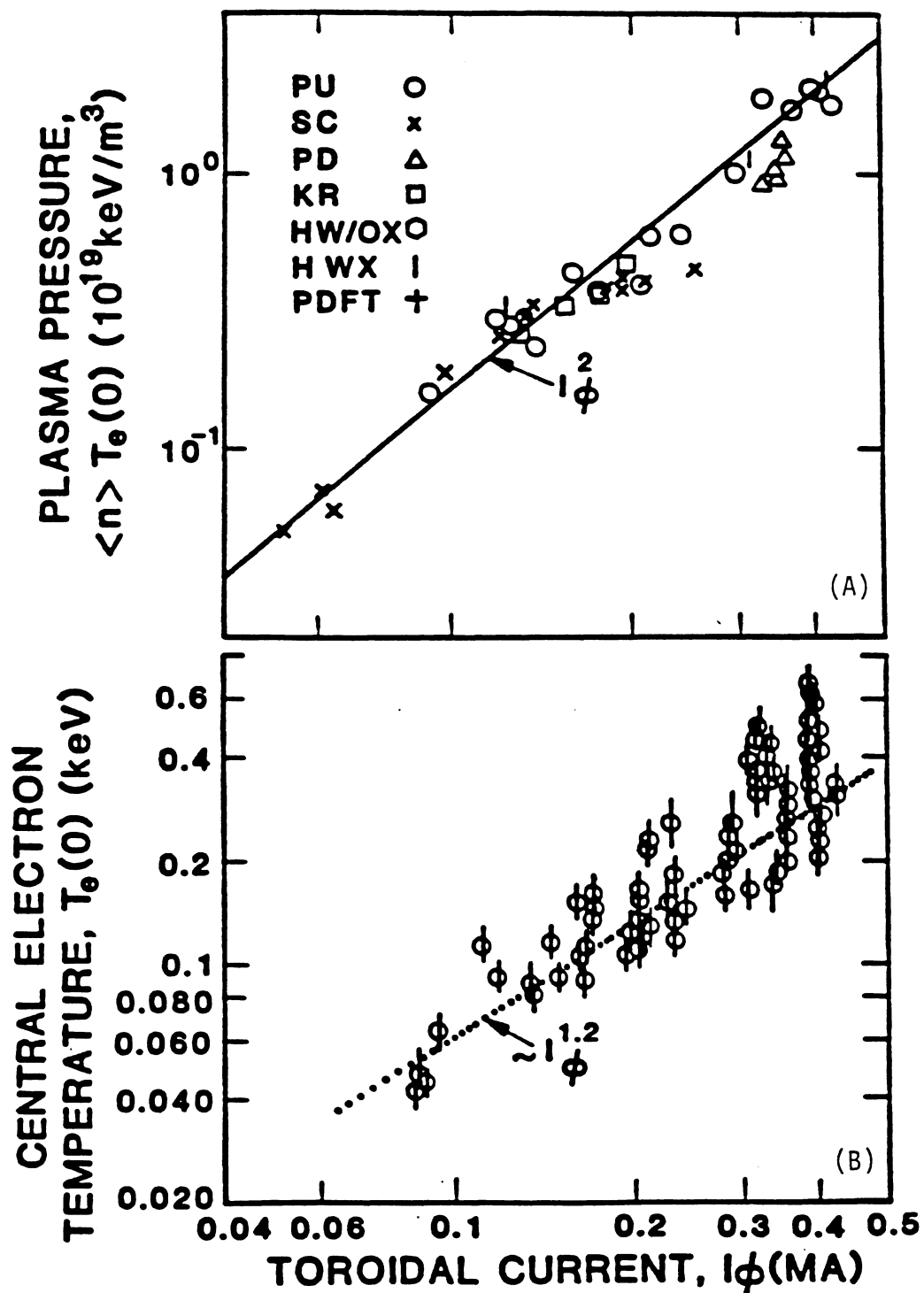


Figure 2.3-17. Variation of the product of central electron temperature with the average electron density current (A) and central electron temperature (B) with the plasma current for the ZT-40M experiment.

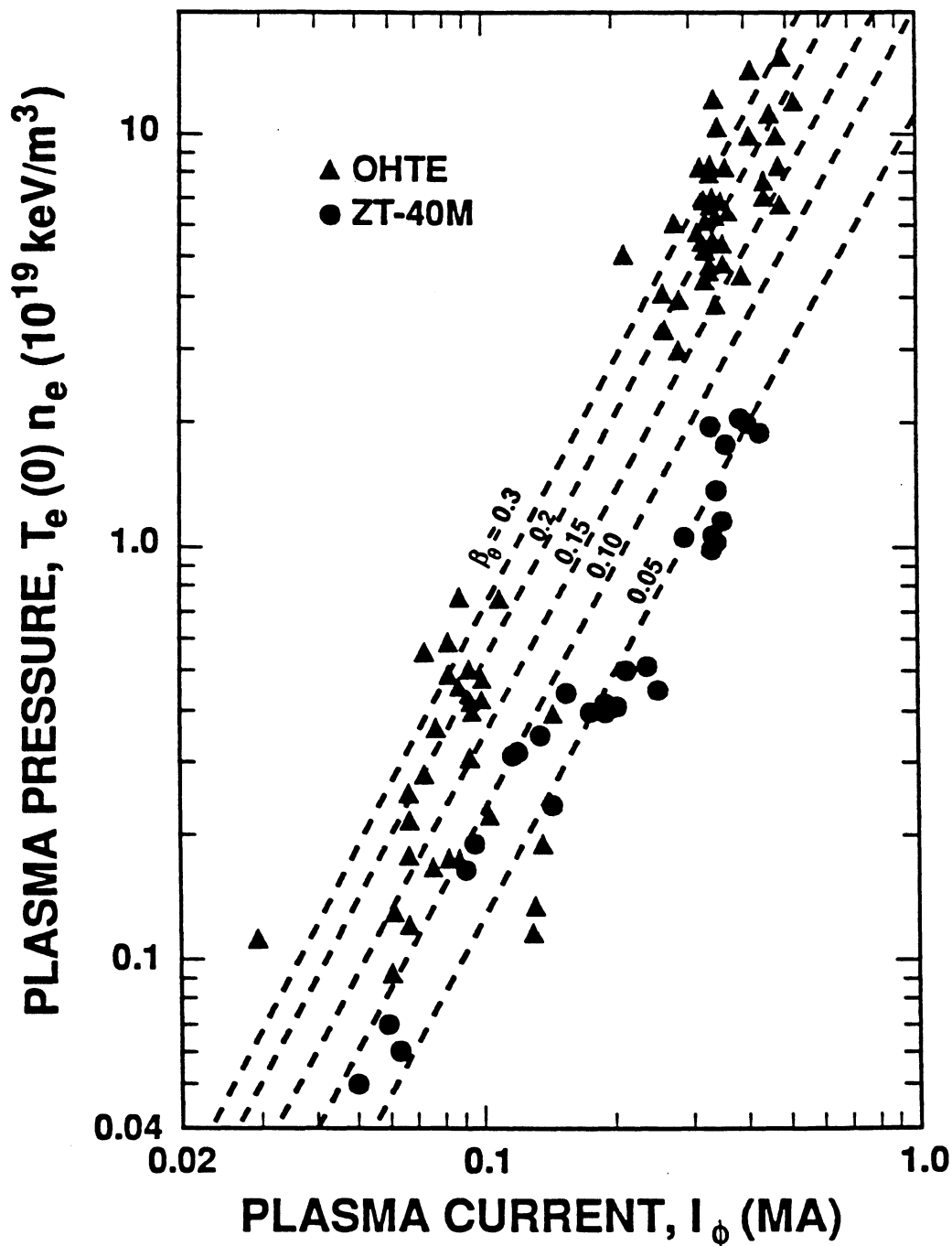


Figure 2.3-18. Correlation of ZT-40M and OHTE/RFP pressure-scaling data with Equation 2.3-1 for a range of β_θ and assuming $T_e(0)/T \approx 2.0$.

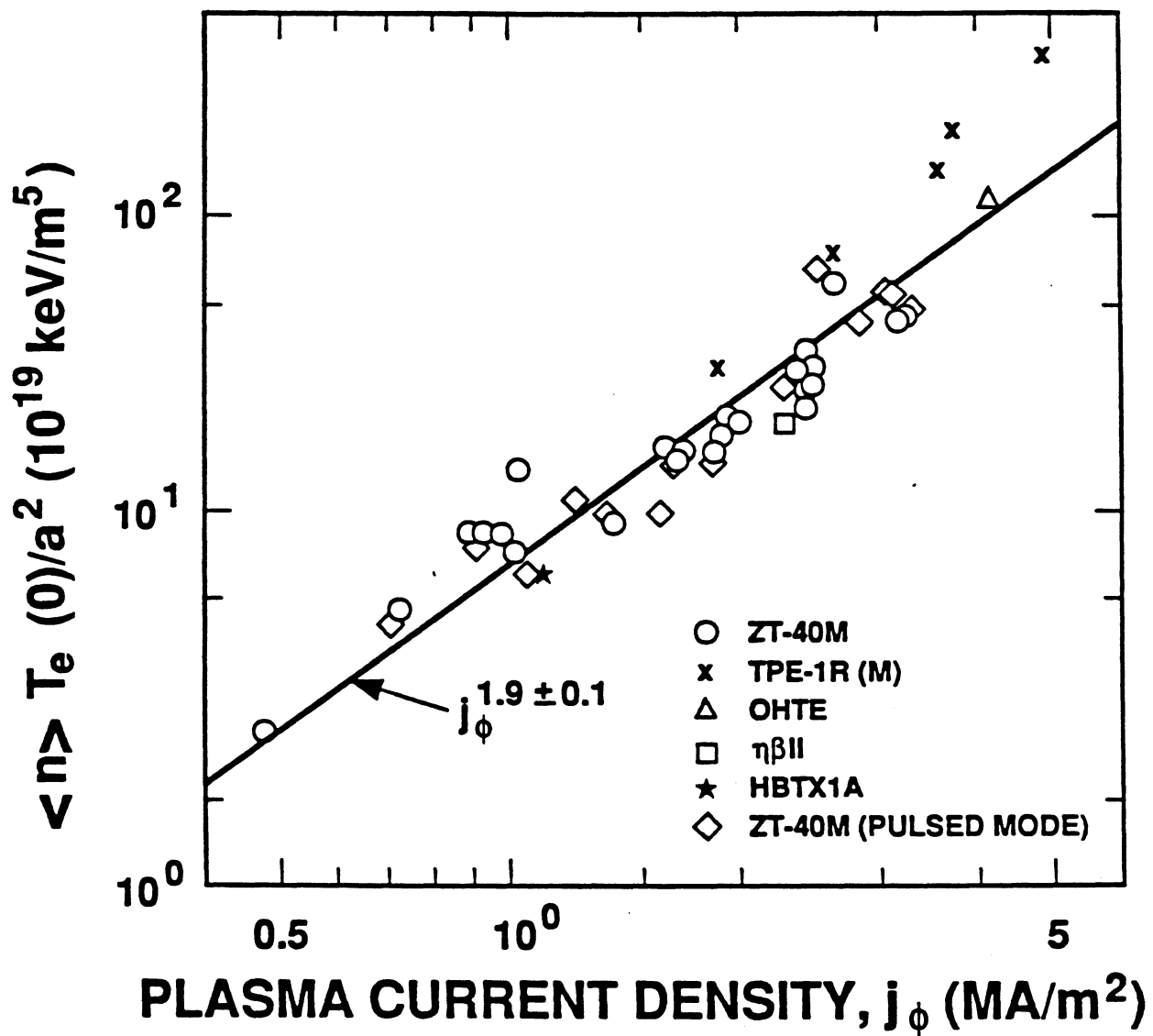


Figure 2.3-19. Correlation of plasma pressure with current and geometry for a number of RFP experiments. The “best-fit” curve gives $\beta_\theta \simeq 0.064$ under the assumption that $T_e(0)/T \simeq 2.0$.

2.3.5.3. Transport scaling

As noted previously, only a heuristic approach to the scaling of τ_B and $n\tau_B$ is possible until plasma profiles and transport are intrinsically and reproducibly measured. Combining Equations 2.3-1 and 2.3-3 and using the previously stated expression for Spitzer resistivity with $\ln \Lambda \simeq 15$ gives the following expression for τ_B and $n\tau_B$:

$$\tau_B = 1.86 \times 10^{13} \frac{r_p^2 \beta_\theta^{5/2}}{g_{OHM} Z_{eff}} \left(\frac{I_\phi}{N} \right)^{3/2} I_\phi^{3/2}, \quad (2.3-4)$$

$$n\tau_B = 5.9 \times 10^{12} \frac{\beta_\theta^{5/2}}{g_{OHM} Z_{eff}} \left(\frac{I_\phi}{N} \right)^{1/2} I_\phi^{5/2}. \quad (2.3-5)$$

For constant β_θ , g_{OHM} , Z_{eff} , and I_ϕ/N , τ_B should scale as $I_\phi^{3/2}$, $n\tau_B$ should scale as $I_\phi^{5/2}$ and, according to Equation 2.2-1, $T \propto I_\phi$. Figure 2.3-20 gives an early data correlation used to formulate and calibrate the following scaling in previous RFP reactor studies [8] as well as the present one

$$\tau_B = C_\nu I_\phi^\nu r_p^2 f(\beta_\theta), \quad (2.3-6)$$

where the coefficient, C_ν , and exponent, ν , are fitting parameters to the extrapolation shown in Figure 2.3-20 and are given in Table 3.2-III.

More recent and extensive measurements on ZT-40M [77] show that the invariability of I_ϕ/N is not sufficient to assume this parameter constant, and that $\tau_B \propto (I^2/N)^{3/2}$ gives a better correlation with recent data. Figure 2.3-21 gives this correlation with ZT-40M data. The deviation from the ideal slope of $\sim 3/2$ on this figure could be explained by increasing values of Z_{eff} ($\tau_B \propto 1/Z_{eff}$) as the plasma current and heat loads on in-vacuum components are increased. Unfortunately, a measurement of Z_{eff} is not yet available; the curves on Figure 2.3-22 are derived from Equation 2.3-4. Figure 2.3-22 correlates these ZT-40M data according to $\chi_B \equiv (3/16)r_p^2/\tau_B$ and extrapolates to the TITAN reactor requirement.

It should be noted that recent scaling experiments on the ZT-40M device [77] have generated considerably more data points than reported on Figures 2.3-21 and 2.3-22. Many of these additional discharges have been performed at lower currents (70 to 100 kA) and in this region show improved performance (e.g., increased β_θ and τ_B). These newer, low-current data skew the distributions when combined with higher-current data, which do not show improvement relative to past experiments on ZT-40M. The result is an

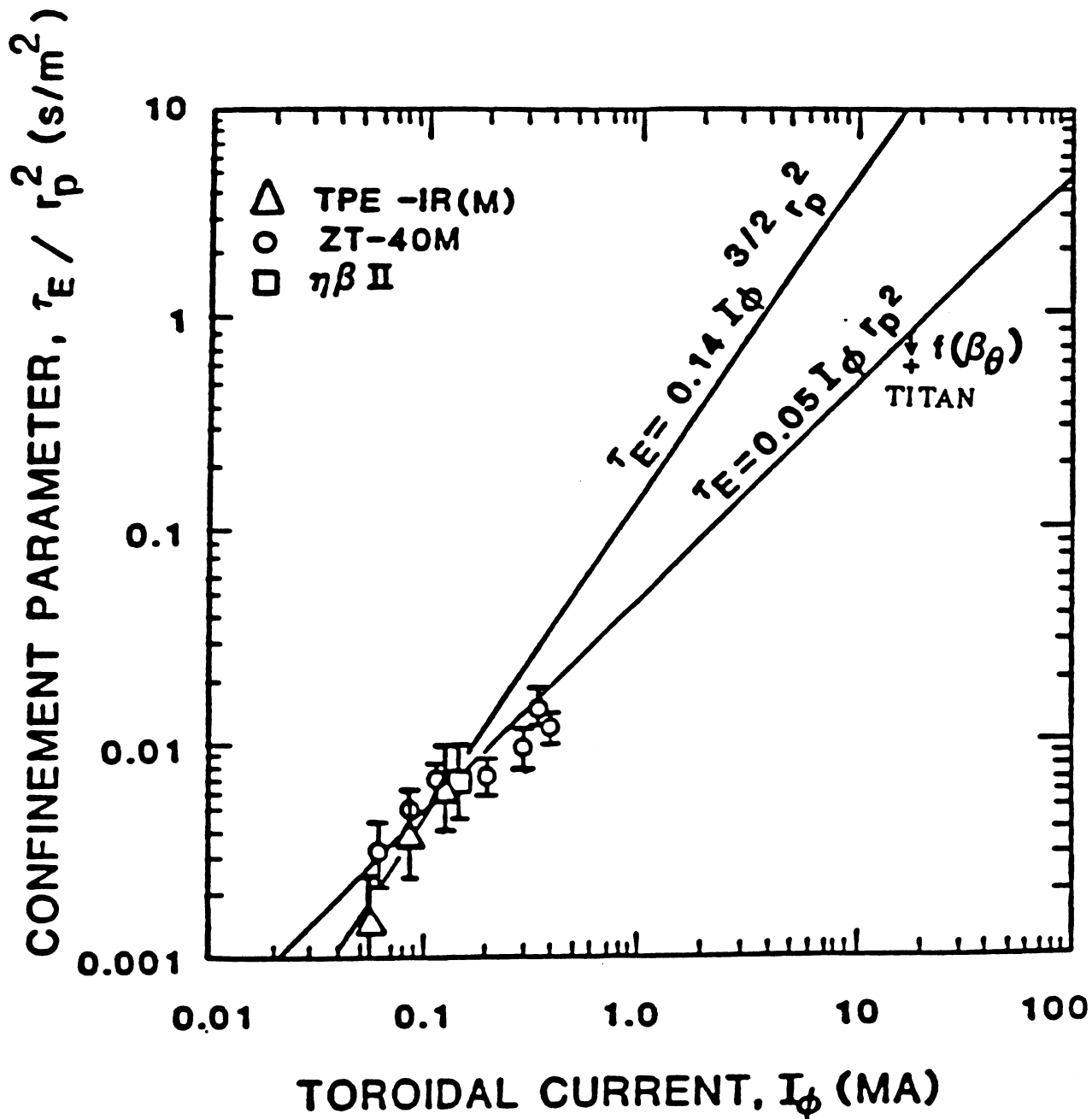


Figure 2.3-20. Variation of the confinement parameter with plasma current with data from several experiments. These early data formed the basis of scaling relationships used in early studies of the RFP reactor [8].

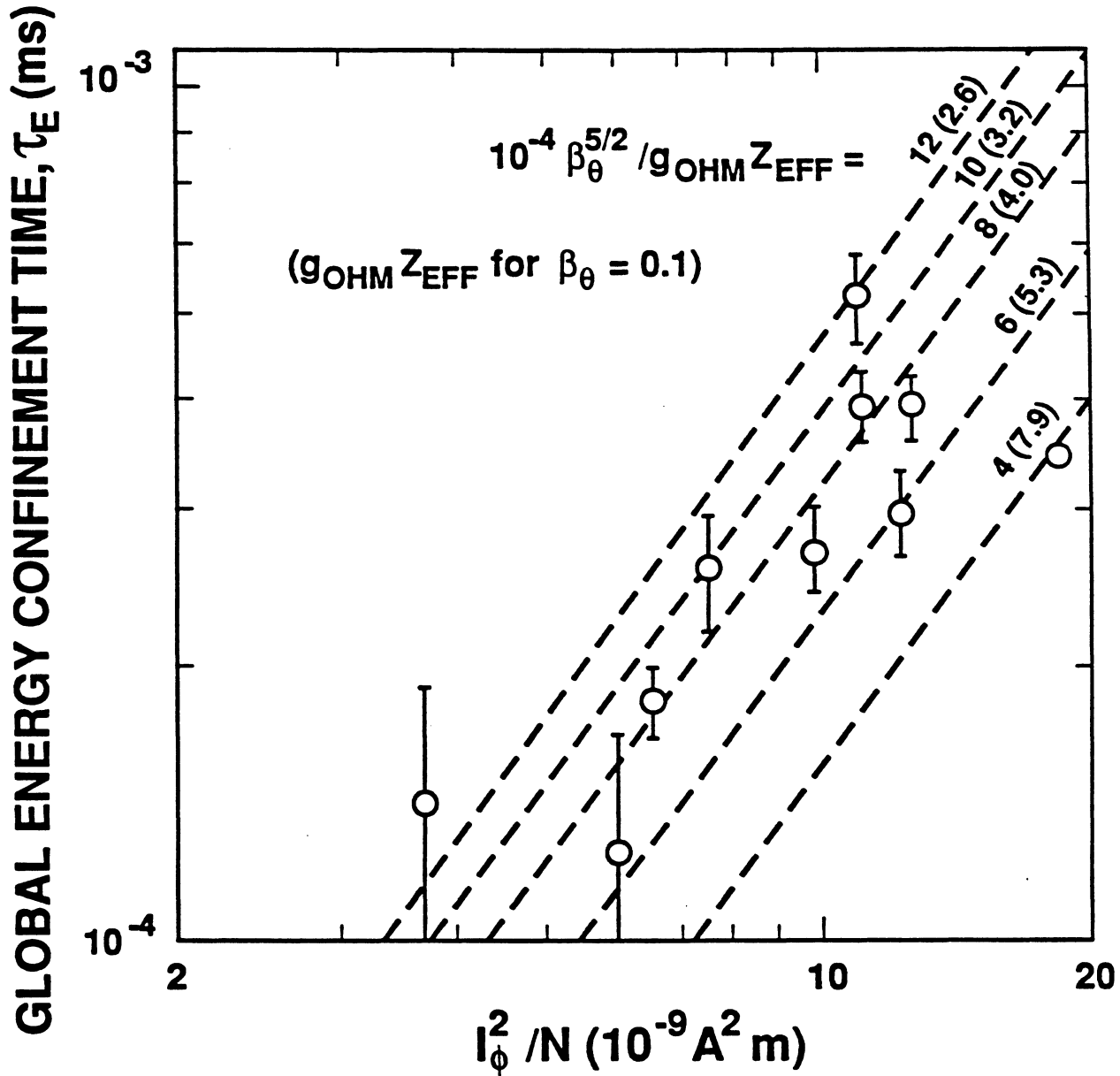


Figure 2.3-21. Correlation of global energy confinement time in ZT-40M with the parameter $(I_\phi^2/N)^{3/2}$ in order to accommodate variability in the parameter I_ϕ/N . The lines of constant $\beta_\theta^{5/2} / g_{OHM} Z_{eff}$ are generated by Equation 2.3-4. The values of $g_{OHM} Z_{eff}$ are given in parenthesis for $\beta_\theta = 0.1$.

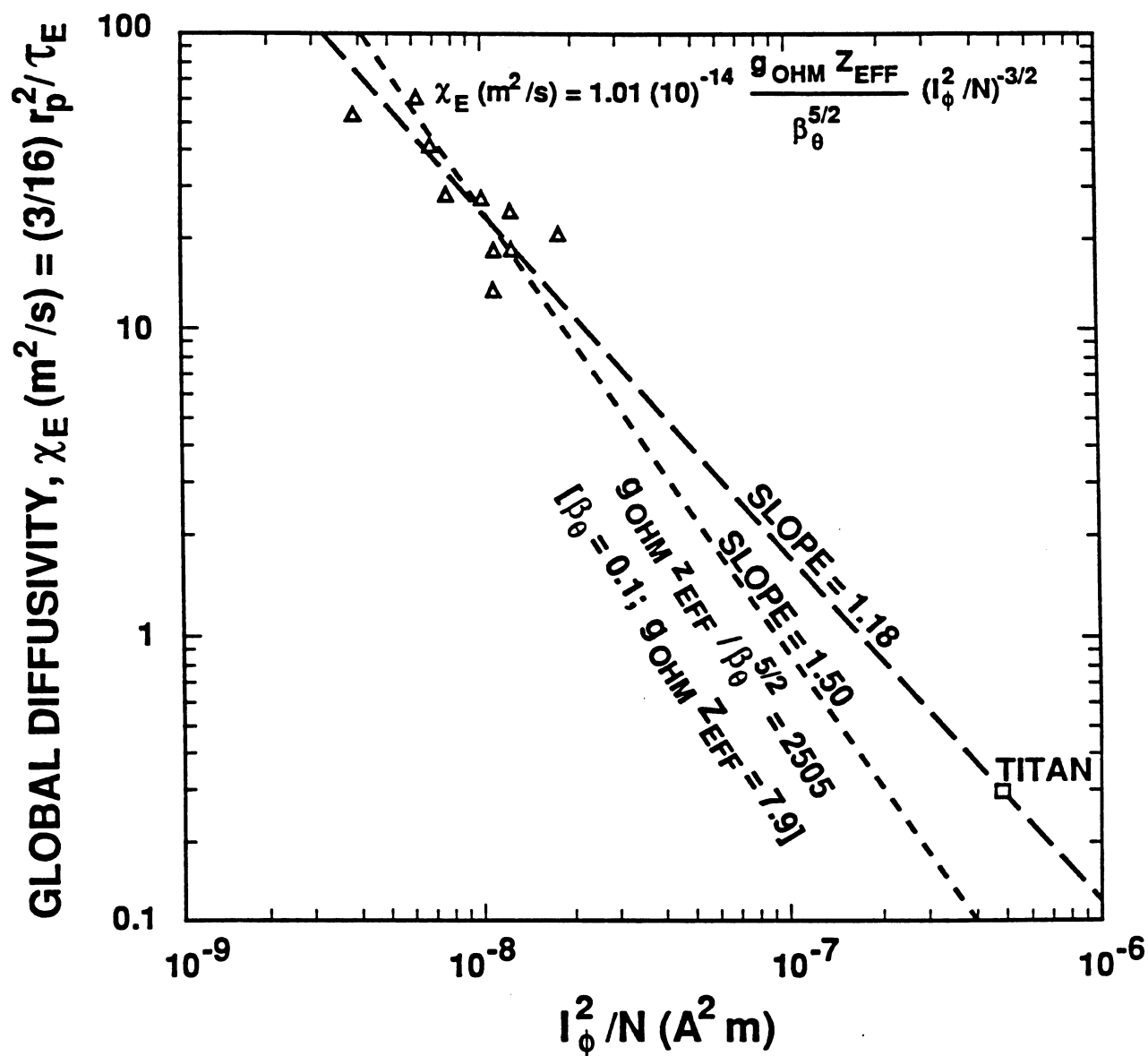


Figure 2.3-22. Correlation of global diffusivity for ZT-40M [77] and an extrapolation to the TITAN reactor conditions using Equation 2.3-4.

overall current scaling that is less favorable than indicated on Figures 2.3-21 and 2.3-22. Data from higher-current discharges with better density control, and with improved and extended diagnostics of Z_{eff} and profiles are required. It is likely that these issues will not be fully resolved until data from the higher-current RFP devices [24] become available.

Equation 2.3-5 shows that a correlation of transport with plasma current using a Lawson-like parameter, $n\tau_B$, should reduce the impact of uncontrolled variations in I_ϕ/N . Figure 2.3-23 gives such a plot for both ZT-40M and OHTE/RFP experiments. The line drawn on this figure has the slope of 5/2 which, taking a nominal value of $I_\phi/N \simeq 8 \times 10^{-14} \text{ A/m}$, has an intercept that predicts $g_{OHM} Z_{eff} \simeq 1650 \beta_\theta^{5/2}$. Hence, for $\beta_\theta \simeq 0.1$, $g_{OHM} Z_{eff} \simeq 5.2$. Both the ZT-40M and OHTE/RFP data show a derivation from the ideal $n\tau_B \propto I_\phi^{5/2}$ scaling at the higher currents, again possibly reflecting increases in heat load and Z_{eff} and/or changing (flattening) profiles for the higher-current discharges.

In summary, experimental results a few years ago [78,79] suggested that the scaling of temperature with current might be described by the postulate of a constant β_θ and $n\tau_B \propto I_\phi^2$, with the slope of T_e versus I_ϕ being determined by I_ϕ/N . More recent data correlations from both ZT-40M and HBTX1A indicate that the scaling of $nT_e(0)$ with current could under certain circumstances be less than quadratic, with a lower limit of $nT_e(0) \propto I_\phi^{1.7}$ being suggested by some data analyses [77,80]. Preliminary indications that β_θ may be decreasing somewhat with current awaits a better experimental resolution. As for TITAN, parametric results on the impact of reduced β_θ on the reactor performance are given in Sections 3 and 8.

Also of great interest is the scaling of transport with plasma size, a variable which to date is limited in range. In many respects the main issue for the compact, small-FPC approach to commercial fusion is the degree to which size (r_p) and current can be traded to give the smallest plasma exhibiting bulk-like plasma properties and acceptable first-wall and divertor heat loads. Central to this goal is the achievement of highly radiating, but well-confined plasmas.

2.3.6. Highly Radiating Plasma

The observed scaling of plasma pressure with the toroidal current, $nT_e(0) \propto I_\phi^2$, is suggestive of operation near a beta limit. Under this condition, the intrinsic transport would adjust by MHD activity, radiation, or other mechanism to lose energy at a sufficient rate to maintain β_θ constant. To test this hypothesis, experiments were performed on

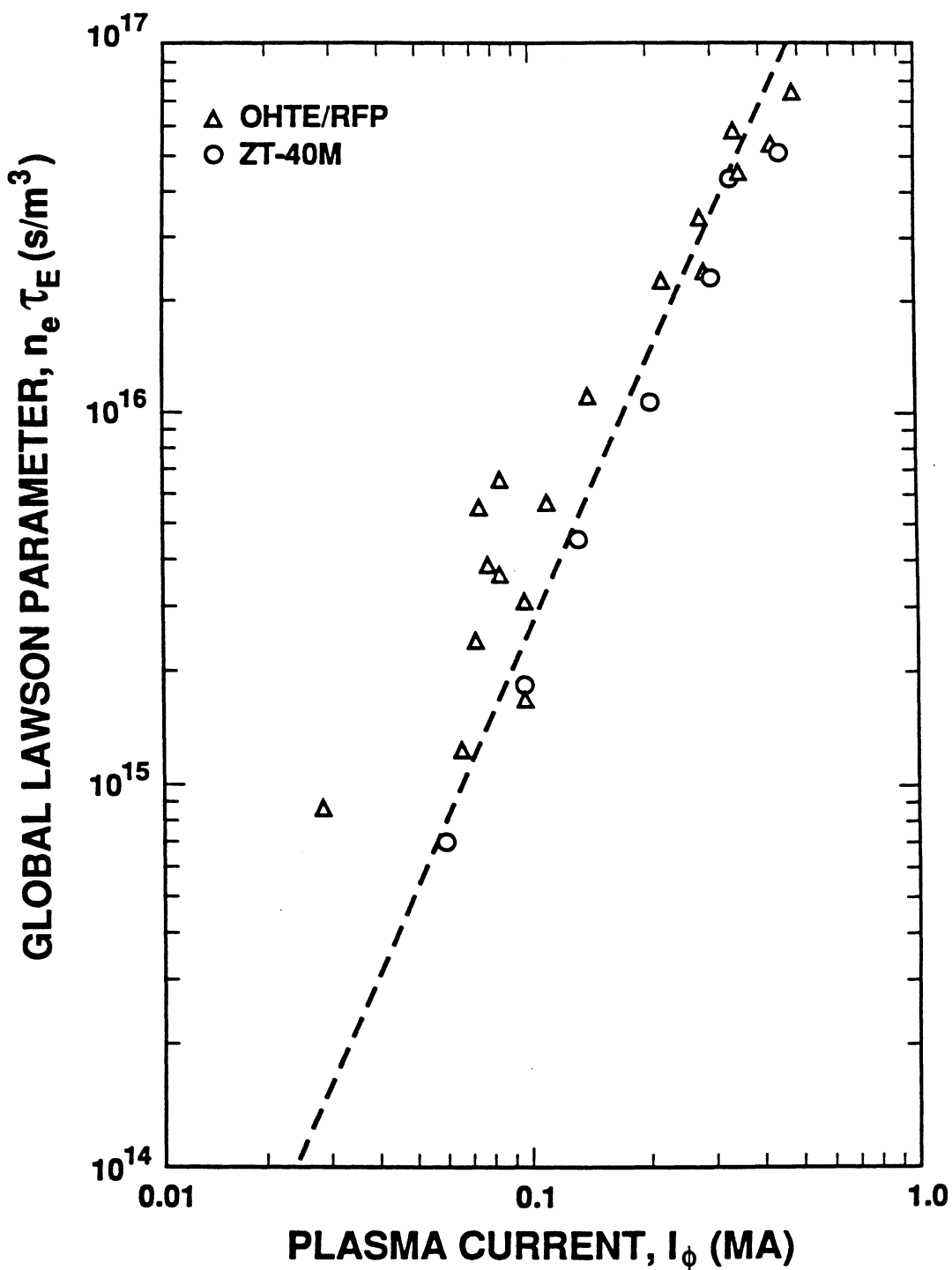


Figure 2.3-23. Correlation of a Lawson-like global energy confinement parameter, $n\tau_E$, with plasma current for both OHTE/RFP and ZT-40M devices.

ZT-40M by adding trace quantities of krypton impurity [81] to enhance the radiative losses. Krypton was chosen to maximize the ratio of radiated power to the ohmic-heating power. It was found that as the impurity was injected, the rate of radiation loss, P_{RAD} , was increased, but simultaneously, the ohmic power, P_{OHM} , only slightly increased. Most importantly, β_θ remained constant. This observation suggests that as radiation losses are increased, the non-radiative or “intrinsic” transport losses, P_{NR} , decrease to maintain the beta constant.

A simplified zero-dimensional power-balance model for a steady-state plasma gives $P_{OHM} = P_{RAD} + P_{NR}$. Using the definitions of the global energy confinement time, τ_B , and a non-radiative (intrinsic) energy-confinement time, τ_E^{NR} , the following expression results:

$$\tau_E^{NR} = \tau_B \left(1 - \frac{P_{RAD}}{P_{RAD} + P_{NR}} \right)^{-1}. \quad (2.3-7)$$

For the assumed constant-beta scaling and self-similar profiles of density and electron temperature before and after krypton injection, the values of the total energy loss ($P_{RAD} + P_{NR}$) and τ_B remain unchanged. Equation 2.3-7 indicates that as the radiative losses increase, the non-radiative losses decrease (or τ_E^{NR} increases) to maintain the energy content of the plasma and hold β_θ constant. The data from the krypton impurity experiments are plotted in Figure 2.3-24, and close agreement with predictions of Equation 2.3-7 is indicated.

A second experimental test was made of the beta-limit hypothesis. The energy confinement scaling given by Equation 2.3-4 predicts that the total energy confinement scales inversely with Z_{eff} . By injecting krypton impurities, the plasma resistance was varied and the total confinement time was measured. These experimental data shown on Figure 2.3-24 indicate that τ_B scales as Z_{eff} , as suggested by Equation 2.3-4.

It is important to point out that, while suggestive of a beta-limit hypothesis, these results are not conclusive. Furthermore, it appears that far more power is being supplied to the discharge than is needed to maintain the plasma at a given beta limit [81]. Therefore, these experiments are not expected to exhibit an underlying transport which is not affected by the beta-limit hypothesis. Beta-limited plasma operation with a high radiation fraction, $f_{RAD} \equiv P_{RAD}/(P_{OHM} + P_\alpha)$, is crucial to the compact high-power-density devices in order to meet realistic constraints on heat and particle loads on the first wall and divertor plates.

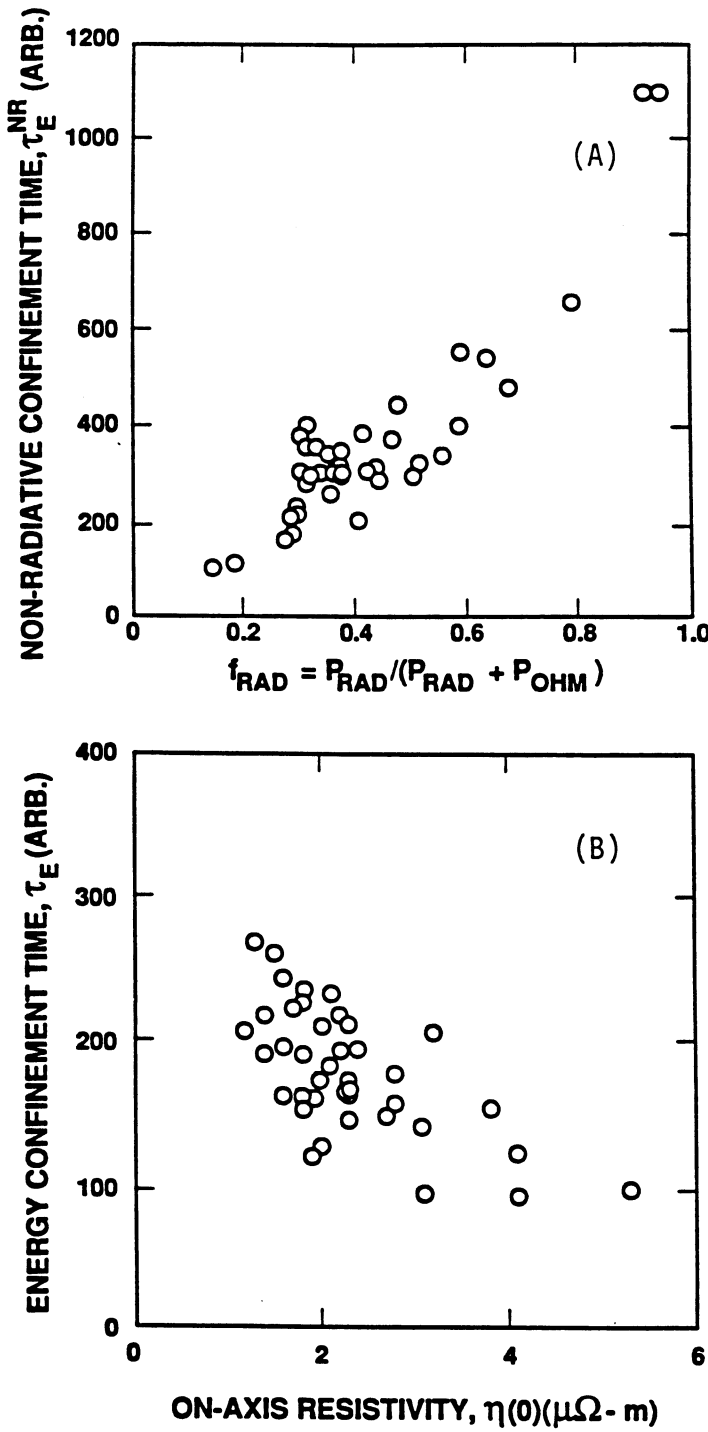


Figure 2.3-24. Scaling of the non-radiative energy confinement time with the fractional radiative power loss (A) and dependence of τ_E on the effective plasma resistivity (B) in the krypton-seeded ZT-40M discharges [81].

2.3.7. Current Termination

Operating RFP experimental discharges usually end with a current-termination phase, wherein the plasma current is rapidly reduced to approximately zero (Figure 2.3-2). The current termination occurs in a few tenths of a microsecond in small devices and up to a few hundred microseconds in the larger machines. Current terminations are accompanied by a positive voltage spike and large density and magnetic-field fluctuations. A number of variables, such as plasma radius, density, toroidal-field reversal, magnetic-field errors, and impurities appear to affect the termination. A complete and satisfactory explanation of RFP current terminations is not yet available. Because of large stored magnetic energy in the plasma, current termination at TITAN reactors at full plasma current must be avoided in favor of controlled ramp-down of the plasma current.

Evidence suggests that the onset of termination may be related to a loss of density and confinement, possibly leading to a streaming parameter, ξ , that exceeds a critical value for runaway electrons. Studies on ZT-40M indicate [80] that termination occurs when I_ϕ/N approaches ~ 1 to 2×10^{-13} A/m, which is consistent with the occurrence of a critical drift threshold when ξ approaches unity.

Rapid current termination can have severe consequences in large, high-current experiments or reactors because of the large voltage spikes and the localized heating of the walls. A method of controlled “run-down” has been tested experimentally on HBTX1B [61,63,82] in which the toroidal-field-coil circuit is controlled so that the pinch parameter, Θ , is maintained at a given value as the current is decreased. The field reversal in this case is maintained until the current reaches a relatively low level. Maintaining reversal in this way is found to delay termination, and the current can be reduced to between 10% and 20% of the maximum value before the termination occurs. Controlled ramp-downs of this kind forestall the loss of toroidal-field reversal as long as possible and will be required of the reactor.

2.3.8. Current Drive

Because of the relatively small values for L_p/R_p in the compact RFP reactor, inductive pulse lengths in excess of 100 to 200 s are not possible, and some form of current drive is required. Although the use of radio-frequency (RF) fast-wave current-drive scheme has not been fully explored for the RFP, the high plasma density and currents relative to those for the tokamak indicate problems with the efficiency of RF current-drive schemes (Section 7). On the other hand, because of the relaxation processes in RFPs, there is no

need to drive the current at the plasma center and some of the issues related to wave penetration may be negated.

Bootstrap current, given by $j_{BC} = -(\epsilon^{1/2}/B_\theta)(\partial p/\partial r)$ [83], is also expected to be low (if such current exists at all in RFPs) since β_θ and $\epsilon = r_p/R_T$ are small. For example, if the pressure profile is given by $p/p_o = 1 - (r/r_p)^\nu$, then the contribution of bootstrap current to the overall current density is given by

$$\frac{j_{BC}}{j_\phi} = \beta_\theta \epsilon^{1/2} \frac{\nu^2}{4(\nu + 2)}, \quad (2.3-8)$$

which for $\nu \simeq 2$, $\beta_\theta \simeq 0.2$, and $\epsilon \simeq 1/6$ (TITAN plasma conditions) gives $j_{BC}/j_\phi \simeq 0.02$.

The close coupling of poloidal and toroidal currents and magnetic fields that determine the near-minimum-energy states of the RFP offers the possibility of a current-drive method based on “magnetic helicity injection” [17]. Current drive through “electrostatic helicity injection” has been experimentally demonstrated in spheromaks [18], which are also relaxed-state systems like RFPs. Another helicity-injection technique is the oscillating-field current drive (OFCD) [17,19]. In this scheme, audio-frequency oscillating voltages are applied to the toroidal and poloidal circuits in the appropriate phase ($\delta = \pi/2$) to drive a DC toroidal current in the plasma with the plasma, in effect, behaving as a nonlinear rectifier. As originally proposed [17], OFCD is based on the premise that maintenance of the RFP configuration simply requires the supply of magnetic helicity at a rate equal to its dissipation. The helicity balance is given by [17,84]

$$\frac{dK}{dt} = 2\Phi V_\phi - 2 \int \mathbf{E} \cdot \mathbf{B} dV_p, \quad (2.3-9)$$

where the integral gives the rate of helicity dissipation throughout the plasma volume and the remaining product of toroidal flux and voltage gives the rate of helicity injection or ejection through the plasma surface. Helicity is effectively injected into the plasma if Φ and V_ϕ are sinusoidal and are oscillated in phase with each other (e.g., $V_\theta = -\dot{\Phi}$ and V_ϕ are in quadrature), even though the time-averaged electric fields are zero. Hence, with the F - Θ diagram providing the required connection between V_θ and V_ϕ , a noninvasive and potentially efficient means to drive currents in high-density thermonuclear plasma is possible. Current drive by helicity injection has also been proposed for tokamaks [85 - 87], provided that a similar, globally nondisruptive mechanism for profile relaxation exists.

The effects of AC magnetic-field oscillations on ZT-40M were first studied using a zero-dimensional simulation, assuming that the plasma evolved through a series of quasi-relaxed equilibrium states. The OFCD was predicted for these experiments, provided that

the plasma relaxation time was shorter than the modulation period and that such field modulations did not adversely affect plasma performance. Subsequent field-oscillation experiments on ZT-40M [19] showed relaxation times of ~ 0.1 ms without deleterious impacts, provided toroidal-field reversal was maintained. Based on these RFP relaxation experiments a full test of OFCD on ZT-40M was conducted [16,21,88].

The test of OFCD on the relatively cold, $T_e(0) \simeq 200$ eV, resistive ZT-40M plasma was anticipated to be difficult because of the strong field oscillations and high frequencies required to observe an effect. The main OFCD discharge variables that have to be optimized relative to RFP physics and machine limitations are V_ϕ , V_θ , δ , $\bar{\Theta}$, and ω , where $\bar{\Theta}(F)$ is the pinch parameter about which the oscillations would occur at frequency ω . This optimization procedure is described in References [16] and [21]. Operational constraints on ω lie in the range 5 to 500 kHz, although consideration of the shell electrical penetration time forced an upper limit of 5 kHz, and a lower limit of 2 kHz was set by temporal characteristics of sawtooth oscillations [40]. Ideally, $\bar{\Theta}$ is selected as the point of minimum plasma resistance ($\bar{\Theta} \simeq 1.45$, Figure 2.3-3). Maximum OFCD power, however, required V_θ to be maximized which forced deeper reversal, larger $\bar{\Theta}$ (more negative F), increased plasma resistance (Figure 2.3-3), and required more power. Lastly, as previously noted, the maximum OFCD effect is expected for $\delta \simeq \pi/2$.

High-power (~ 40 MVA) OFCD tests on $I_\phi = 180$ to 200 kA discharges were first performed and the results are given in Figure 2.3-25. The real rms power input amounts to ~ 20 MW compared to 7 MW for the DC power input. “Anti-OFCD” conditions, wherein helicity is drawn out from the plasma at an accelerated rate, could be obtained if $\delta = -\pi/2$. These high-power OFCD tests showed an increasing plasma resistance, total radiation power, and metal line radiation which, together, indicate a strong plasma-wall interaction. A slight decrease in I_ϕ was seen because of increased plasma resistance related to increased impurity content. Calculations indicated that the adverse effect of the plasma-wall interaction was comparable to any expected OFCD current enhancement.

The low-power OFCD tests (~ 7 MVA, $I_\phi \simeq 60$ to 70 kA), also shown in Figure 2.3-25, were conducted to reduce the extent of the increase in plasma resistance caused by the plasma-wall interaction. These ramped discharges, however, were at lower temperature and, hence, higher plasma resistance. In this case, no substantial increase in plasma resistance was observed between the OFCD and DC discharge. With optimal phasing ($\delta \simeq \pi/2$), an approximately 5% increase in poloidal flux was observed when OFCD was applied. Furthermore, the amplitude and phase of the on-axis oscillation of the toroidal field compared to that in the edge-plasma region were what would be expected if the mean magnetic fields remained in a quasi-relaxed state, as described by a modified BFM [17,89].

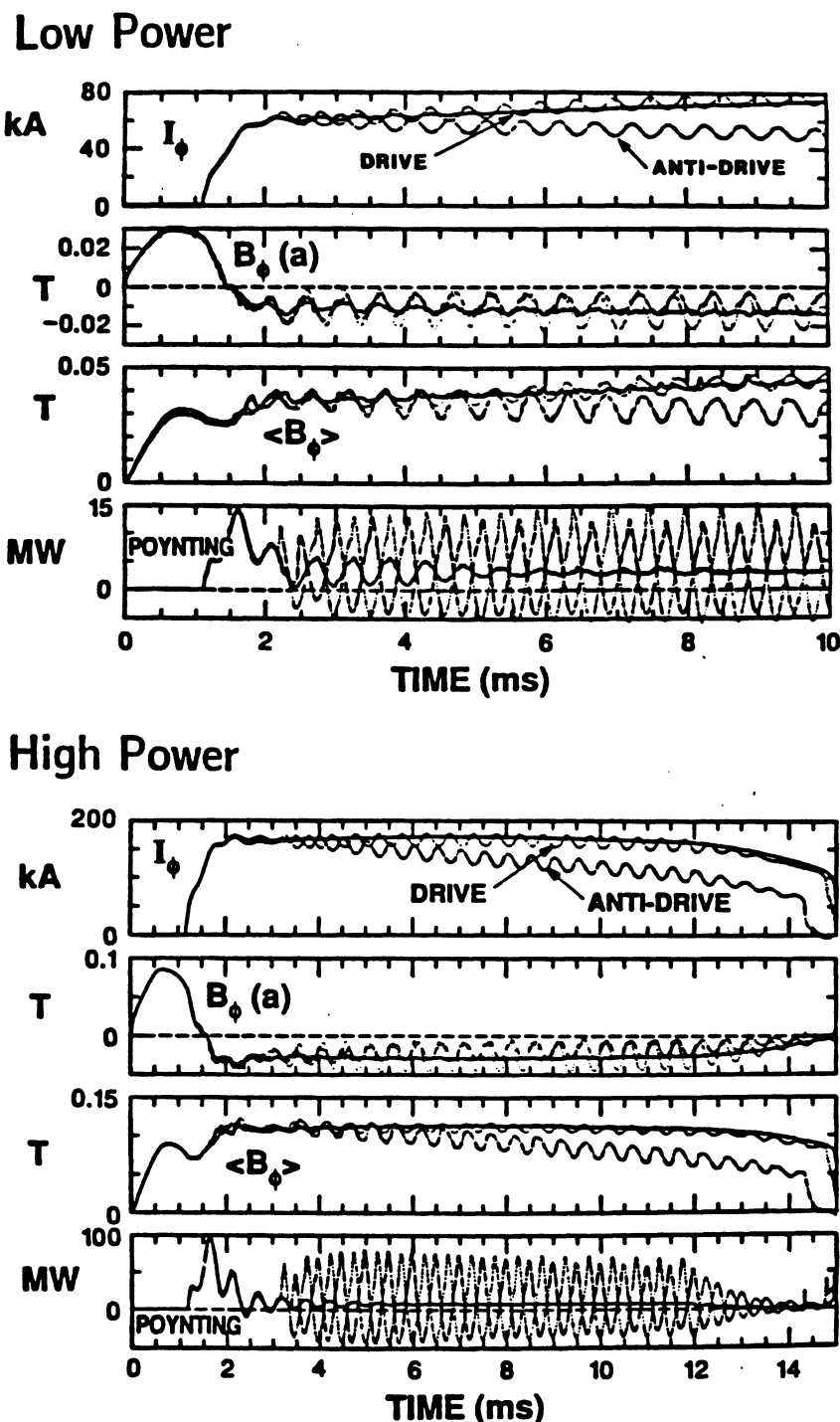


Figure 2.3-25. The OFCD results from ZT-40M [16,21] for low-power (~ 7 MVA, $I_\phi = 60$ to 70 kA) and high-power (~ 40 MVA, $I_\phi = 180$ to 200 kA) tests.

While a clear demonstration of substantial current drive by OFCD must await RFPs operating with hotter plasmas and reduced wall interaction [24], the strong dependence of the plasma response on δ and the spatial and temporal behavior of the mean magnetic fields are in general agreement with magnetic helicity models and simulations.

2.3.9. Operation with Resistive Shells

Since the confinement in an ohmically heated discharge is related to the plasma resistance ($\chi_B = g_{OHM} \eta / \mu_0 \beta_\theta$), the key to increased τ_B and reduced χ_B is the reduction in plasma resistivity through increased plasma temperature and reduced wall interactions. Improved plasma performance is expected if the magnetic-helicity dissipation occurring in the edge-plasma region can be significantly reduced. For a number of present-day RFP experiments, a better control of the plasma position through an externally applied vertical field has led to improved plasma parameters and extended discharge durations. Increased external control on the plasma, however, requires thinner stabilizing shells.

Historically, RFP experiments have closely surrounded the plasma with thick conducting shells to stabilize against kink instabilities [9,33,38]. The crucial trade-off between the desire and/or need for active control of the plasma position and the plasma-wall interaction on the one hand, and the control of instabilities to a level that also minimizes the plasma-wall interaction on the other (both being directly but inversely dependent upon the thickness of the stabilizing shell) represents a crucial issue for the next major RFP experiments [24] as well as for reactors.

Table 2.3-II and Figure 2.3-26 show that the characteristic time for vertical-field or shell diffusion in most present day RFPs is greater than or comparable to typical discharge times. Those experiments that apply an external vertical field, B_V , do so in a preprogrammed mode; active feedback of B_V is yet to be done in any RFP experiment. The impact of this preprogrammed vertical field on the plasma performance can be significant [12,15,51,52]. The results from the most recent experiments on OHTE [90] are given in Figure 2.3-26, which shows the time dependence of the plasma current and radial displacement for a number of vertical-field conditions. The plasma-position control indicated on this figure was made possible by decreasing the shell time constant from 25 to 1.5 ms [91]. There was no change in the gross MHD modes when operating with the more resistive shell, although linear MHD theory predicts RFP plasmas surrounded by a resistive shell should be unstable [33]. A toroidally localized kink mode was observed [92]. This mode perhaps resulted from nonlinear coupling of internal kink modes and seemed to grow initially and then self-heal. If in fact a relatively resistive shell can

Table 2.3-II.
VERTICAL-FIELD TIME CONSTRAINTS
FOR A NUMBER OF RFP EXPERIMENTS

Device	R_T (m)	r_p (m)	I_ϕ (kA)	τ_v (ms) ^(a)	τ_d (ms) ^(a)
Reversatron	0.50	0.08	25.	0.004	0.28
TPE-1RM15	0.50	0.09	130.	100.	7.
ETA-BETA-II	0.65	0.125	150.	8.	2.
HBTX1B	0.80	0.26	320.	80. ^(f)	10.
ZT-40M	1.14	0.20	400.	65.	38.
OHTE	1.24	0.20	500.	1.5 ^(b)	14.
CPRF/ZTH ^(c)	2.40	0.40	4,000.	~ 50. ^(d)	~ 800.
RFX ^(c)	2.00	0.48	2,000.	300.	~ 250.
TITAN	3.80	0.60	18,000.	10.	∞

(a) Characteristic resistive shell time for vertical-field diffusion, $\tau_v = \mu_0 r_s \delta_s / (2\eta_s)$, where r_s is the shell minor radius and δ_s is the shell thickness.

(b) Decreased from an original value of 25 ms [91,92].

(c) Planned experiments.

(d) Original design was 250 ms.

(e) Maximum discharge time.

(f) Plans exist to install a $\tau_v = 2$ -ms shell in early 1988.

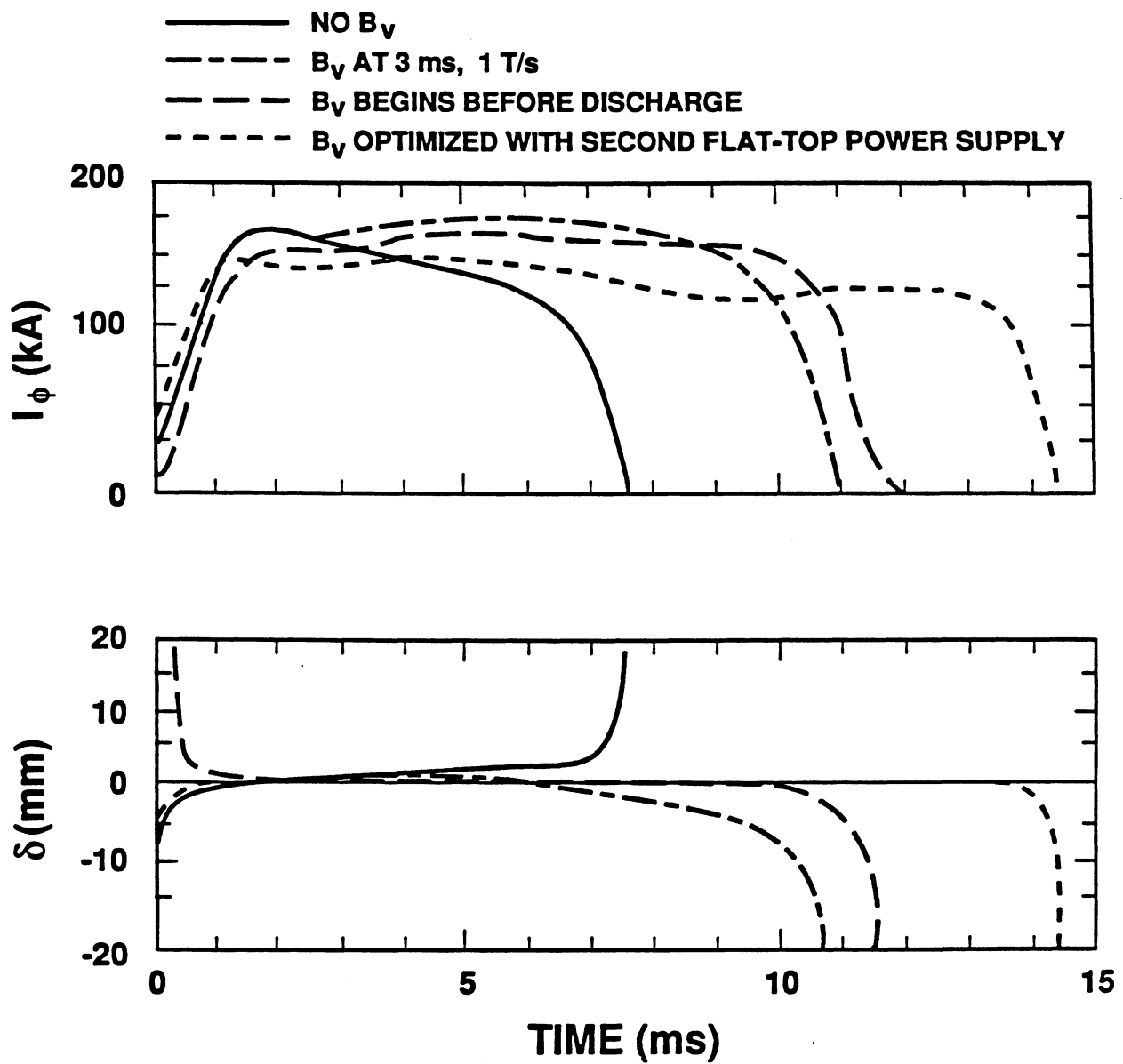


Figure 2.3-26. Impact of vertical field on OHTE discharges carried out in resistive shells with $\tau_v = 1.5$ ms [90].

provide a boundary that is adequately stabilizing, major design simplification and optimization for both the next generation RFPs and reactors may be possible. Field-error constraints become less important. Also, active control of plasma position should reduce the plasma-wall interaction, edge-plasma dissipation, and the loop voltage, and should thereby increase the energy confinement time [92]. This trend towards $\tau_D > \tau_v$ and the ability to exert more external control on the plasma is reflected in the RFX and ZTH experiments (Figure 2.3-27), and is a major step towards reactor-relevant operation of RFPs.

The Reversatron experiment [93] is pursuing the limits of RFP operation with virtually no conducting shell (Table 2.3-II). This device is somewhat small in size and is subject to large field errors, but nevertheless the Reversatron has the flexibility to operate as an RFP or as a high-aspect-ratio spheromak (*i.e.*, $F \rightarrow 0$). Shell-less discharges in both RFP and spheromak configurations are terminated by global MHD modes with toroidal mode numbers $n = 1$ and 2. Depending on the vertical-field index, n' , this shell-less RFP is found to be unstable to the $n = 1$ tilt or shift modes. The growth time scales for the “rigid” (vertical) shift and tilt modes, respectively, were shown to scale as follows [94]:

$$\left(\frac{1}{\gamma}\right)_{SFT} = \left(\frac{2A^2}{|n'| \Lambda - 1}\right) \tau_v \simeq A^2 \tau_v , \quad (2.3-10)$$

$$\left(\frac{1}{\gamma}\right)_{TLT} = \left(\frac{4}{\pi}\right)^2 \left(\frac{A^2}{\Lambda |1 - n'|} - 1\right) \tau_v , \quad (2.3-11)$$

where $\Lambda = \ln(8A) + \ell_i/2 + \beta_\theta - 3/2$, $n' = -(R_T/B_{V0})(\partial B_V/\partial R)$, and $A = R_T/r_p$ is the plasma aspect ratio, with $|n| \Lambda/2 \simeq 1$. On the basis of this simplified theory, the OHTE discharges given on Figure 2.3-26 have not reached a point where these instabilities should be seen ($\tau_v = 1.5$ ms, $A = 6.3$, or $1/\gamma \simeq 60$ ms).

In summary, considerable experimental and theoretical work is required to resolve the role of the close-fitting, stabilizing shell that ideal-MHD theory has historically demanded for the RFP. The longer-pulsed, higher-current, higher-power-density RFPs of the future, however, must operate with active control of the plasma position to achieve a better control of the edge-plasma conditions and better confinement. The first steps in this direction are being taken by the new OHTE and Reversatron experiments, but considerably more remains to be done in this crucial area.

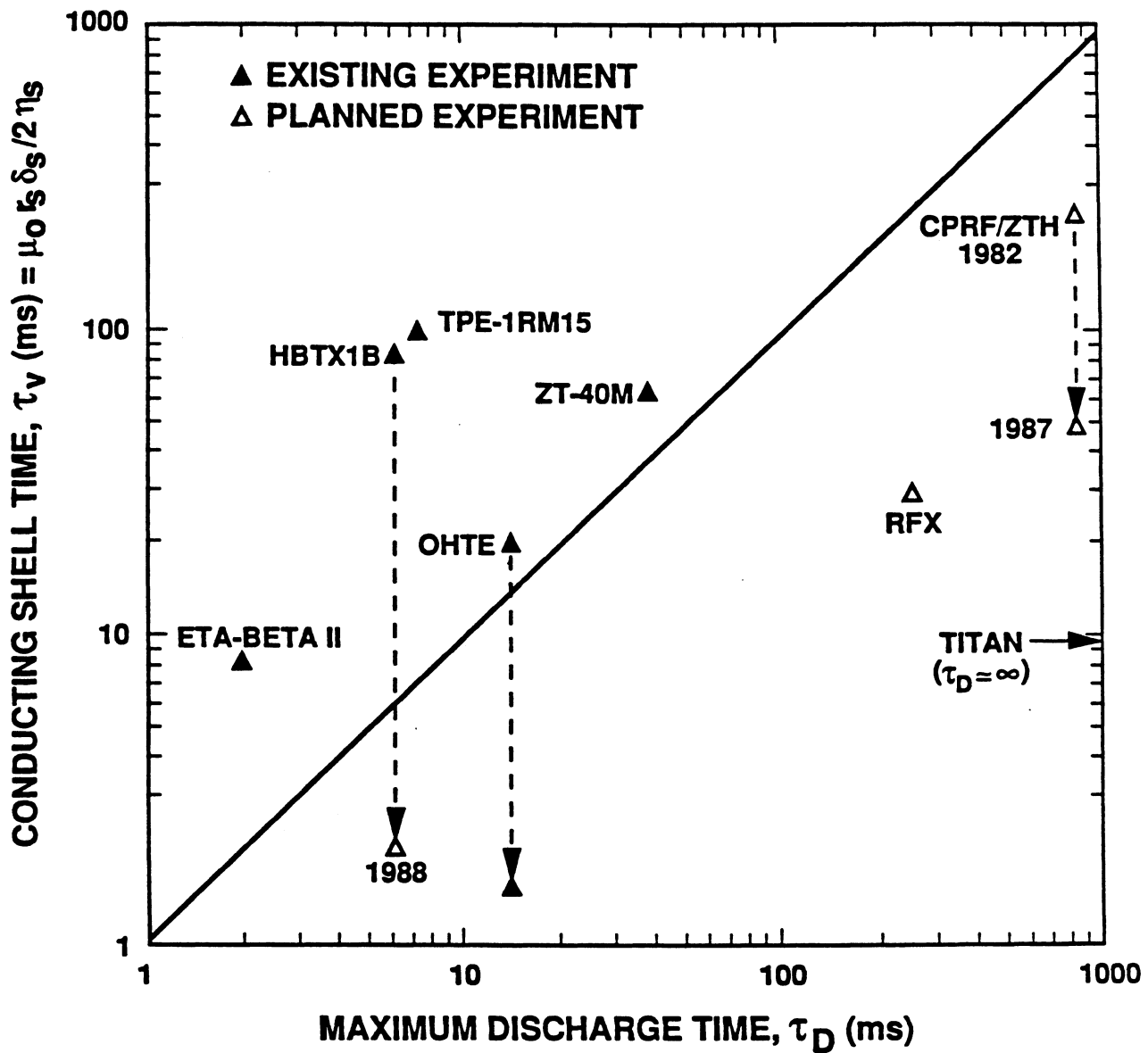


Figure 2.3-27. Relationship between shell and discharge times for a range of existing and planned RFP experiments.

2.4. SUMMARY

The principles of the RFP confinement concept were discussed and the experimental data base was briefly reviewed. This data base is not as extensive as that of tokamaks and, therefore, requires a larger extrapolation to reactor-relevant regimes. Modern RFP experiments such as those of Table 2.3-I, however, have demonstrated the robustness of the RFP dynamo and an emerging commonality of the basic physical processes operative in RFPs.

The key physics requirements and uncertainties for a RFP reactor include heating, transport, plasma-wall interaction, current drive, and impurity control and particle exhaust with pumped limiters or magnetic divertors. The largest uncertainties in the existing RFP data base remain in the confinement physics and, in particular, in the mechanism, magnitude, and the regional extent of cross-field transport in the near-minimum-energy-state RFP configuration. Experiments with higher currents (and possibly higher current densities) and variable plasma size are needed to distinguish between possible scaling laws.

The modern RFP experiments are physically small, but operate close to ohmic-power and current densities expected for the reactor. These experiments, therefore, can be strongly influenced by plasma-wall interaction. The increased particle and heat load on the first wall and impurity-control system, and the need to control field errors and the plasma-wall interaction in general, also represent major challenges for the next-step multi-mega-ampere experiments [24]. Data from these next-generation experiments are expected in the early 1990s. These data are of the utmost importance in resolving key physics requirements and uncertainties for RFP reactors. Furthermore, these next-step experiments can provide valuable technological insight for devising a development path towards economically and technologically attractive RFP fusion reactors with strong safety and environmental attributes.

REFERENCES

- [1] F. Najmabadi, N. M. Ghoniem, R. W. Conn, *et al.*, "The TITAN Reversed-Field Pinch Reactor Study, Scoping Phase Report," joint report of University of California Los Angeles, General Atomics, Los Alamos National laboratory, and Rensselaer Polytechnic Institute, UCLA-PPG-1100 (1987).
- [2] R. W. Conn (chairman and Ed.), "Magnetic Fusion Advisory Committee Panel X Report on High Power Density Fusion Systems," (May 8, 1985).
- [3] J. Sheffield, R. A. Dory, S. M. Cohn, J. G. Delene, L. F. Parsley, *et al.*, "Cost Assessment of a Generic Magnetic Fusion Reactor," Oak Ridge National Laboratory report ORNL/TM-9311 (1986) 103.
- [4] R. A. Krakowski, R. L. Miller, and R. L. Hagenson, "The Need and Prospect for Improved Fusion Reactors," *J. Fusion Energy* **5** (1986) 213.
- [5] R. A. Krakowski, R. L. Hagenson, N. M. Schnurr, C. Copenhaver, C. G. Bathke, R. L. Miller, and M. J. Embrechts, "Compact Reversed-Field Pinch Reactors (CRFPR)," *Nuclear Eng. Design/Fusion* **4** (1986) 75.
- [6] H. A. Bodin, R. A. Krakowski, and O. Ortolani, "The Reversed-Field Pinch: from Experiment to Reactor," *Fusion Technol.* **10** (1986) 307.
- [7] R. L. Hagenson, R. A. Krakowski, C. G. Bathke, R. L. Miller, M. J. Embrechts, *et al.*, "Compact Reversed-Field Pinch Reactors (CRFPR): Preliminary Engineering Considerations," Los Alamos National Laboratory report LA-10200-MS (1984).
- [8] C. Copenhaver, R. A. Krakowski, N. M. Schnurr, R. L. Miller, C. G. Bathke, *et al.*, "Compact Reversed-Field Pinch Reactors (CRFPR)," Los Alamos National Laboratory report LA-10500-MS (1985).
- [9] H. A. B. Bodin and A. A. Newton, "Review Paper: Reversed-Field Pinch Research," *Nucl. Fusion* **20** (1980) 1255.
- [10] D. A. Baker and W. E. Quinn, "The Reversed-Field Pinch," *FUSION I, Part A*, Edward Teller (Ed.), Academic Press, NY (1981) p. 438.
- [11] J. B. Taylor, "Relaxation of Toroidal Plasma and Generation of Reversed Magnetic Field," *Phys. Lett.* **33** (1974) 1139.

- [12] H. A. B. Bodin, "Reversed-Field Pinch: Status and Trends," *Plasma Phys. and Cont. Fusion* **29** (1987) 1297.
- [13] V. Antoni, D. Merlin, S. Ortolani, and R. Paccagnella, "MHD Stability Analysis of Force-Free Reversed-Field Pinch Configurations," *Nucl. Fusion* **26** (1987) 1711.
- [14] J. A. Phillips, D. A. Baker, R. F. Gribble, and C. Munson, "Start-up of Reversed-Field Pinches and Current Ramping Using Dynamo Action," submitted to *Nucl. Fusion* (1987).
- [15] R. S. Massey, R. G. Watt, P. G. Weber, G. A. Wurden, D. A. Baker, C. J. Buchenauer, *et al.*, "Status of the ZT-40M RFP Experimental Program," *Fusion Technol.* **8** (1985) 1571.
- [16] G. A. Wurden, K. F. Schoenberg, M. M. Pickrell, and the RFP Experimental Team, "RFP Experiments: Results From ZT-40M and ZT-P," in *Proc. Int. School of Plasma Phys. Course and Workshop on Physics of Mirrors, Reversed-Field Pinches, and Compact Tori*, Varenna, Italy (September 1987).
- [17] M. K. Bevir and J. W. Gray, "Relaxation, Flux Consumption and Quasi Steady State Pinches," *Proc. RFP Theory Workshop*, Los Alamos National Laboratory report LA-8944-C (January 1982) 176.
- [18] C. W. Barnes, J. C. Fernandez, I. Henins, H. W. Hoida, T. R. Jarboe, S. O. Knox, G. J. Marklin, and K. F. McKenna, "Experimental Determination of the Conservation of Magnetic Helicity from the Balance Between Source and Spheromak," *Phys. Fluids* **29** (1986) 3415.
- [19] K. F. Schoenberg, C. J. Buchenauer, R. S. Massey, J. G. Melton, R. W. Moses, R. A. Nebel, and J. A. Phillips, " $F - \Theta$ Pumping and Field Modulation Experiments on a Reversed Field Pinch Discharge," *Phys. Fluids* **27** (1984) 548.
- [20] K. F. Schoenberg, C. P. Munson, D. A. Baker, R. F. Gribble, R. W. Moses, P. G. Weber, R. A. Nebel, and R. F. Scardovelli, "Oscillating-Field Current Drive Experiments on the ZT-40M RFP," *Bull. Am. Phys. Soc.* **31** (1986) 1547.
- [21] K. F. Schoenberg, J. C. Ingraham, C. P. Munson, P. G. Weber, D. A. Baker, R. F. Gribble, *et al.*, "Oscillating-Field Current Drive Experiment in ZT-40M Reversed Field Pinch," submitted to *Phys. Fluids* (1988).
- [22] V. D. Shafranov, "Plasma Equilibrium in a Magnetic Field," *Reviews of Plasma Physics* **2**, Consultant Bureau, New York (1966) 103.

- [23] V. S. Mukhovatov and V. D. Shafranov, "Plasma Equilibrium in a Tokamak," *Nucl. Fusion* **11** (1971) 605.
- [24] D. B. Thomson (Ed.), *Proc. Int. Workshop on Engineering Design of Next Step Reversed Field Pinch Devices*, Los Alamos National Laboratory (July 13-17, 1987).
- [25] B. B. Kadmontsev, "Disruptive Instabilities in Tokamaks," *Sov. J. Plasma Phys.* **1** (1975) 389.
- [26] T. R. Jarboe and B. Alper, "A Model for Loop Voltage of a Reversed-Field Pinch," *Phys. Fluids* **30** (1987) 1177.
- [27] H. Y. W. Tsui, "Helicity Transport and Anomalous Resistance in Reversed-Field Pinch," in *Proc. 14th European Conf. on Cont. Fusion and Plasma Phys.* Madrid, Spain (June 22-26, 1987).
- [28] A. R. Jacobsen and R. W. Moses, "Non-local DC Electrical Conductivity of a Lorentz Plasma in a Stochastic Magnetic Field," *Phys. Rev. A* **29** (1984) 3335.
- [29] R. W. Moses, K. F. Schoenberg, and D. A. Baker, "Empirical Modelling and Dependence of RFP Loop Voltage on Edge Plasma Conditions," private communication, Los Alamos National Laboratory (December 1987).
- [30] I. B. Bernstein, E. A. Frieman, M. D. Kruskal, and R. M. Kulsrud, "An Energy Principle for Hydromagnetic Stability Problems," *Proc. Royal Soc.* **244** (1958) 17.
- [31] B. R. Suydam, "Stability of Linear Pinch," *Proc. 2nd United Nations Int. Conf. on the Peaceful Uses of Atomic Energy*, Geneva, Switzerland (September 1958), United Nations, Geneva **31** (1958) 157.
- [32] C. Mercier, "A Necessary Criterion for the Hydrodynamic Stability for an Axisymmetric Plasma," *Nucl. Fusion* **1** (1960) 47.
- [33] D. C. Robinson, "High- β Diffuse Pinch Configurations," *Plasma Phys.* **13** (1971) 439.
- [34] I. H. Hutchinson, "Plasma Resistance Studies in HBTX1A Reversed-Field Pinch," in *Proc. 11th European Conf. on Cont. Fusion and Plasma Phys.*, Aachen, F. R. G. (September 1984).
- [35] R. G. Watt and E. M. Little, "RFP Energy Evolution and Containment in the Presence of Giant Sawteeth," *Phys. Fluids* **27** (1984) 784.

- [36] D. C. Robinson, "Tearing-Mode-Stable Diffuse-Pinch Configurations," *Nucl. Fusion* **18** (1978) 939.
- [37] J. W. Connor and J. B. Taylor, "Resistive Fluid Turbulence and Energy Confinement," *Phys. Fluids* **27** (1984) 2676.
- [38] A. D. Merlin, S. Ortolani, and R. Paccagnella, "Free Boundary MHD Stability Configurations," in *Proc. 14th European Conf. on Cont. Fusion and Plasma Phys.*, Madrid, Spain (June 22-26, 1987).
- [39] S. Ortolani, in *Proc. Int. School of Plasma Phys. Course on Mirror-based and Field-Reversed Approaches to Magnetic Fusion*, Varenna, Italy (1983).
- [40] R. G. Watt and R. A. Nebel, "Sawteeth, Magnetic Disturbances, and Magnetic Flux Regeneration in the Reversed-Field Pinch," *Phys. Fluids* **26** (1983) 1168.
- [41] D. D. Schnack, E. J. Caramana, and D. C. Barnes, "Simulation of Current Ramp Operation in the Reversed- Field Pinch," *Bull. Am. Phys. Soc.* **30** (1985) 1399.
- [42] M. G. Rusbridge, "A Model of Field Reversal in the Diffuse Pinch," *Plasma Phys.* **19** (1977) 499.
- [43] M. G. Rusbridge, "Field-Line Reconnection and Density Fluctuations in ZETA," *Plasma Phys.* **22** (1980) 331.
- [44] Z. G. An *et al.*, "Role of Multiple Helicity Non-Linear Interaction of Tearing Modes in Dynamo and Anomalous Thermal Transport in Reversed Field Pinch," *Proc. 10th Int. Conf. Plasma Phys. and Cont. Nucl. Fusion Res.*, London, U. K. (September 1984), IAEA, Vienna, **2** (1985) 231.
- [45] N. T. Gladd and N. A. Krall, JAYCOR report J530-84-221 (1984).
- [46] S. Briguglio, F. Romanelli, and G. Vlad, "Current Driven Drift Waves as a Possible Mechanism for Dynamo Effect and Transport in Reversed Field Pinches," *Nucl. Fusion* **26** (1986) 1293.
- [47] D. C. Robinson and R. E. King, "Factors Influencing the Period of Improved Stability in ZETA," *Proc. 3rd Int. Conf. on Plasma Phys. and Cont. Nucl. Fusion Res.*, Novosibirsk, U. S. S. R. (Aug. 1968), IAEA, Vienna, **1** (1969) 263.
- [48] A. Buffa *et al.*, "First Results from the ETA-BETA-II RFP Experiment," *Proc. 9th European Conf. on Cont. Fusion and Plasma Phys.*, Oxford, U. K. (September 1979), Culham Laboratory (1979) 544.

- [49] V. Antoni *et al.*, "Studies on High-Density RFP Plasmas in the ETA-BETA-II Experiment," *Proc. 9th Int. Conf. on Plasma Phys. and Cont. Nucl. Fusion Res.*, Baltimore, U. S. A. (September 1982), IAEA, Vienna, **1** (1983) 619.
- [50] V. Antoni *et al.*, "Reversed Field Pinch Plasma with Current Flat-Top in ETA-BETA-II," *Proc. 10th Int. Conf. on Plasma Phys. and Cont. Nucl. Fusion Res.*, London, U. K. (September 1984), IAEA, Vienna, **2** (1985) 487.
- [51] K. Ogawa, Y. Maejima, T. Shimada, Y. Hirano, P. G. Carolan, C. W. Gowers, A. Nagata, H. Ashida, T. Amano, and Y. Kondoh, "Experimental and Computational Studies of Reversed-Field Pinch on TPE-1R(M)," *Proc. 9th Int. Conf. on Plasma Phys. and Cont. Nucl. Fusion Res.*, Baltimore, U. S. A. (September 1982) IAEA, Vienna, **1** (1983) 575.
- [52] Y. Hirano, T. Shimada, Y. Maejima, and K. Ogawa, "Improved Stability Period in High-Current-Density Operation of Reversed-Field Pinch of ETL-TPE-1R(M)," *Nucl. Fusion* **22** (1982) 1613.
- [53] D. A. Baker, M. D. Bausman, C. J. Buchenauer, L. C. Burkhardt, G. Chandler, and J. N. DiMarco, "Performance of the ZT-40M Reversed-Field Pinch with an Inconel Liner," *Proc. 9th Int. Conf. on Plasma Phys. and Cont. Nucl. Fusion Res.*, Baltimore, U. S. A. (September 1982) IAEA, Vienna, **1** (1983) 587.
- [54] D. A. Baker, C. J. Buchenauer, L. C. Burkhardt, E. J. Caramana, J. N. DiMarco, J. N. Downing, *et al.*, "Experimental and Theoretical Studies of the ZT-40M Reversed-Field Pinch," in *Proc. 10th Int. Conf. on Plasma Phys. and Cont. Nucl. Fusion Res.*, London, U. K. (September 1984) IAEA, Vienna (1985).
- [55] H. A. B. Bodin *et al.*, *Proc. 9th Int. Conf. on Plasma Phys. and Cont. Nucl. Fusion Res.*, Baltimore, U. S. A. (September 1982), IAEA, Vienna, **8** (1983) 641.
- [56] P. Carolan *et al.*, "New Results from HBTX1A Reversed Field Pinch," *Proc. 10th Int. Conf. on Plasma Phys. and Cont. Nucl. Fusion Res.* London, U. K. (September 1984), IAEA, Vienna, **2** (1985) 449.
- [57] T. Tamano *et al.*, "Pinch Experiments in OHTE," *Proc. 9th Int. Conf. on Plasma Phys. and Cont. Nucl. Fusion Res.*, Baltimore, U. S. A. (September 1982), IAEA, Vienna, **1** (1983) 609.
- [58] T. Tamano, W. D. Bard, T. N. Carlstrom, C. Chu, B. Curwe, R. K. Fisher, *et al.*, "High Current, High Beta Toroidal Pinch Experiment in OHTE," in *Proc. 10th Int.*

- Conf. on Plasma Phys. and Cont. Nucl. Fusion Res.*, London, U. K. (September 1984) IAEA, Vienna (1985).
- [59] C. G. Bathke, R. A. Krakowski, R. A. Krakowski, and R. L. Miller, "A DT Neutron Source Based on the Reversed Field Pinch," *Proc. 12th IEEE Symp. on Fusion Eng.*, Monterey, CA (October 1987) 829.
 - [60] G. Malesani (Chair.), *Trilateral Workshop to Promote International Cooperation on RFP Research*, Padova, Italy (September 1987) Instituto Gas Ionizzati del C.N.R. report IGI 87/03 (1987).
 - [61] A. A. Newton and P. G. Noonan, "Controlled Termination of Reversed-Field-Pinch Discharges," *Nucl. Instr. and Methods A*245 (1986) 167.
 - [62] J. A. Phillips, "Improved Start-up of Reversed-Field Pinches Using Current Ramping with Toroidal Flux Generation," *Bull. Am. Phys. Soc.* 32 (1987) 1785.
 - [63] P. G. Noonan, C. G. Gimblett, and A. A. Noonan, "Plasma Behavior During Programmed Current Decay and Ramping in the Reversed-Field Pinch," in *Proc. 14th European Conf. on Cont. Fusion and Plasma Phys.*, Madrid, Spain (June 1987).
 - [64] B. Alper and H. Y. W. Tsui, "Effect of a Moveable Tile Limiter on the Loop Voltage in HBTX1B RFP," in *Proc. 14th European Conf. on Cont. Fusion and Plasma Phys.*, Madrid, Spain (June 1987).
 - [65] J. A. Phillips, L. C. Burkhardt, A. Haberstich, R. B. Howell, J. C. Ingraham, E. M. Little, K. S. Thomas, and R. G. Watt, "ZT-40M Current Risetime Study," Los Alamos National Laboratory report LA-9717-MS (1983).
 - [66] R. G. Watt, G. A. Wurden, P. G. Weber, K. Buechl, and E. K. Spanos, "Pellet Injection on the ZT-40M Reversed-Field Pinch," *Rev. Sci. Instr.* 58 (1987) 1401.
 - [67] G. A. Wurden, P. G. Weber, R. G. Watt, C. P. Munson, T. E. Cayton, and K. Buchl, "Refueling and Density Control in the ZT-40M Reversed-Field Pinch," in *Proc. Int. School of Plasma Phys, Course and Workshop on Physics of Mirrors, Reversed-Field Pinches, and Compact Tori*, Varenna, Italy (September 1987).
 - [68] V. Antoni, E. Baseggio, L. Carraro, L. Flora, L. Gabellieri, and L. Giudicotti, " D_2 Pellet Injection in ETA-BETA-II Plasma," in *Proc. 14th European Conf. on Cont. Fusion and Plasma Phys.*, Madrid, Spain (June 1987).

- [69] I. H. Hutchinson *et al.*, "The Structure of Magnetic Fluctuations in HBTX1A Reversed-Field Pinch," *Nucl. Fusion* **14** (1984) 59.
- [70] V. Antoni and S. Ortolani, "Characteristic of the Magnetic-Field Fluctuations in the ETA-BETA-II Reversed Field Pinch Experiment," *Plasma Phys.* **25** (1983) 799.
- [71] D. Brotherton-Ratcliffe, C. G. Gimblett, and I. H. Hutchinson, "Analysis of Internal Magnetic Fluctuations in HBTX1A Reversed Field Pinch," Culham Laboratory report CLM-P742 (1985).
- [72] R. J. LaHaye *et al.*, "Measurements of Magnetic-Field Fluctuations in the OHTE Toroidal Pinch," *Phys. Fluids* **27** (1984) 2576.
- [73] H. Y. W. Tsui, J. Cunnane, and D. E. Evans, "Magnetic Island Fluctuations in the HBTX1B Reversed-Field Pinch," in *Proc. 14th European Conf. on Cont. Fusion and Plasma Phys.*, Madrid, Spain (June 1987).
- [74] V. Antoni, P. DeSimone, P. Innocente, P. Martin, S. Martini, S. Ortolani, *et al.*, "Fluctuation Studies on the ETA-BETA-II Experiment," in *Proc. 14th European Conf. on Cont. Fusion and Plasma Phys.*, Madrid, Spain (June 1987).
- [75] G. A. Wurden, "Soft X-ray Array Results on ZT-40M Reversed Field Pinch," *Phys. Fluids* **27** (1984) 551.
- [76] V. Antoni and S. Ortolani, "Magnetic Field Fluctuation Studies on ETA-BETA-II," *Proc. of the Workshop on Mirror-Based and Field-Reversed Approaches to Magnetic Fusion*, Varenna (September 1983), Monobypia Franchi, Perugia, **2** (1984) 97.
- [77] G. Wurden, private communication, Los Alamos National Laboratory (December 1987).
- [78] B. Alper *et al.*, "RFP Confinement Studies in ETA-BETA-II," *Proc. 12th European Conf. on Cont. Fusion and Plasma Phys.*, Budapest, Hungary (September 1985), *European Phys. Soc.* **1** (1985) 578.
- [79] P. G. Weber *et al.*, "Results from the Los Alamos RFP Experiments," *Proc. 12th European Conf. on Cont. Fusion and Plasma Phys.*, Budapest, Hungary (September 1985), *European Phys. Soc.* **1** (1985) 570.
- [80] T. Cayton, private communication, Los Alamos National Laboratory (1987).

- [81] M. M. Pickrell, J. A. Phillips, C. J. Buckenauer, T. Cayton, J. N. Downing, A. Haberstich, *et al.*, "Evidence for a Poloidal Beta Limit on ZT-40M," *Bull. Am. Phys. Soc.* **29** (1984) 1403.
- [82] A. R. Jacobsen and M. G. Rusbridge, "Observed Mechanism of Termination in ZT-40M Reversed-Field Pinch," Los Alamos National Laboratory report LA-9589-MS (1982).
- [83] R. Gross, *Fusion Energy*, Wiley and Sons, NY (1984) 118.
- [84] K. F. Schoenberg, R. F. Gribble, and D. A. Baker, "Oscillating Field Current Drive for Reversed Field Pinch Discharges," *J. Appl. Phys.* **56** (1984) 2519.
- [85] J. T. Hogan, *Bull. Am. Phys. Soc.* **31** (1986) 1548.
- [86] J. M. Finn and T. M. Antonsen, Jr., "Anomalous Current Penetration and Oscillating Current Drive in Tokamaks," *Phys. Fluids* **30** (1987) 2450.
- [87] M. Ono, G. J. Greene, D. Dajrrow, C. Forest, H. Park, and T. H. Stix, "Steady-State Tokamak Discharge via Helicity Injection," *Phys. Rev. Lett.* **59** (1987) 2165.
- [88] W. A. Reass, R. F. Gribble, and C. F. Hammer, "Design Construction and Electrical Test Results of Dual Phase Controlled Multi-Megawatt Oscillators for Oscillating-Field Current Drive on ZT-40M," *Proc. IEEE 11th Symp. Fusion Eng.* (1985) 1214.
- [89] K. F. Schoenberg, G. A. Wurden, P. G. Weber, J. C. Ingraham, C. P. Munson, *et al.*, *Proc. 11th Int. Conf. on Plasma Phys. and Cont. Nucl. Fusion Res.*, Kyoto, Japan (November 1986) IAEA, Vienna, **2** (1987) 423.
- [90] S. Ortolani, V. Antoni, S. Martini, R. LaHaye, M. Schaffer, T. Tamano, and P. Taylor, "Reversed-Field Pinch Operation with a Thin Shell," in *Proc. 14th European Conf. on Cont. Fusion and Plasma Phys.*, Madrid, Spain (June 1987).
- [91] R. R. Goforth, T. N. Carlstran, C. Chu, B. Curwen, D. Grauman, P. S. C. Lee, *et al.*, "Reversed-Field Pinch Experiment with a Resistive Shell," *Nucl. Fusion* **26** (1986) 414.
- [92] T. Tamano, W. D. Bard, C. Chu, T. N. Carstram, R. R. Goforth, Y. Kondoh, *et al.*, "Characteristics of Reversed-Field Pinch Plasmas with a Resistive Shell," in *Proc. 11th Int. Conf. on Plasma Phys. and Cont. Nucl. Fusion Res.*, Kyoto, Japan (November 1986).

- [93] P. Schmid and S. Robertson, "Design of an Air-Core Reversed-Field Pinch," *IEEE Trans. Plasma Sci.* (June 1986).
- [94] S. Robertson and P. Schmid, "Instability of a Reversed Field Pinch Without a Conducting Shell," private communication, University of Colorado, Boulder (1987).